CHARACTERIZING PIAS1 FUNCTION DURING EMBRYOGENESIS AND

LUNG CANCER PROGRESSION

APPROVED BY SUPERVISORY COMMITTEE

_____

Pier P. Scaglioni, M.D. (PhD Mentor)
Associate Professor
Internal Medicine

_____

Rolf A. Brekken, Ph.D. (Chairman)
Professor
Surgery, Pharmacology

_____

Jerry W. Shay, Ph.D.
Professor
Cell Biology

_____

Hongtao Yu, Ph.D.
Professor
Pharmacology

DEDICATION

To my mother and grandmother Fior and Elsa Constanzo who supported my education on anything that I decided to do. To my brothers Juan and Chris, whom I hope, to serve as a good example to pursue anything they want in life with honesty, dedication and dignity. To my wife Mariya for always supporting me and providing encouragement when I needed it most.

CHARACTERIZING PIAS1 FUNCTION DURING EMBRYOGENESIS AND LUNG CANCER PROGRESSION

By

JERFIZ D. CONSTANZO

DISSERTATION

Presented to the Faculty of the Graduate School of Biomedical Sciences

The University of Texas Southwestern Medical Center

In Partial Fulfillment of the Requirements

For the Degree of

DOCTOR OF PHILOSOPHY

The University of Texas Southwestern Medical Center

Dallas, Texas

May 2016

ACKNOWLEDGEMENTS

I would like to acknowledge my PhD mentor Dr. Pier Paolo Scaglioni for welcoming me into his laboratory to pursue my PhD training. I am forever grateful for his mentorship, infinite patience and support during my arduous years of training. Thank you for helping me successfully submitting independent grant applications, progress evaluations and completion of three research manuscripts. Thank you for the collaborative environment, the ability to ask my own questions and for continuously striving to make me a better scientist.

In addition, I am extremely grateful to Drs. Rolf A. Brekken, Jerry W. Shay and Hongtao Yu for the opportunity to continuously interact during my PhD training, priceless feedback on my research progress and opening their laboratories for collaboration, reagents and expertise. I honestly could have not done it without your help.

I also would like to thank my wife Mariya Ilcheva for all the support and encouragement, and for being patient with my unforgiving work-schedule and all the "just to change media" moments that lasted more than five minutes.

I am very thankful to my friends and colleagues: Drs. Kristina Y. Aguilera, Kacey Rajkovich, Ke-jing Tang, Carlos Gil Del Alcazar and Pavlina Todorova for being my support group, for all their help and friendship during my PhD training and all our lets go have a drink moments, I could not have come this far without you guys.

I would like to thank current and former lab members: Drs. Georgia Konstantinidou, Smita Rhindhe, Margherita Melegari, Mahesh Padanad, Andrea

Rabellino, Haopeng Yan and Niranjan Venkateswaran for technical training, help with experiments and feedback on my project(s) during lab meetings and informal coffee breaks.

I also like to give special thanks go to Dr. Ondine Cleaver, Dr. Douglas Millay and Dr. Mi Deng, for Developmental Biology advise, recommendations and collaborative help needed for moving my project forward. Thank you for sharing your expertise and having the wonderful open door policy for which UTSW is characterized and greatly successful for.

ABSTRACT

The main focus of this work is to provide a better understanding about the function of small ubiquitin like modifiers (SUMO) conjugating enzymes in eukaryotes during embryonic organogenesis, tissue differentiation and human tumor progression; with a focus on non-small cell lung cancers (NSCLC).

The SUMO E3 ligase protein inhibitor of activated STAT-1 (PIAS1) is one the few known SUMO conjugating enzymes known to date. PIAS1 was first discovered as a negative regulator of signal transducer and activator of transcription 1 (STAT-1), from which its name is derived. PIAS1 facilitates STAT-1 conjugation with SUMO, which subsequently blocks STAT-1 ability to interact with DNA and promote gene transcription. PIAS1 is also known for its involvement in the coordinated response to DNA damage repair and immune repression. During DNA damage PIAS1 SUMOylation of target proteins, such as, breast cancer susceptibility gene 1 (BRCA1) promotes its recruitment to sites of DNA damage and promotes efficient DNA repair. In contrast, PIAS1 repression of necrosis factor kappa B (NFκB), blocks interaction with downstream target genes and suppresses the secretion of inflammatory cytokines by immune cells. Thus, the ability to interact with widely diverse targets, including transcription factors and genome integrity proteins places PIAS1 at the epicenter of SUMOylation biology making it a valuable protein to study in this field.

We used mice (Mus musculus) as our model system for studying the function of *Pias1* by global inactivation of this gene in mammals to discover tissues and biological processes affected by the loss of *Pias1*. We found that, in agreement with previous reports, inactivation of *Pias1* results in embryonic lethality in 90% of mouse embryos, while the remaining 10% are born about 40% smaller and anemic. Upon close examination of mouse embryos prior to their death, we discovered severe growth retardation, anemia and defective angiogenesis. We determined that hematopoietic cells in the embryonic yolk sac (YS) were depleted early during development as a result of defective differentiation and reduced cell survival. Although blood differentiation and angiogenic defects were detected first, the lack of blood circulation and a deficient endothelial cell layer in the vasculature of *Pias1* null embryos also results in loss of myocardium muscle mass and defective heart formation. However, with *in vivo* analysis we could not rule out heart tissue intrinsic defects. In contrast, *in vitro* studies show that PIAS1 may cooperate with the cardiac transcription factors Myocardin and GATA-4 in promoting cardiac differentiation.

Because *Pias1* loss primarily affects erythrogenesis and vascular development of the YS, we also tested how conditional *Pias1* deletion in endothelial cells of the YS would affect erythrogenesis and vascular development.

Pias1 loss in endothelial cells recapitulates the erythroid and angiogenic defects in the YS of *Pias1* null embryos, but not the growth retardation phenotype.

In this study we also examined PIAS1 involvement in tumorigenesis with the hypothesis that PIAS1 functions during tissue growth and survival can be exploited by malignant neoplasms during tumor progression. Previous studies have found that PIAS1 can either repress or enhance tumorigenesis depending on tumor type. In prostate cancer, PIAS1 has been found to promote tumor proliferation by repression of the p21 tumor suppressor. In addition, PIAS1 protein loss correlates with colon cancer development. Previous reports suggested that amplification of the *PIAS1* gene locus is observed in human NSCLC. Using single nucleotide polymorphism (SNPs) data we identified concurrent copy number alterations for *PIAS1* and the focal adhesion kinase (FAK) in a subset of NSCLC cell lines. PIAS1 and FAK were previously found to interact by a yeast two-hybrid screen. Moreover, FAK SUMOylation by PIAS1 was reported to increase its active phosphorylation at Tyrosine 397 (Y397). We decided to characterize FAK-PIAS1 interaction further and discovered that upon mitogenic stimulation, endogenous FAK and PIAS1 proteins interact in endosomes in the cytoplasm of NSCLC cells. Moreover PIAS1 promotes a modest increase in FAK SUMOylation and C-terminal cleavage by the calcium dependent protease Calpain. Ectopic expression of PIAS1 induces FAK nuclear accumulation and affects gene transcription favoring DNA damage repair and metabolism.

Importantly, we found that pharmacologic inhibition of FAK protein or its deletion by CRISPR/CAS9 technology results in susceptibility to DNA damage *in vitro* and *in vivo*, providing a valuable strategy for combination therapy using FAK inhibitors (FAKi) and ionizing radiation (IR) in the treatment of human NSCLC. Our results provide new knowledge about PIAS1 and FAK requirement for basic biology and in human disease.

TABLE OF CONTENTS

PUBLICATIONS

1. **Constanzo J.D.,** Deng M., Rhindhe S., Tang K., Zang C. and Scaglioni P.P., *Pias1* Deficiency Induces Failure of Cardiovascular Development and Yolk Sac Erythropoiesis in Mice. (Manuscript under review)

2. **Constanzo J.D.,** Tang K. and Scaglioni P.P. *FAK-PIAS1* Interaction Promotes the Survival and progression of Metastatic Lung Cancer cells. (Manuscript under review)

3. Tang K., **Constanzo J.D.,** Venkateswaran N.V., Melegari M. and Scaglioni P.P. Focal Adhesion Kinase regulates the DNA damage response and its inhibition leads to radiosensitizing effects in lung cancer. (Manuscript under review)

LIST OF FIGURES AND TABLES

LIST OF ABBREVIATIONS

SUMO	Small ubiquitin like modifier
UBC9	Ubiquitin conjugating enzyme 9
PIAS1	Protein inhibitor of activated STAT-1
STAT-1	Signal transducer and activator or transcription 1
PML	Promyelocytic leukemia
BIM	BCl2- protein family member 11 (Apoptosis Facilitator)
GATA-1	GATA binding transcription factor 1
GATA-4	GATA binding transcription factor 4
FACS	Fluorescence associated cell sorting
FAK	Focal adhesion kinase
VCL	Vinculin
CDK1	Cyclin-dependent kinase 1
LAMP1	Lysosome associated protein 1
RAB11	Ras-related GTP-binding protein 11
DAPI	4', 6-diamidino-2-phenylindole
DMEM	Dulbecco's Modified Eagle Medium
DMSO	Dimethyl sulfoxide
FBS	Fetal Bovine Serum
PKCi	Protein kinase C inhibitor
EGF	Epithelial growth factor

shRNA	Short hairpin ribonucleic acid
siRNA	Small interfering ribonucleic acid
SNP	Single nucleotide polymorphism
TMA	Tissue microarray
DNA	Deoxyribonucleic acid
RAC1	Ras related C3 botulinum toxin substrate 1
ROCK1	Rho-associated, coiled-coil containing protein kinase 1
GAPDH	Glyceraldehyde-3-phosphate dehydrogenase
PBS	Phosphate buffered saline
PFA	Paraformaldehyde
TUNEL	Terminal deoxynucleotidyl transferase-mediated dUTP-nick end labeling
UV	Ultraviolet
WT	Wild-type
PECAM	Platelet/endothelial cell adhesion molecule 1
SEMA3E	Semaphorin3E
ANGP2	Angiopoietin 2
VCAM-1	Vascular cell adhesion molecule 1
VEGFR2	Vascular endothelial growth factor receptor 2
BMP2	Bone morphogenetic protein 2
ZEB1	Zinc finger E-box binding homeobox 1

MMP1	Matrix metallopeptidase 1
MMP7	Matrix metallopeptidase 7
MMP28	Matrix metallopeptidase 28
WNK1	Lysine deficient protein kinase 1
THBS1	Thrombospondin 1
CRISPR	Clustered regularly interspaced short palindromic repeats
CAS9	CRISPR associated protein 9
γ-H2AX	Histone 2A variant X
Gy	Gray
BRCA1	Breast cancer susceptibility gene 1
CHK1	Checkpoint kinase 1
ATM	Ataxia telangiectasia mutated kinase
ATR	Ataxia telangiectasia and Rad3 related kinase
HR	Homologous recombination
NHEJ	Non-homologous end joining
ATP	Adenosine triphosphate
RANBP2	Ran binding protein 2
PC2	Polycomb protein 2
ZNF451	Zinc finger protein 451

CHAPTER I

General introduction

1.1.0 SUMOylation in eukaryotic cell biology

SUMOylation is a reversible covalent posttranslational modification with small ubiquitin like modifier (SUMO) used by cells to modify and alter the function of transcription factors, DNA repair proteins, kinases and GTPases (Jackson and Durocher, 2013; Melchior et al., 2003). SUMO proteins share about 20% sequence homology with ubiquitin proteins and go through a similar conjugation process (Rytinki et al., 2009).

SUMOylation can alter the target protein stability, binding partners and cellular localization in a relatively short amount of time, allowing cells to respond to stress signals and also changing extracellular environments. However, only a small fraction of the SUMO-recipient protein is modified at any given time, suggesting a tight regulation of the SUMOylation system (Hay, 2005; Niskanen et al., 2015).

To date, four SUMO isoforms have been identified in higher vertebrates: SUMO1-SUMO4, but mostly SUMO1-SUMO3 have been meticulously studied thus far (Eifler and Vertegaal, 2015; Eisenhardt et al., 2015; Vertegaal, 2007). While SUMO1 shares 50% sequence identity with the other SUMO proteins, SUMO2 and SUMO3 share over 97% sequence identity and are referred collectively as SUMO2/3 (Rytinki et al., 2009). SUMO can also be bound by ubiquitin in three potential Lysine residues found in the N-terminal domain of the protein sequence (K10, K23 and K42). Moreover, all SUMO proteins share a C-

terminal double Glycine (GG) domain that is made available for Lysine conjugation (KCD) following the removal of a small peptide sequence by Sentrin-specific proteases (SENP). Finally, during conjugation to protein substrate, SUMO2/3 can form poly-SUMO chains due to the presence of a SUMOylation acceptor sequence (SAS) or motif (ΨKxD/E), whereas SUMO1 does not have a SAS motif and is thought to be either a single modifier or chain terminator (Figure 1.1) (Johnson and Gupta, 2001).

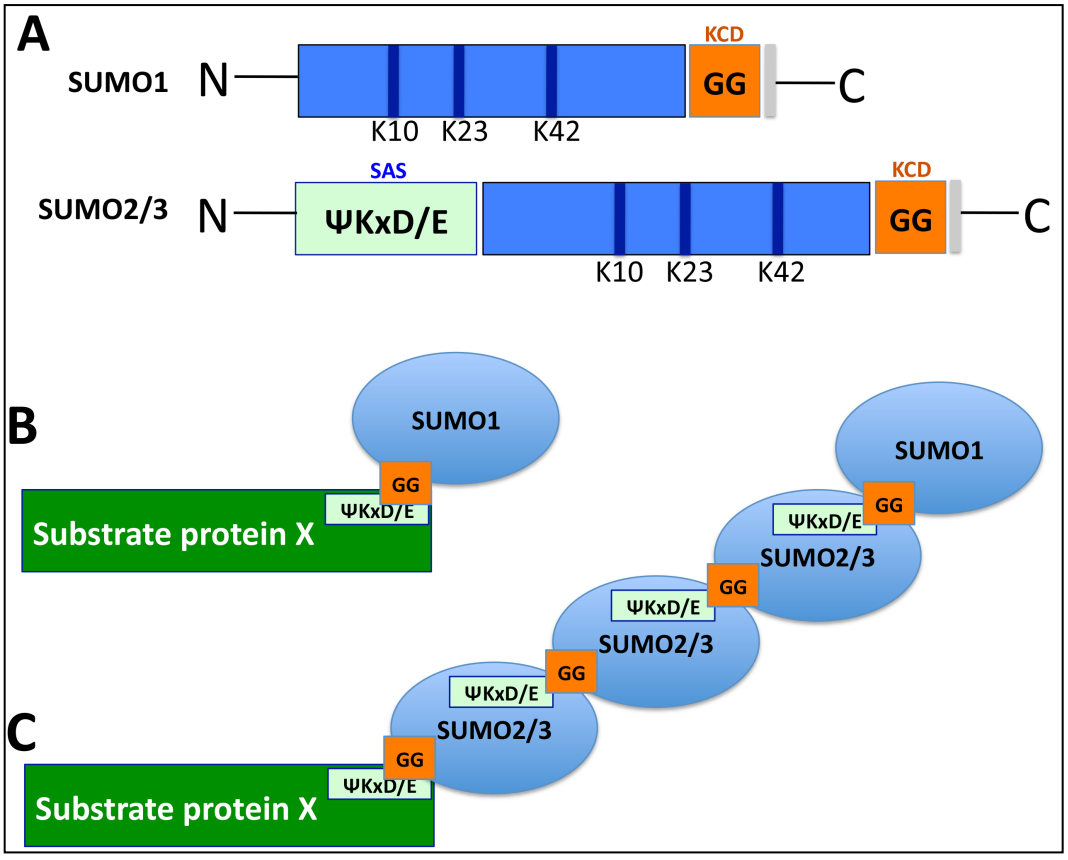

Figure 1.1 Functional domains of SUMO proteins. **A,** Diagram representation of SUMO protein domains. Lysine 10 (K10), Lysine 23 (K23) and Lysine 42 (K42) are putative ubiquitin recognition sites; C-terminal double Glycine site (GG), exposed following SENP protease C-terminal peptide cleavage (grey) are used during covalent bond formation. Note that SUMO2/3 have the SUMO acceptor site (SAS: ΨKxD/E) that allows them to become conjugated to another SUMO protein and form poly-SUMO-chains. The putative SUMO acceptor motif ΨKxD/E, in which Ψ is a large hydrophobic amino acid, K is the acceptor lysine, x is any amino acid followed by aspartic or glutamic acid, can be found on almost all SUMOylated proteins. **B-C,** Cartoon shows an example of mono and poly SUMOylation respectively.

SUMOylation is a multistep process that involves at least three regulatory enzymes. SUMOylation enzymes called E1, E2 and E3 ligases. Following the removal of the short C-terminal peptide sequence by SENPs, producing a GG end in the C-terminal domain of SUMO, E1 enzymes, also known as SUMO activating enzyme 1/2 (SAE1/UBA2) bind SUMO proteins and use the newly exposed GG (double Glycine) C-terminal domain to promote SUMO conjugation to a E2 ligase (Geiss-Friedlander and Melchior, 2007). E2 ligases can then proceed to conjugate SUMO directly onto substrate or use an E3 ligase to aid target recognition (Figure 1.2).

Many reports have described that SUMOylation can be achieved *in vitro* by the addition of E1 and E2 ligases without a need for E3 ligases. Nevertheless, addition of a E3 Ligases can dramatically increase the efficiency of SUMOylation of the target protein (Cappadocia et al., 2015; Choi et al., 2015; Gupta et al., 2014; Johnson and Gupta, 2001; Spektor et al., 2011).

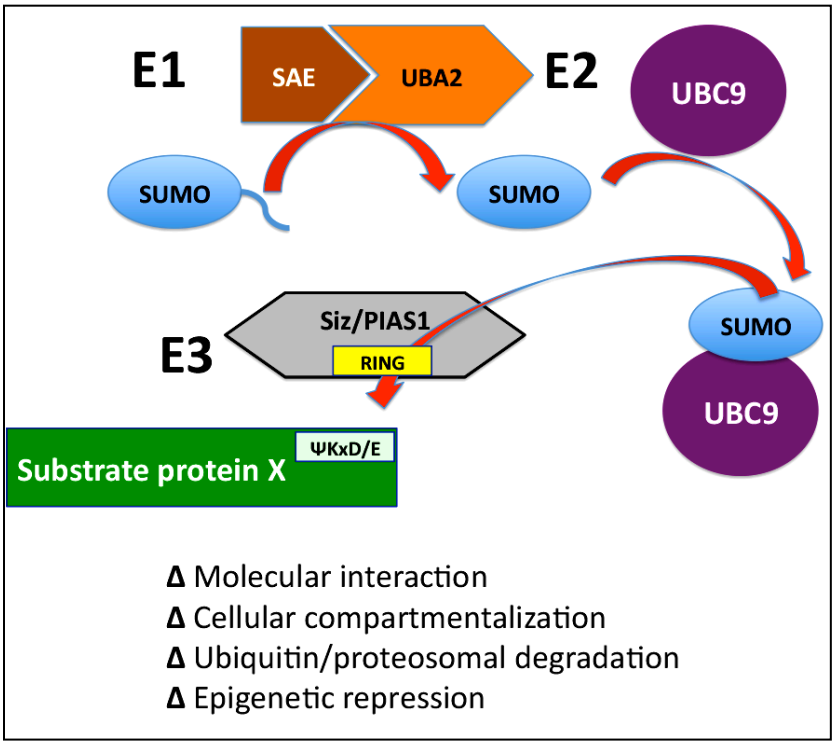

Figure 1.2 Overview of the SUMOylation pathway. Diagram shows E1, E2 and E3 enzymes involved in the various steps of the SUMO activation and conjugation pathway. The Greek letter delta (Δ) signifies the change suffered by the target protein after SUMOylation, followed by some of the potential outcomes.

Ubiquitin conjugating enzyme 9 (UBC9) is currently the only-known example of a SUMO carrier or E2 ligases (Johnson and Blobel, 1997). Disruption of the *Ubc9* gene or its SUMO ligase activity promotes G2/M cell cycle arrest in yeast and impairs proliferation in mammalian cells (Nacerddine et al., 2005; Seufert et al., 1995). For instance, *Ubc9* disruption in mammalian cells results in chromosome segregation defects, loss of stem cell potential, DNA damage and deregulation of tumor suppressor networks (Buschmann et al., 2000; Ivanschitz et

al., 2015; Nowak and Hammerschmidt, 2006; Qin et al., 2011). In this regard is important to note that various members of the SUMOylation pathway have been associated with mitotic progression. These include: SENP/1/2, SUMO2/3, UCB9 and the E3 ligase Ran Binding Protein 2 (RanBP2), which localize to centromeres and kinetochores and are reported to aid in chromosomal segregation during meiosis and mitosis (Figure 1.3).

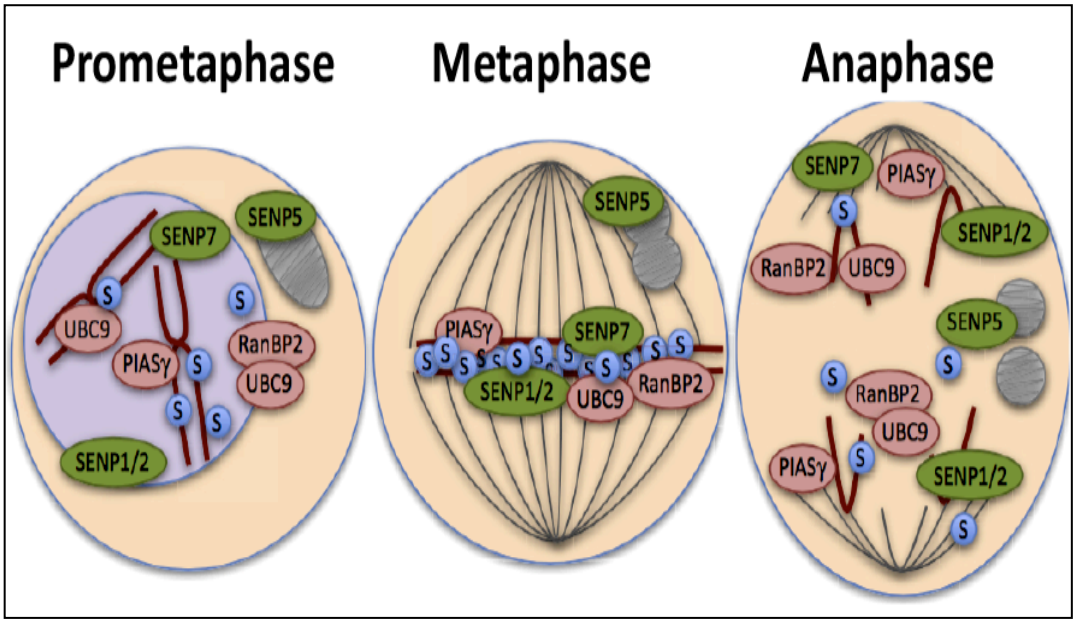

Figure 1.3 SUMOylation during mitosis. During early mitosis, the chromosomes (dark red) condense and align at the equator of the cell. Similarly, SUMOylation machinery components (SENP1/2, SUMO2/3, UBC9, RanBP2, PIASγ and SEMP5/7) accumulate at the metaphase plate and have been reported to help coordinate proper chromosome segregation. During anaphase, after sister chromatids separation, SUMOylation components disperse and can be seen scattered in the cytoplasm; (Figure adapted from Eifler et al., 2015).

Over the last two decades, studies on SUMO and E1/E2 ligases highlight several important mechanisms regulated by the SUMOylation machinery. Few examples of these include control of cell cycle progression, epigenetic gene regulation, proper chromosome segregation and DNA repair (Dieckhoff et al., 2004; Johnson and Blobel, 1997; Seufert et al., 1995). Importantly, these mechanisms are now known to be conserved from yeast to humans. However, although we know much more about SUMO and the regulatory proteins in the SUMO conjugation machinery, more work is still needed surrounding the specific cues that drive SUMOylation or how substrate specificity is achieved in a spatiotemporal manner.

1.2.0 SUMO conjugating enzymes: SUMO E3 ligases

SUMO E3 ligases are important regulatory members of the SUMOylation cascade. Part of the SUMO E3 ligase function is to provide target specificity from a large pool of potential targets inside the cell (Hochstrasser, 2001). The study of SUMO E3 ligases in eukaryotic cell biology has recently gained some traction, and much is been learned about these versatile enzymes. This subchapter will focus on providing a brief overview on the current knowledge of SUMO E3 ligases and the role they play in various cellular processes during cellular homeostasis and disease.

SUMO E3 ligases are usually grouped into families of related proteins and/or isoforms. Some of the few known E3 ligases and E3 families include: Ran-binding protein 2 (RanBP2), Polycomb protein family member 2 (PC2), zinc finger 451 (ZNF451) and protein inhibitor of activated STAT (Siz/PIAS) family members (Johnson and Gupta, 2001; Kagey et al., 2003; Karvonen et al., 2008; Mahajan et al., 1997).

RanBP2: The RanBP2 protein is over 350 KDa in size and normally localizes to the nuclear periphery in association with the nuclear pore complex (NPC) proteins, but can also be seen associated with metaphase bodies during chromosome segregation and cytokinesis (Figure 1.3) (Bolhy et al., 2011). RanBP2 SUMOylates RanGAP proteins, promoting nuclear import by the NPC at the expense of Adenosine triphosphate (ATP) consumption (Gorlich and Mattaj, 1996; Mahajan et al., 1997; Pichler et al., 2002; Sakin et al., 2015; Stade et al., 2002). Moreover, RanBP2 facilitates mRNA nuclear export by binding to nuclear RNA export factor 1 (NXF1) and inducing its nuclear exclusion (Forler et al., 2004). Thus, RanBP2 E3 ligase functions and site of residence makes it a gatekeeper of cyto-nuclear transport and essential for cell survival (Figure 1.4).

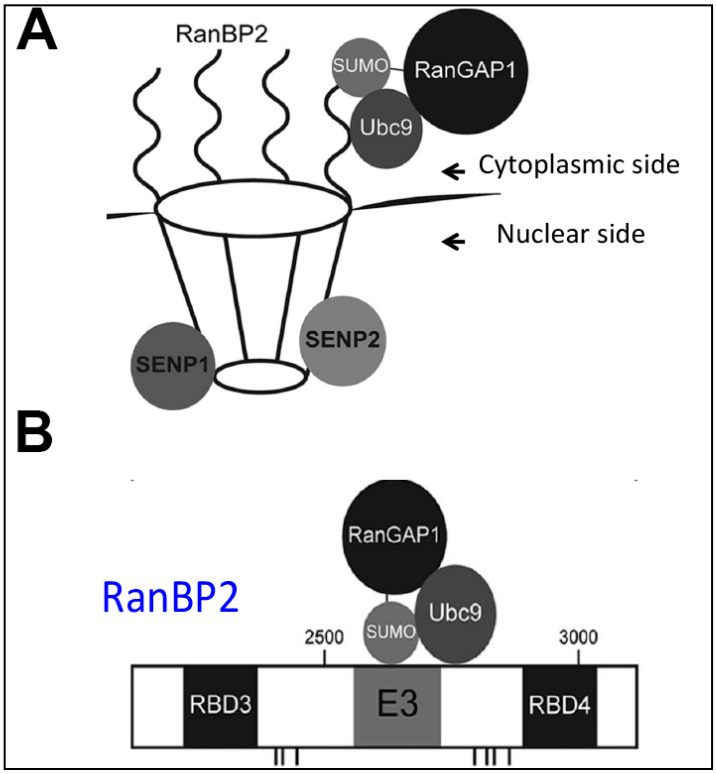

Figure 1.4 Regulation of nuclear transport by RanBP2. A, Cartoon of RanBP2 positioned at the cytoplasmic side of the nuclear pore complex (NPC) and SENP proteases on the nuclear side. **B**, Schematic representation of RanBP2 Ran-binding domains (RBD3 and RBD4) in association with components of the SUMOylation pathway. In this diagram, RanBP2 has two Ran-binding domains (RBD3 and RBD4) and E3 ligase motif that, in conjunction with the E2 ligase Ubc9, are used to transfer SUMO onto RanGAP1; (Figure modified from Sakin et al, J. Biol. Chem. 2015).

Given its essential functions in cells, mutations in the *RANBP2* gene in humans are rare, yet they do exist. Acute necrotizing encephalopathy (ANE) is a (familial) pediatric disease associated with, and potentially lethal, viral illness caused by a missense mutation in the *RANBP2* gene (Neilson et al., 2009; Singh et al., 2015). The missense mutation in *RANBP2* found in ANE patients results in

a substitution of Cytosine to Thymine at position 18180 that changes the coding sequence for Threonine into Methionine (*RANBP2*$^{18180C\text{-}T(Thr\text{-}Met)}$). Despite a high correlation with viral infections and central nervous system (CNS) inflammation, it is still unclear as to how *RANBP2*$^{18180C\text{-}T\ (Thr\text{-}Met)}$ affects the E3 ligase protein function or the extent to which it contributes to ANE (Lopez-Laso et al., 2009; Neilson, 2010). Importantly, how the mutation affects RANBP2 ability to bind nuclear inbound-outbound cargo in ANE has yet to be defined. However, recent studies have successfully attempted to characterize transgenic null mice with *Ranbp2* deletions (*Ranbp2*$^{-/-}$) or knock-in inactivation of the RanGTPase binding domains 2/3 (*Ranbp2*$^{TgRBD2/3}$) in retinal epithelium (Patil et al., 2014). In these animal studies, it was discovered that retinal pigment epithelium degeneration (RPED) in *Ranbp2*$^{-/-}$ mice can be recapitulated using the *Ranbp2*$^{TgRBD2/3}$ mutant, which directly affects RanGTPase binding. Together, these results suggest that mutations in *RANBP2* that affect binding to RanGTP proteins may result in the phenotypic consequences of ANE or RPED in humans.

PC proteins: Another group of very interesting E3 ligases, the Polycomb (PC) family of E3 ligases, has been heavily studied in the field of epigenetic gene regulation and tumorigenesis (Chen et al., 2015; Davidovich et al., 2015; Paro and Hogness, 1991; Poux et al., 2001). PC family proteins are associated with stable epigenetic repression of target histones and regulation of non-coding RNAs (ncRNA) accessibility (Gil et al., 2005; Yang et al., 2011a). PC proteins form

Polycomb bodies or granules (PcG) that associate tightly with heterochromatin and whose level of association is dependent on growth signals and transcription factor co-regulators (Yang et al., 2011a). PcGs exist in hetero-multimeric complexes named Polycomb repression complex 1 (PRC1), Polycomb repression complex 2 (PRC2) and their antagonizing complex Trithorax (TRX) (Garcia-Dominguez and Reyes, 2009; Khan et al., 2015) act together to carry out Histone3-Lysine27 (H3K27) tri-methylation/demethylation, exerting their gene repressive/activating functions.

PC2 genes are essential for stable cell differentiation and loss of PRC1 or PRC2 function is associated with the development of brain, prostate, malignant peripheral nerve sheet tumors (MPNST), and also breast cancers (Choi et al., 2015; Lewis et al., 2013; Prieto-Granada et al., 2015; Wassef et al., 2015). Moreover, PC2 can promote E2F SUMOylation and initiation of gene transcription and PC2 inhibition has been linked to the repression of prostate cancer proliferation (Yang et al., 2011a).

In addition to their impact on gene regulation, PC2-like family members PCL1-PCL3 regulate cell proliferation by either negative regulation of INK4A (PCL2/3) or binding and stabilization of the p53 tumor suppressor (PCL1) (Brien et al., 2015).

ZNF451: ZNF451 is a recent addition to the group of SUMO E3s ligases. ZNF451 was initially discovered associated with the promyelocytic leukemia

tumor suppressor (PML), in PML nuclear bodies, and ZNF451 SUMOylation promotes its nuclear recruitment and retention (Karvonen et al., 2008). The initial findings suggest that ZNF451 functions as a transcriptional co-regulator, but does not seem to activate transcription directly. Moreover, later studies propose ZNF451 as a transcriptional repressor, and showed that ZNF451 expression promotes the decrease in transforming growth factor beta (TGF-β) gene expression (Feng et al., 2014). Recently, two studies have inducted ZNF451 as a novel member of the SUMO E3 ligases family and as a SUMO chain elongator (Cappadocia et al., 2015; Eisenhardt et al., 2015).

ZNF451 ability to form SUMO-chains is attributed to two N-terminal SUMO interacting motifs (SIM) located in tandem and bridged by a Pro-Leu-Arg-Pro (PLRP) motif that is thought to incur in SUMO conjugation while facilitating the secondary addition of SUMO from a donor E2 Ligase (Figure 1.5). These two independent examples are the first to show a defined molecular mechanism of SUMO-chain elongation, giving insight into a novel SUMO E3 ligase function. With this new information and available crystal structure for ZNF451, it is plausible that other E3 ligases with chain elongation ability will soon be discovered or better defined.

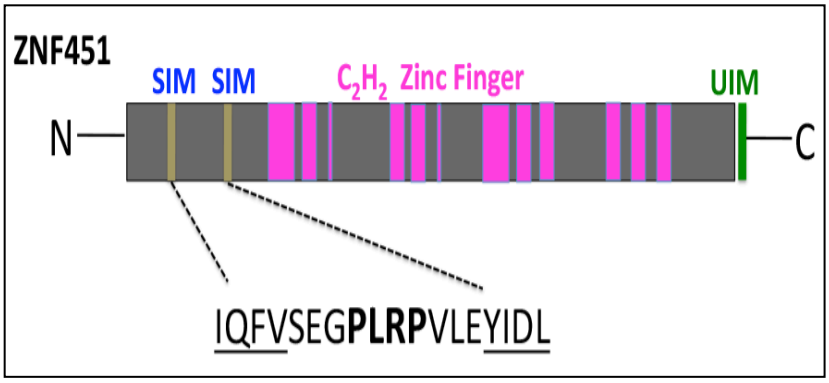

Figure 1.5 ZNF451 a model SUMO E3 for poly-SUMO conjugation activity. Cartoon shows the domain organization of ZNF451. Gold colored boxes represent predicted SUMO interacting motifs (SIM). ZNF451 contains two SIM motif, 12 C_2H_2-type zinc fingers (Pink) and one ubiquitin interacting motif (UIM) on the C-terminal domain (Green). The sequence of the fragment containing the Pro-Leu-Arg-Pro (PLRP) SIM flanked motif is displayed below the diagram. Residues belonging to the two SIMs are underlined and the Pro-Leu-Arg-Pro (PLRP) bridge motif is in bold; (Figure adapted from Cappadocia et al., 2015).

1.3.0 Siz/PIAS family of SUMO E3 ligases

The Siz/PIAS family of E3 ligases are among the oldest founding members of SUMO E3 ligases and share a conserved really interesting new gene (RING) motif (Moilanen et al., 1999). Siz proteins were initially identified in yeast as the putative Smt3/SUMO E3 ligases for the GTP binding proteins collectively called Septins (Cdc3, Cdc10 and Cdc11), which are important for the formation of a filamentous ring between mother-daughter yeast cells during mitosis (Chung et al., 1997; Takahashi et al., 2001). Septins SUMOylation, specifically at the mother side of the budding-neck, promotes neck resolution and

separation from daughter cell. Conversely, deletion of Siz1/Siz2 in yeast is characterized by a G_2/M cell cycle arrest and unresolved bud-neck.

The PIAS proteins are the mammalian orthologs of Siz1/2 in yeast. There are four widely recognized PIAS family members arising from separate gene loci (PIAS1, PIAS2/xα, PIAS3 and PIAS4/y). As their names indicate, PIAS are the proteins inhibitors of signal transducer and activator of transcription (STAT) family of transcription factors. PIAS proteins inhibit STATs binding to DNA in a stimulus dependent manner and with well-defined substrate specificity (Arora et al., 2003; Liu et al., 1998). However, STAT inhibition may not be entirely SUMOylation dependent and groups have reported STAT inhibition by PIAS without SUMO modification (Rogers et al., 2003). In agreement with this, various functions of E3 ligases are independent of their ability to facilitate SUMOylation of a target protein. For example, E3 ligases can interact non-covalently with SUMOylated proteins using their SUMO interacting motifs (SIM); or bind DNA using a scaffold attachment factor-A/B, acinus and PIAS (SAP) to alter gene transcription (Palvimo, 2007; Rytinki et al., 2009). For instance, the N-terminal SAP domain of PIAS1, which contains a four helix-loop-helix like structure, preferentially binds AT-rich DNA sequences (Okubo et al., 2004). Moreover, recent studies demonstrated that endogenous PIAS4 preferentially binds DNA sequences associated with the nuclear matrix together with other co-regulators of gene transcription (Sachdev et al., 2001). Finally, PIAS proteins themselves can

be SUMOylated and form multi-protein complexes with the aid of the RING motif, altering their cellular compartmentalization (Weissman, 2001).

Human PIAS proteins share many of the functional domains found on E3 ligases in flies and yeast. They have a nuclear localization signal (NLS), an scaffold attachment factor-A/B, acinus and PIAS (SAP) motif, a Proline-Isoleucine-Asparagine-Isoleucine-Threonine (PINIT) motif, Siz/PIAS-really interesting new gene (SP-RING) motif, and SUMO interacting (SIM) motif (Cheong et al., 2009; Minty et al., 2000). However, PIAS proteins differ in the length and sequence of a C-terminal regulatory region containing Serine and Threonine residues substrates subject to mitogenic/regulatory kinase phosphorylation (Heo et al., 2013; Liu et al., 2007; Stehmeier and Muller, 2009) (Figure 1.6).

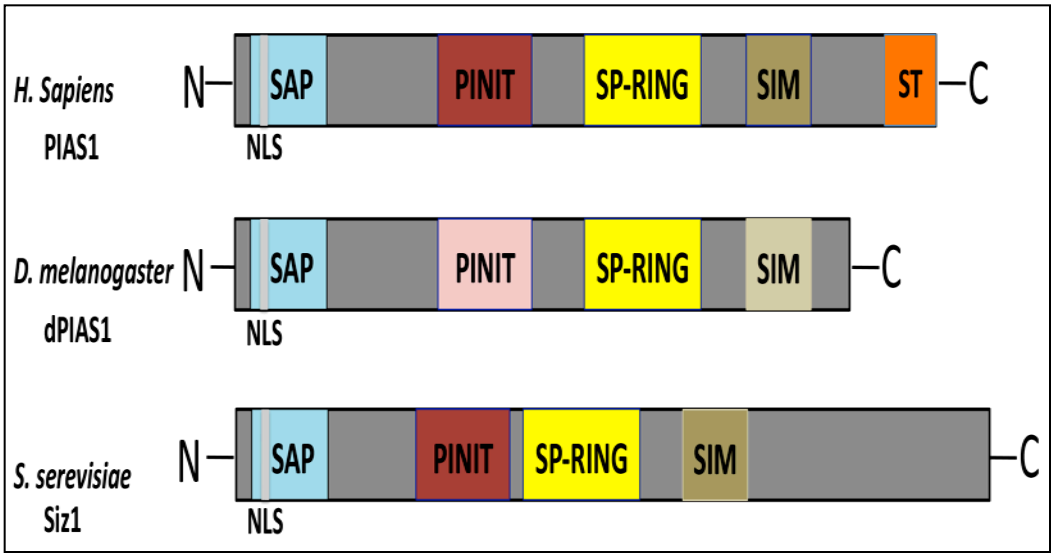

Figure 1.6 Conserved functional domains of Siz/PIAS family of E3 ligases. PIAS protein motif are highly conserved from yeast to humans. Except for a complete lack of a Serine/Threonine C-terminal regulatory motif in the drosophila PIAS (dPIAS) and Siz1 (the yeast ortholog) the functional domains of these E3 ligases are almost identical. All E3 ligases contain a nuclear localization signal (NLS), an scaffold attachment factor-A/B, acinus and PIAS (SAP) motif, a Proline-Isoleucine-Asparagine-Isoleucine-Threonine (PINIT) motif, Siz/PIAS-really interesting new gene (SP-RIN) motif, and SUMO interacting (SIM) motif; (Adapted from Rytinki et al, 2009).

1.4.0 SUMOylation in the regulation of development

It is now clear that SUMOylation plays a role in many fundamental processes within cells. Thus, genetic deletion, silencing with small interfering RNA (siRNA) or chemical inhibition of members of the SUMO pathway results in phenotypes ranging from cell cycle arrest, reduced cell viability and embryonic lethality. The purpose of the next section is to provide a brief overview of how affecting SUMOylation at the various steps of the pathway can negatively affect mammalian development.

SUMO specific protease 1 (SENP1), for instance, is essential for activation of SUMO proteins following translation and for SUMO removal from target substrate (Bailey and O'Hare, 2004). Deletion of SENP1 in mice leads to anemia and embryonic lethality correlating with hyper-SUMOylation of GATA-1 and impairment of downstream transcriptional activation (Yu et al., 2010). Moreover, deletion of SENP2 is associated with cardiac development defects, which correlate with repression of GATA4/GATA6 chromatin regions by the Polycomb repression complex 1 (PCRC1) (Kang et al., 2010).

Interestingly, deletion of SUMO1 or SUMO3 genes does not to affect mouse development, while deleting SUMO2 results in severe growth retardation and embryonic lethality by embryonic day 10.5 (E10.5) (Wang et al., 2014; Zhang et al., 2008). These findings suggest that because SUMO2 and SUMO3 are almost identical SUMO2 protein levels, but not SUMO3s, may be limiting during development and thus with a larger contribution to global SUMOylation and survival.

UBC9 is the only known E2 member of the SUMOylation pathway with few or no redundancies for its SUMO-donor function. *Ubc9* deletion results in embryonic lethality soon after implantation or its conditional inhibition in zebrafish cells causes cell death (Nacerddine et al., 2005; Nowak and Hammerschmidt, 2006). RanBP2 is another essential member of the SUMO machinery and because of its unique function at the NPC and metabolism its

deletion is lethal in mice (Aslanukov et al., 2006). Conditional inactivation of RanBP1/2, however, has provided molecular insights into its requirement for nuclear import and how binding to Ran proteins is required for function (Dawlaty et al., 2008; Hamada et al., 2011; Nagai et al., 2011; Singh et al., 2015).

PIAS family members differ in their requirement for embryogenesis. While *Pias1* loss is embryonic lethal with 10% incomplete penetrance, *Pias2*/xα and *Pias4/y* are not associated with lethality, but the combined deletion of *Pias1* and *Pias4/y* significantly impairs embryonic survival (Liu et al., 2004; Santti et al., 2005; Tahk et al., 2007). Together, these findings suggest that PIAS1 compensates for the functions of other PIAS family members. This also suggests that PIAS1 target substrates are essential regulatory genes and that their dysfunction is incompatible with life.

1.4.1 *Pias1* embryonic Lethality

PIAS1 is an E3 ligase with a well-known involvement in STAT1 transcriptional inhibition and suppressive effects on the immune system. The surviving 10% of *Pias1* null mice are significantly smaller than their littermates, are prone to pre/post-natal death and have defects in hematologic differentiation patterns and reduced stem cell potential (Liu et al., 2004; Liu et al., 2010; Liu et al., 2014b). Although these reports on *Pias1* null mice offer some insight into the function of PIAS1, they are incomplete and do not fully characterize its biological

properties. Thus, close to 90% of *Pias1* null mice die during development of unknown causes.

Investigating and characterizing the cause of *Pias1* embryonic lethality provides a great opportunity to learn more about the processes regulated by SUMOylation at the organismal level. Moreover, these investigations could shed insights into novel mechanisms wherein PIAS1 protein is an essential regulator.

The first part of this thesis work will focus on identifying the cause of *Pias1* embryonic lethality via the generation of novel mouse strains and characterizing the molecular events leading to lethality. This work fills a gap in our knowledge on the biological properties of the PIAS1 SUMO E3 ligase and SUMOylation in eukaryotes.

1.5.0 PIAS1 in human cancers

It was not long after the discovery of SUMOylation association with chromosome integrity, cell differentiation and cellular growth that scientist started to probe for potential ways to characterize or target SUMO machinery component during disease. Many years after their discovery, SUMOylation has been found to be deregulated in several human neoplasms including brain, lung, colon and prostate cancers (Eifler and Vertegaal, 2015).

One of the first identified SUMO modified proteins was the acute promyelocytic leukemia (APL) tumor suppressor PML and its fusion with the

retinoic acid receptor alpha (PML-RARα). PML interacting clone 1 (PIC-1; SUMO) protein localizes with PML nuclear bodies in NIH-3T3 cells, but not with PML-RARα in APL cell line NB4, suggesting a biological marker of APL (Boddy et al., 1996). Later studies discovered that all-trans retinoic acid (ATRA) and arsenic trioxide (As2O3) treatment results in PML and its fusion protein PML-RARα SUMOylation, inducing their degradation and complete APL remission (Guo et al., 2001; Muller et al., 1998a; Muller et al., 1998b; Wang et al., 2004a).

1.5.1 PIAS1 in lung cancer progression

Recently, it was discovered that SUMOylation of PML or the PML-RARα oncoprotein promotes its proteosomal degradation in a PIAS1 and casein kinase 2 (CK2) dependent manner (Rabellino et al., 2012). This study also shows that PIAS1 gene is amplified in a subset of lung tumors wherein it degrades the PML tumor suppressor.

Thus, the second and third part of this thesis work is to determine the role of PIAS1 in lung tumorigenesis and identifying PIAS1 targets required for tumor progression respectively

1.6.0 Hypothesis and specific aims

Given our current knowledge about SUMOylation and SUMO E3 ligases, we hypothesize that PIAS1 function is required for developmental processes essential for embryonic survival and cell differentiation. Moreover we hypothesize that PIAS1 gene amplification in human NSCLC tumors promotes tumor progression and that PIAS1 downstream targets can be used as biological markers of tumor progression or as potential therapeutic targets.

Aims:

1.6.1 Identify the underlying cause for embryonic lethality in PIAS1 deficient mouse embryos

1.6.2 Address the effect of PIAS1 inhibition in human tumors cells and investigate the molecular mechanisms behind potential phenotypes

1.6.3 Characterize PIAS1 downstream targets in human lung cancer cells for potential therapeutic intervention

CHAPTER II

Pias1 is essential for erythroid and vascular development in the mouse embryo

2.1.0 Introduction

The cardiovascular system is critical during embryonic development. The vasculature supplies the developing embryo with oxygen, nutrients and removes metabolic waste. Consequently, inactivation of genes that impair vascular or erythroid development result in mouse embryonic lethality (Conway et al., 2003; Maeda et al., 2009; Pang et al., 2012; Shalaby et al., 1995). The first nucleated RBCs, also called primitive erythrocytes, are visible within the yolk sac (YS) blood islands approximately at embryonic (E) days 7.5-8.5 days post conception. These nucleated red blood cells begin circulating the embryo proper at E8.5 after the YS and dorsal aorta (DA) blood vessels have fused (Conway et al., 2003). Vasculogenesis, the generation of blood vessels, starts following new blood cells formation, between E7.5 and E8.5 (Coffin et al., 1991; Coffin and Poole, 1991). The vascular and erythroid cell compartments cooperate to promote embryonic growth via nutrient delivery and gaseous exchange.

Endothelial cells are essential for the onset of erythropoiesis in the mouse embryo. For instance, they give rise to the primitive erythroid cell lineage in the YS and blood vessels from a common progenitor called the hemangioblast (Auerbach et al., 1996; Lacaud et al., 2001). These cells then colonize the fetal liver and therein maintain hematopoiesis until birth. In addition, a direct interaction between hematopoietic stem and progenitor cells (HSPCs) and the vascular endothelium has been reported during asymmetric cell divisions in zebrafish

(Jacobsen et al., 2014; Tamplin et al., 2015). To achieve this complex multicellular task, key transcription factors, cytokines, growth factors and their plasma membrane receptors are required to orchestrate proper erythroid and vascular development. For instance, transcription factors GATA-1, GATA-4 and MYC are required for proper cardiovascular and RBC development in mice.

Disruption of either *Gata1* or *Myc* alters the gene expression profiles of hematopoietic stem cells, resulting in anemia, endothelial cell apoptosis and embryonic lethality (Baudino et al., 2002; Pang et al., 2012; Yu et al., 2010), while disruption of *Gata-4* results in cardiovascular failure and abnormal heart development (Ip et al., 1994; Kelley et al., 1993). Plasma membrane receptors controlled by *Gata1* or *Myc*, such as vascular endothelial growth factor receptors 1/2 (VEGFR1/2) and their ligand VEGF enhance pro-survival signaling and define the formation and directionality of new blood vessels and the lymphatic systems (Dellinger et al., 2013; Shalaby et al., 1995; Stefater et al., 2011). Moreover, vascular cell adhesion molecule-1 (*Vcam-1*) gene expression in endothelial cells regulates the interaction between the vascular endothelium and RBCs, promoting RBCs survival and differentiation (Jacobsen et al., 2014; Sturgeon et al., 2012).

On the other hand, three key regulatory proteins Semaphorin-3A/E (SEMA3A; SEMA3E), Thrombspondin-1 (THBS1) and bone morphogenesis protein 2 (BMP2), provide the restrictive signals that block blood and lymphatic vessel formation in the mouse. SEMA3A/E protein, for instance, promotes

retraction of cell projections and inhibits endothelial cell adhesion to extracellular matrix, while THBS1 and BMP2 proteins are anti-angiogenic by inhibiting migration and proliferation of endothelial cells (Dunworth et al., 2014; Feng et al., 2015; McKenna et al., 2014; Meadows et al., 2013).

An emerging layer of complexity in these developmental processes is the contribution of posttranslational modifications on transcription factors and heterochromatin remodeling. Modifications with small ubiquitin-like modifiers (SUMO) have recently gained attention because of their participation in activation/repression of gene transcription (Costa et al., 2011; Liu et al., 2014a; Yu et al., 2010). SUMOylation of target proteins alters their function by promoting changes in protein-protein interaction and/or heterochromatin accessibility.

SUMOylation is a hierarchical process in which SUMO proteins are added onto substrates by the stepwise transfer of SUMO from activating enzyme E1, cargo enzyme E2 and finally onto conjugating enzyme E3 ligase (Palvimo, 2007; Rytinki et al., 2009). For instance the E2 ligase UBC9 is essential for proper chromosome segregation and genomic stability in mice and for hematopoietic stem cell self-renewal in Drosophila melanogaster (Kalamarz et al., 2012; Nacerddine et al., 2005). Moreover, PIAS-like protein ZIMP10 was shown to contribute to vascular and hematopoietic development in mice (Beliakoff et al., 2008).

PIAS1 loss was reported to result in embryonic and perinatal lethality in mice, but a detailed examination of these events has not been performed (Beliakoff

et al., 2008). The goal of our study was to provide a better understanding of the role of PIAS1 in the regulation biological processes in multicellular organisms during embryonic development. To do this, we generated two novel mouse mutant strains that constitutively or conditionally inactivate the *Pias1* gene. We analyzed embryos at different stages of development and characterized the individual tissues affected for defects in cell proliferation and differentiation.

2.2.0 Materials and Methods

Mouse ES Cells and Mouse genotyping. Embryonic stem (ES) cells for *Pias1* gene constitutive inactivation were generated by the UC DAVIS mutant mouse resource and research centers (MMRRC; www.mmrrc.org). Genotyping primers used for RT-PCR: FW, ATGGCGGACAGTGCGGAACTAA; RV1, CTGTTGTGGTGTCAAGGCAAAT; RV2, GACAGTATCGGCCTCAGG AAG. ES cells for *Pias1* gene conditional inactivation was generated by the NIH Knock-Out Mouse Project (KOMP) and obtained from the KOMP Repository (www.komp.org). Genotyping primers for PCR: FW1.GAGATGG CGCAACGCAATTAATG; R1.ATGCCCTCAGAAGCAATGAAAGAGC; FW2.CAGCAGATCAGCAGCTCCAT; RV2.CAGATGCAGCTTCC GGACTA. All experimental procedures involving animals in this study were reviewed and approved by the University of Texas Southwestern Medical Center's Institutional Animal Care and Use Committee.

LacZ reporter assay and X-gal staining. For whole-mount X-gal staining, embryos were fixed in cold 4% PFA/1xPBS buffer (0.1% deoxycholic acid; 0.2% Igepal-NP40) for 45 min at 4°C with gentle shaking. Embryos were rinsed twice with cold 1xPBS, stained overnight using staining buffer (5 mM $K_3Fe(CN)_6$; 5 mM $K_4Fe(CN)_6$; 2 mM $MgCl_2$; 1 mg/ml X-gal in 1xPBS) followed by two 1xPBS washes and post-fixing with 4% PFA/PBS and glutaraldehyde (Millay et al., 2013).

Cryosection and immunofluorescence. Frozen sections of E7.5-E8.0 embryos were used. Tissues sections were permeabilized with 0.3% Triton X-100 in 1xPBS, blocked with 20% Aquablock with 0.02% sodium azide for 1 hour, incubated with Ki67 1:500 (Cell signaling), PML 1: 500 (Santa Cruz, No.: sc-5621), C. CASPASE 3 1:500 (Cell signaling, No.: 9665) Overnight. Primary antibodies were washed of tissue-slides twice with 1xPBS; slides were incubated in Alexa-Fluor secondary antibodies and 1:800 4', 6-diamidino-2-phenylindole (DAPI) for 30 mines, rinsed and coverslipped. 40x magnification pictures were taken with a Leica DMI6000 inverted microscope. Picture analysis was performed with ImageJ software for quantification of pixel intensity averages.

Whole mount immunohistochemistry. Endogenous peroxidase was neutralized by incubating the embryos in 5% hydrogen peroxide for 5 hours RT.

Background signal was reduced by incubating embryos in 20% aquablock (East Coast Biologics, cat no.: PP82-P0691), 0.1% TritonX-100 overnight. Finally, embryos were incubated with primary antibody against *Pecam* (CD31) in 5% aquablock 0.1% TritonX-100 overnight, washed 4 times in 0.1% Triton/1xPBS at 4°C with gentle agitation, incubated with HRP-conjugated secondary antibody, washed 3 times in 5% aquablock/0.1% Triton/1xPBS for 30 minutes at RT, rinsed with 1xPBS for 20 min and stained using the DAB kit (Vector labs, No.: SK 4100).

Quantitative PCR (qPCR). Total RNA was extracted from fresh/frozen tissues using the total RNA extraction kit from SIGMA (SIMA-Aldrich, No.: RTN350) following manufacturer's protocols. cDNA synthesis was done using Superscript III reverse transcriptase with random hexamer primers (Invitrogen, No: 18080-400). For qPCR analysis, we used Power SYBR Green (Applied Biosystems, No.: 4368577) detection-dye and followed manufacturer's protocol. To analyze the samples we used the *Applied Biosystems 7500 Fast Real-Time PCR System* (Applied Biosystems, No.: ABI-7500). Data values were plotted in histograms using GraphPad Prism 6.0 software.

Methocult cell differentiation assays. YS were isolated at 9.5. Approximately $1x10^3$ cells diluted in 100 μL serum free media were mixed with 2

mL Methocult media (Stem cell tech. no.: 03436) supplemented with either recombinant mouse erythropoietin (rEPO) (R&D systems no.: 959-ME) or recombinant mouse granulocyte-macrophage colony stimulation factor (rGMCSF) (Millipore No.: GF206). Cells were allowed to form colonies for 5 days and then imaged in phase contrast using DMI6000 inverted microscope (Leica).

Isolation and culture of primary myoblast. Five *Pias1*$^{+/+}$ E15.5 hearts were dissociated by mincing using a sterile surgical blade and 250μL 0.25% Trypsin for 5-10mins. Trypsin was neutralized with in 9.5mL 20% FBS/ DMEM. Cells were transferred to 15mL falcon tube followed by centrifugation at 1,000g for 5 min at 37C. The pellet was re-suspended in 10 ml of growth media (20% FBS/Ham F10 with 2.5ng rFGF and plated on a 60 mm Laminin treated cell culture dish.

Cardiogenic differentiation. To induce cardiac differentiation following *Pias1* expression, primary myoblasts and MEFs cell cultures were placed in differentiation media (2% horse serum, DMEM) for 3 days (Millay et al., 2013) followed by qPCR analysis.

Western blotting. Cells lysate was prepared with radioimmuno-precipitation assay buffer (RIPA buffer) with protease and phosphatase inhibitors.

40ug of proteins was resolved on 8% SDS-PAGE gel, transferred to nitrocellulose membrane and probed for the indicated antibodies.

In vitro tube formation assays. HUVECs cells were transfected with dsRED-*Pias1* or dsRED-Empty vector using Lipofectamine 3000 reagent (Life Technologies). Positive transfectants were FACS sorted to 98% purity. For tube formation assay cells were cultured on top of growth factor reduced Matrigel (Dbouk et al., 2014). To monitor the rate of tube formation, pictures were taken at 0, 4 and 6 hours after plating using an Andor spinning disc confocal microscope (Nikon).

Flow cytometry. Embryos from E9.5 to E12.5 were washed in cold 1xPBS, YS were processed to obtain single-cell suspensions using 1 mg/mL collagenase D (Roche)/ 3% FBS in PBS, gently rocking at 37C for 30 min. Finally single cells were washed 1X in PBS, resuspend in 3% FBS in DMEM, treated with fluorescently labeled CD71, Ter119, Mac1 and Gra1 antibodies and analyzed by fluorescence associated cell sorting (FACS).

RNAi interference. Stable *PIAS1* knockdown was performed with pGIPZ vectors containing shRNA against *PIAS1* (5'-CCGGATCATTCTAGAGCTTTA-3' No.: TRCN0000231898); and non-targeting scramble shRNA controls (Open

biosystems, No.: RHS4346). Lentiviral particles were generated by transfection of HEK-293T cells with pGIPZ and helper plasmids (Addgene, No.: 84545; 8455). 4μg/mL Polybrene (SIGMA, No.: H9268) was used with viral supernatant to enhance transduction efficiency.

Plasmid constructs

Flagged-*Pias1*; Addgene, No.: 15206

dsRED-Empty; available upon request

dsRED-*Pias1;* available upon request

qPCR primers

1. m*Angpt-2* FW. GGACAGTCATCCAACACCGAG
2. m*Angpt-2* RV. GACTCTTCACCAGCGAGGTAG
3. m*Pml* FW: AGTGTGAACAGCTCATTTGCAG
4. m*Pml* RV: GGAGCAGAAGATATTGGACTTG
5. m*Bmp-2* FW: GGGACCCGCTGTCTTCTAGT
6. m*Bmp-2* RV: TCAACTCAAATTCGCTGAGGAC
7. m*Vcam-1* FW: GTTCCAGCGAGGGTCTACC
8. m*Vcam-1* RV: AACTCTTGGCAAACATTAGGTGT
9. m*Pecam* FW: CTGCCAGTCCGAAAATGGAAC
10. m*Pecam* RV: CTTCATCCACCGGGGCTATC

11. m*Vegfr-2* FW: GCACATAGAGAGAATGAGCTTCC

12. m*Vegfr-2* RV: CTCCGCTCTGAACAAGGCT

13. m*MyoD* FW: CCACTCCGGGACATAGACTTG

14. m*MyoD* RV: AAAAGCGCAGGTCTGGTGAG

15. m*Myogenin* RV: ATGGAGCTGTATGAGACATCCC

16. m*Myogenin* FW: TTACACACCTTACATGCCCAC

17. m*Myomaker* FW. TTCCTCCCGACAGTGAGCAT

18. m*Myomaker* RV: GCACAGCACAGACAAACCAG

19. m*Myocd* FW: GATGGGCTCTCTCCAGATCAG

20. m*Myocd* RV: GGCTGCATCATTCTTGTCACTT

21. m*Gata1* FW: TGGGGACCTCAGAACCCTT

22. m*Gata1* RV: GGCTGCATTTGGGGAAGTG

23. m*Gata4* FW: CACCCCAATCTGGATATGTT

24. m*Gata4* RV: GTGGTGGTAGTCTGGCAGT

Endothelial primers list:

(Dbouk et al., 2014)

Complete Antibodies list:

1. Ki67; Cell signaling, No.: 9129 (at 1:500)

2. PML; Santa Cruz, No.: sc-5621 (at 1:500)

3. Cleaved CASPASE 3; Cell signaling, No.: 9665 (at 1:500)

4. 4'-, 6-diamidino-2-phenylindole (DAPI); Life technologies, No.: D1306 (1:800).

5. GADPDH; Santa Cruz, No.: sc-32233 (1:2000)

6. BIM; Cell signaling, No.: 2933 (1:1000)

7. ACTIN; SIGMA, No.: A2066 (1:2000)

8. PIAS1; Cell signaling No.: 3350 (1:1000)

9. PIAS1; Abcam No.: Ab32219 (1:100)

10. GATA-1; Santa Cruz, No.: N6 (1:100)

11. GATA-4; Santa Cruz, No.: C20 (1:100)

12. SMA-1; Abcam No.: Ab5694 (1:300)

13. PECAM; Abcam No.: Ab28364 (1:200)

2.3.0 Results

2.3.1 Ablation of *Pias1* impairs YS erythropoiesis in the mouse embryo

We generated two strains of *Pias1* deficient mice using targeted ES cells. *Pias1* was inactivated either by a gene trap insertion after exon 1, introducing a polyadenylation site and a premature stop codon (*Pias1*$^{-/-}$ *mice*), or by Cre recombinase mediated excision of LoxP flanked exons 2 and 3 (*Pias1*$^{f/f}$ *mice*). *Pias1* gene was disrupted in both mouse lines as determined by real-time PCR (RT-PCR) and immunoblotting (Figure 2.1A-C and Figure 2.2A-C).

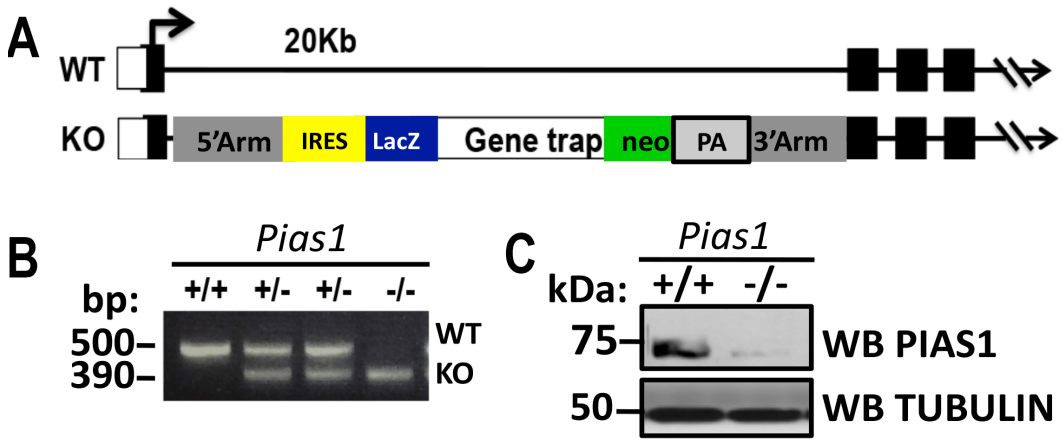

Figure 2.1 Genetrap targeting of *Pias1* loci blocks gene expression. A, Genomic organization of wild type (WT; *Pias1*$^{+/+}$) and *Pias1* null (KO; *Pias1*$^{-/-}$) alleles generated by gene trap insertion. **B-C,** RT-PCR confirmation of *Pias1* gene disruption and immunoblotting confirmation of PIAS1 protein loss**.**

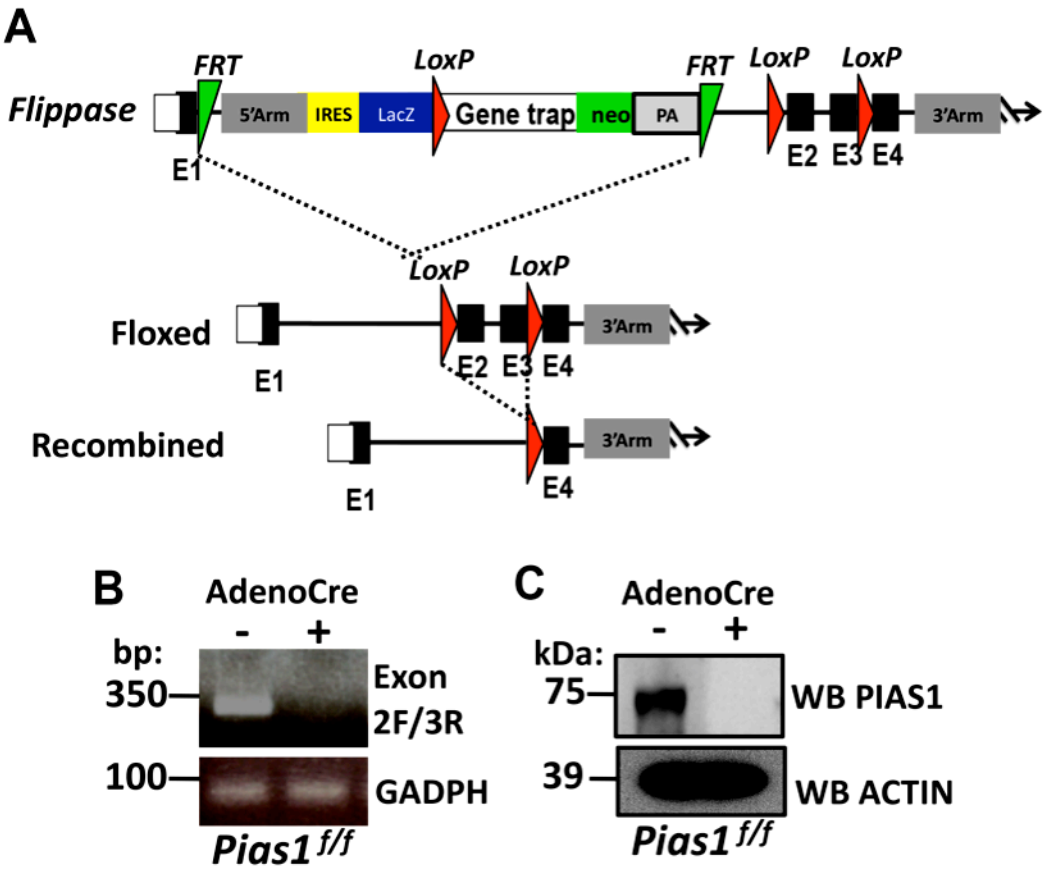

Figure 2.2 Conditional inactivation of *Pias1* by Cre recombinase. A, Diagram shows organization of the KOMP "knockout first" construct used for the generation of *Pias1* conditional null mice and MEFs. Stepwise modification of the knockout first allele by crossing with *Pgk1*$^{+/FlP}$ mice to generate *Pias1* conditional null mice. **B-C,** PCR confirmation of *Pias1* gene disruption and immunoblot confirmation of PIAS1 protein loss.

Next, we determined the pattern of *Pias1* gene expression using the LacZ reporter inserted into the *Pias1* gene locus by the gene trap vector. Consequently, X-gal staining can be used as a proxy to assess *Pias1* gene expression. We found that X-gal staining first appeared in the embryo proper at E8.0-E8.25 and the staining became progressively stronger in the YS at E9.5 and E10.5 (Figure 2.3A).

We noticed that *Pias1* null embryos do not develop obvious defects until E9.5, although they are smaller than their littermates. However, at E10.5, *Pias1*$^{-/-}$ embryos are significantly growth retarded, show a striking reduction in blood content in the YS and severe cardiomegaly (Figure 2.3B). Since the reduction in blood content in the YS is the first macroscopic defect that we detected, we analyzed the YS in more detail. We found that in *Pias1* heterozygous YS, the X-Gal stain is most prevalent in RBCs and endothelial cells lining the blood islands (Figure 2.4A). Strikingly, *Pias1* deficiency leads to loss RBCs content and aberrant capillary structures (Figure 2.4B-C). Notably, we found that GATA-1, a well-known erythroid transcription factor required for YS RBC development and survival, and PIAS1 colocalize in RBCs present in blood islands; and that RBCs are depleted from *Pias1*$^{-/-}$ blood islands (Figure 2.4D). These findings indicate that *Pias1* is expressed and functionally relevant in erythroid precursors and endothelial cells forming the YS blood islands.

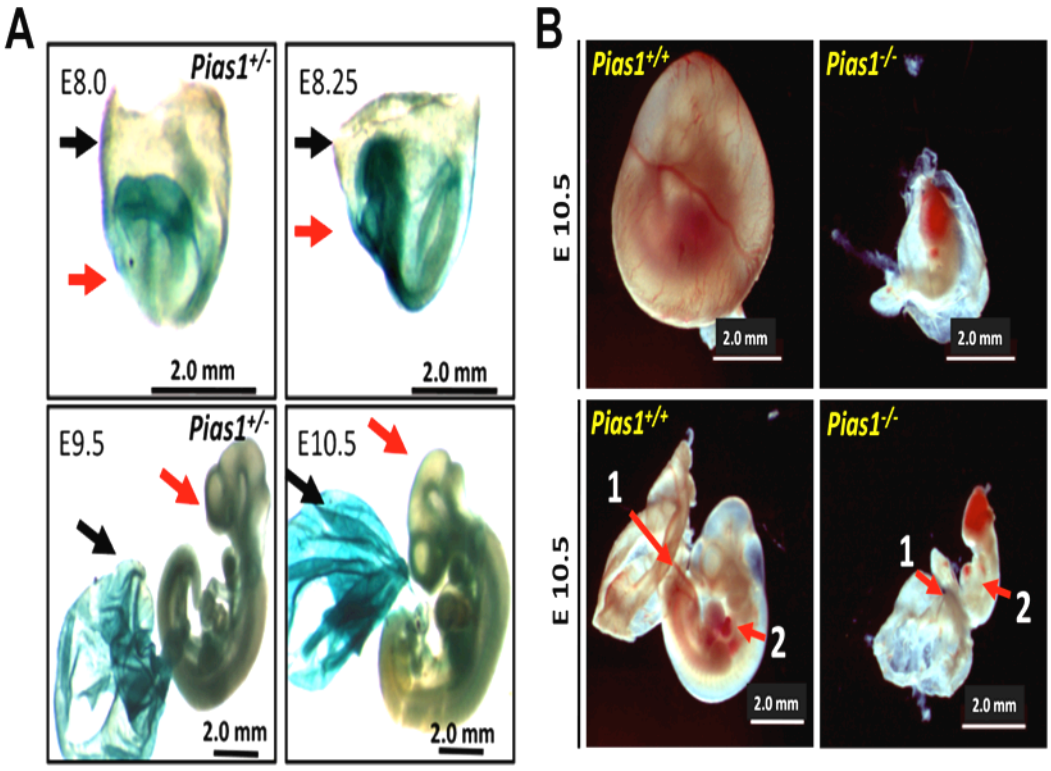

Figure 2.3 *Pias1* is expressed in fast growing and differentiating tissues during development. A, Images show the pattern of *Pias1* gene expression determined by X-gal staining at the indicated days of development. Black arrows indicate the YS and red arrows indicate the embryo proper. Scale bar: 2.0 mm. **B**, Comparison of *Pias1*$^{+/+}$ *vs Pias1*$^{-/-}$ embryos at E10.5. Note the significant growth retardation of the *Pias1*$^{-/-}$ embryo. Red arrows indicate areas with reduced blood content in the YS (1) and cardiomegaly (2) in *Pias1* null embryos as compared to their wild type littermates. Scale bar: 2.0 mm.

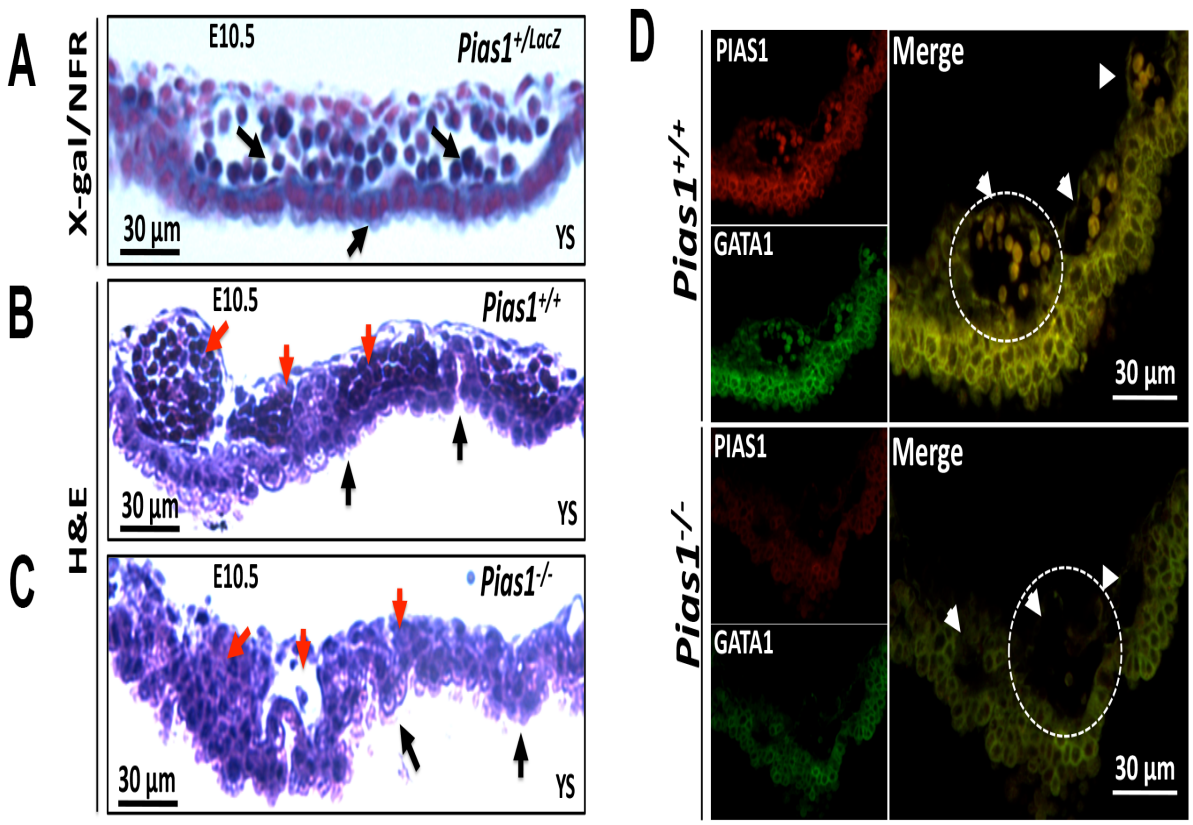

Figure 2.4 *Pias1* is necessary for primitive erythropoiesis in the yolk sac. A, YS stained with X-gal and nuclear fast red (NFR) at E10.5. Arrows indicate LacZ positivity in capillary beds and precursor red blood cells (pRBC) within blood islands. **B-C**, Hematoxylin and eosin (H&E) stained YS sections of the indicated genotypes at E10.5. Red arrows indicate RBCs and black arrows supporting vasculature. Note the significant decrease in RBC and abnormal vasculature in the YS of *Pias1*$^{-/-}$. **D,** IF image shows a comparison of YS blood Islands between *Pias1*$^{+/+}$ and *Pias1*$^{-/-}$ embryos at E10.5. Circles indicate positivity for GATA-1 and PIAS1 in blood islands, which are significantly depleted in *Pias1*$^{-/-}$ embryos (arrowheads). Scale bar: 30 µm.

2.3.2 Ablation of *Pias1* causes embryonic lethality with incomplete penetrance

Although *Pias1*$^{+/-}$ mice appear healthy and are fertile, their intercross leads to a 90% reduction in viable *Pias1*$^{-/-}$ progeny (Table 2.5). To determine the timing of prenatal lethality, we analyzed embryos from timed pregnancies of *Pias1*$^{+/-}$ intercrosses. At E12.5 the percentage of viable *Pias1*$^{-/-}$ embryos dropped to 20% and by E15.5 to approximately 10% (Table 1B). Notably, the defects in the embryo and the YS temporally coincided with the induction of *Pias1* promoter activation, determined by X-Gal staining.

With these findings, we concluded that loss of PIAS1 results in embryonic growth retardation and defective YS erythropoiesis, which becomes limiting after E11.5 and culminates in embryonic lethality.

A Percentage (%) of Pias1 animals of all genotypes 4 weeks post birth

Genotype		Gender		Total %
WT	137	Male 76	Female 61	35.0%
Het	212	Male 113	Female 99	55.0 %
Null	38	Male 17	Female 21	9.8% (*; **)

B Percentage (%) of Pias1 animals of all genotypes during embryogenesis

	WT	Het	Null	Total
7.75- 8.5dpc	9 (25%)	19 (53%)	*8 (22%)	36
9.5dpc	14 (25%)	32 (56%)	*11 (19%)	57
13.5 dpc	9 (26%)	19 (53%)	**7 (20%)	35
15.5 dpc	11 (25%)	30 (67%)	4 (9.%)	45

* Growth retarded embryos **Dying/dead embryos

Table 2.5. *Pias1* loss results in embryonic lethality. A, Mendelian analysis of born mice of all genotypes at 4 weeks of age**. B**, Mendelian analysis of mouse embryos up to E15.5.

2.3.3 *Pias1* regulates germ layer proliferation and survival during development

Aside from growth retardation, we observed no other obvious defects prior to E8.5. Thus, we determined whether there was a defect in cellular proliferation or an increase in apoptosis that could explain this phenotype. We stained by immunofluorescence (IF) cryosections of *Pias1*$^{+/+}$ and *Pias1*$^{-/-}$ embryos at E8.0, using the proliferation marker Ki67, the apoptosis marker cleaved Caspase-3 (C.CASPASE-3) and the PIAS1 regulated tumor suppressor promyelocytic

leukemia (PML). Is important to note that PIAS1 has been reported to directly SUMOylate PML and to promote its ubiquitin-mediated degradation (Rabellino et al., 2012).

We found that *Pias1*$^{-/-}$ embryos have significantly less Ki67 positive cells in the ectoderm and mesoderm germ layers (Figure 2.6A; yellow arrows). In contrast, we observed an increase in Ki67 positive cells in the endoderm germ layer of *Pias1*$^{-/-}$ embryos as compared to *Pias1*$^{+/+}$controls (Figure 2.6A; red arrows). Moreover, *Pias1*$^{-/-}$ embryonic ectoderm germ layers presents with a concomitant increase in PML and C.CASPASE-3 proteins positivity (Figure 2.6 B; yellow arrows). Quantification of these data revealed that the overall Ki67 positivity is consistently reduced and that PML and C.CASPASE-3 protein levels are increased in *Pias1*$^{-/-}$ embryos when compared to *Pias1*$^{+/+}$ littermates (Figure 2.6-E).

PML has a well-known growth suppressive and pro-apoptotic function, which may explain the negative effects on embryonic germ layer development and embryonic growth arrest caused by *Pias1* loss (Bernardi and Pandolfi, 2003; Giorgi et al., 2010). To determine whether the defect in germ layer proliferation is cell autonomous, we dissociated E8.5-E9.5 *Pias1*$^{+/+}$ and *Pias1*$^{-/-}$ embryos into single cells and used them to perform proliferation assays. This analysis revealed that *Pias1* null embryonic cells were significantly fewer in number at the experimental end point, suggesting an intrinsic defect in their proliferative or

survival capacity *in vitro* (Figure 2.6F). Accordingly, we found a significant reduction in cell proliferation in *Pias1* conditional null embryonic fibroblasts (MEFs) following AdenoCre mediated acute *Pias1* gene inactivation (Figure 2.6G). Reduced cell proliferation coincided with an increase in PML and BIM proapoptotic proteins and a decrease in Cyclin D1, a marker of cell proliferation, in *Pias1* conditional null MEFs (Figure 2.6H). These findings suggest that *Pias1* inactivation negatively affects cell survival.

In light of these findings, we concluded that PIAS1 loss result in uncoordinated proliferation of the germ layers at an early stage of embryonic development. This is evident by decreased proliferation of the ectoderm and increased proliferation of the endoderm layer. Furthermore, PIAS1 loss lowers the threshold for apoptosis in cells in vivo and in vitro and is particularly detrimental to hematopoietic-progenitor tissues.

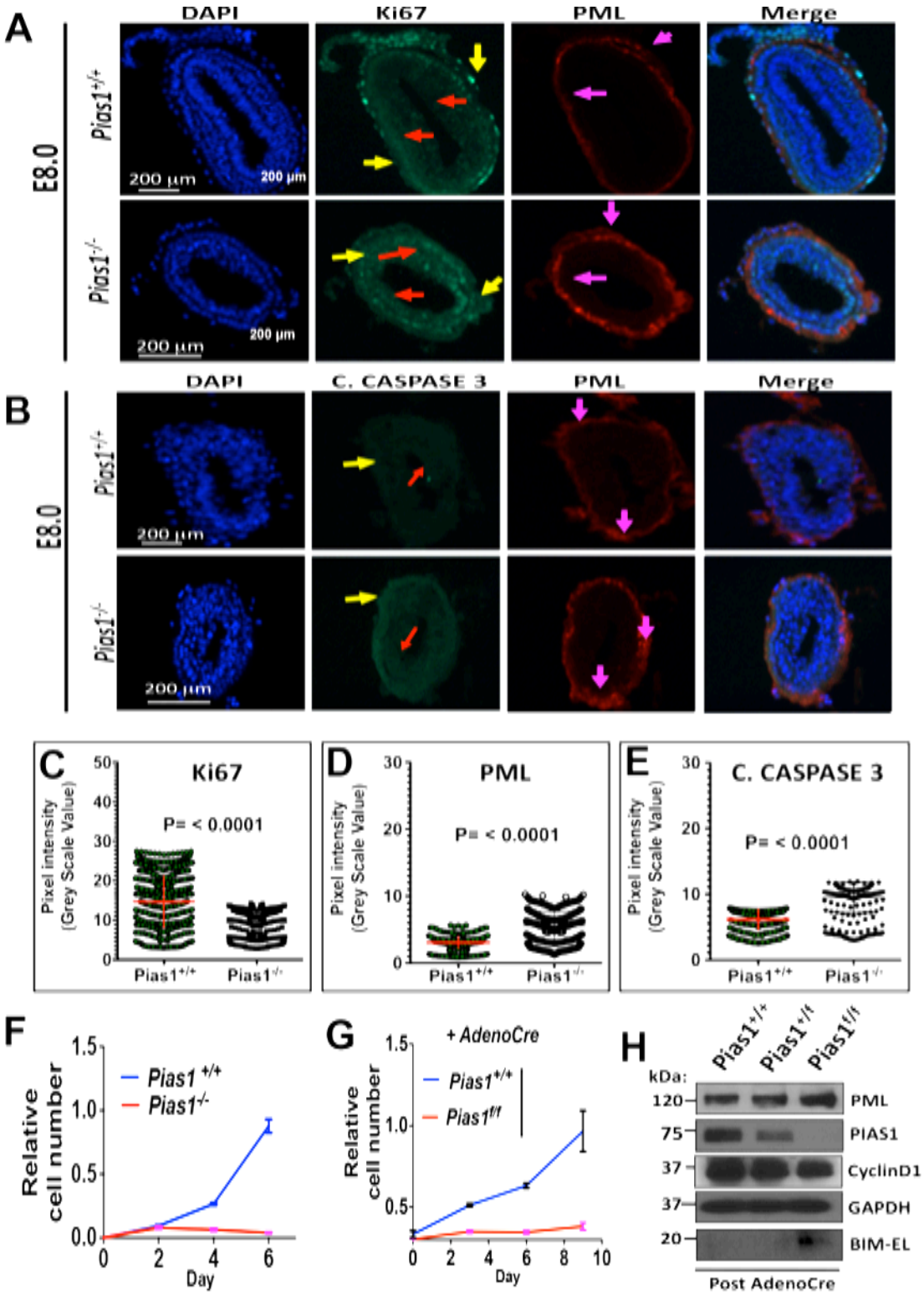
A
DAPI
Ki67
PML
Merge
E8.0
Pias1+/+
Pias1-/-
200 µm
B
DAPI
C. CASPASE 3
PML
Merge
E8.0
C
Ki67
P= < 0.0001
Pixel intensity (Grey Scale Value)
Pias1+/+
Pias1-/-
D
PML
P= < 0.0001
E
C. CASPASE 3
P= < 0.0001
F
Relative cell number
Pias1 +/+
Pias1-/-
Day
G
+ AdenoCre
Pias1+/+
Pias1f/f
H
kDa:
Pias1+/+
Pias1+/f
Pias1f/f
120
75
37
37
20
PML
PIAS1
CyclinD1
GAPDH
BIM-EL
Post AdenoCre

Figure 2.6 *Pias1* regulates cell proliferation and survival during embryonic development. A, IF images of *Pias1*$^{+/+}$ and *Pias1*$^{-/-}$ embryonic germ layers stained as indicated. Yellow arrows indicate ectoderm positivity for Ki67; red arrows indicate Ki67 positivity in the meso-endoderm germ layers. Pink arrows indicate PML positivity in mesoderm and ectoderm germ layers. **B,** IF images of C.CASPASE-3 positivity in *Pias1*$^{+/+}$ and *Pias1*$^{-/-}$ embryos. Red arrows indicate positivity in mesoderm and ectoderm tissue. Scale bars: A-B, 200 μm. **C-E**, Quantification of fluorescence stain intensity from panels A and B; comparison of *Pias1*$^{+/+}$ embryos to *Pias1*$^{-/-}$. n=3 (*: P<0.05). **F**, Proliferation assay of *Pias1*$^{+/+}$ and *Pias1*$^{-/-}$ embryonic cells. Note the reduction in cell proliferation of *Pias1*$^{-/-}$ cells. **G**, Proliferation assay using MEFs of the indicated genotype after exposure to Adeno-Cre. **H**, Immunoblot on MEFs of the indicated genotype after exposure to Adeno-Cre. Note upregulation of the proapoptotic PML and BIM proteins in MEFs after conditional inactivation of *Pias1*.

2.3.4 *Pias1* ablation impairs erythrocyte development in the YS while promoting macrophage differentiation

We determined whether RBC depletion in the YS was a result of an intrinsic defect in erythropoiesis or to a non-cell autonomous process such as loss of interaction with the endothelial niche. We dissociated E9.5 YS into single cell suspensions and induced erythroid differentiation *in vitro* with Methocult™ hematopoietic differentiation media. We used recombinant erythropoietin (rEPO) or recombinant granulocyte macrophage colony stimulating factor (rGMCSF) for 5 days to induce erythroid or myeloid differentiation (Sturgeon et al., 2012; Sturgeon et al., 2014). We discovered that hematopoietic precursors in *Pias1*$^{-/-}$ embryos were deficient at forming mature erythroid cells *in vitro,* determined by detection of heme accumulation (Figure 2.7A, red arrows). We also found that stimulation

with rGMCSF leads to a significant enrichment of the macrophage cell lineage (Figure 2.7B, arrows).

To further characterize this phenotype, we compared hematopoietic cell populations present in the YS at E12.5 using flow cytometry. We used the transferin receptor (CD71) as a marker for erythroid precursors and Ter119 for terminally differentiated erythroid cells. This analysis identifies several cell populations based on their differentiation stage: $CD71^{+}Ter119^{-}$ (R1) pro-erythroblast, $CD71^{+}Ter119^{+}$ (R2) early polychromatophilic erythroblast and $CD71^{-}$ $Ter119^{+}$ (R3) poly/orthochromatophilic erythroblast and enucleated erythroblast (Maeda et al., 2009; Yu et al., 2010). We found a significant increase in the R1 population and a decrease in R2 and R3 cell population in the YS of *Pias1*$^{-/-}$ embryos (Figure 2.7C). This finding indicates that the severe embryonic anemia observed in *Pias1* null mice is not due to lack of erythroid progenitors, but to impaired erythroid maturation.

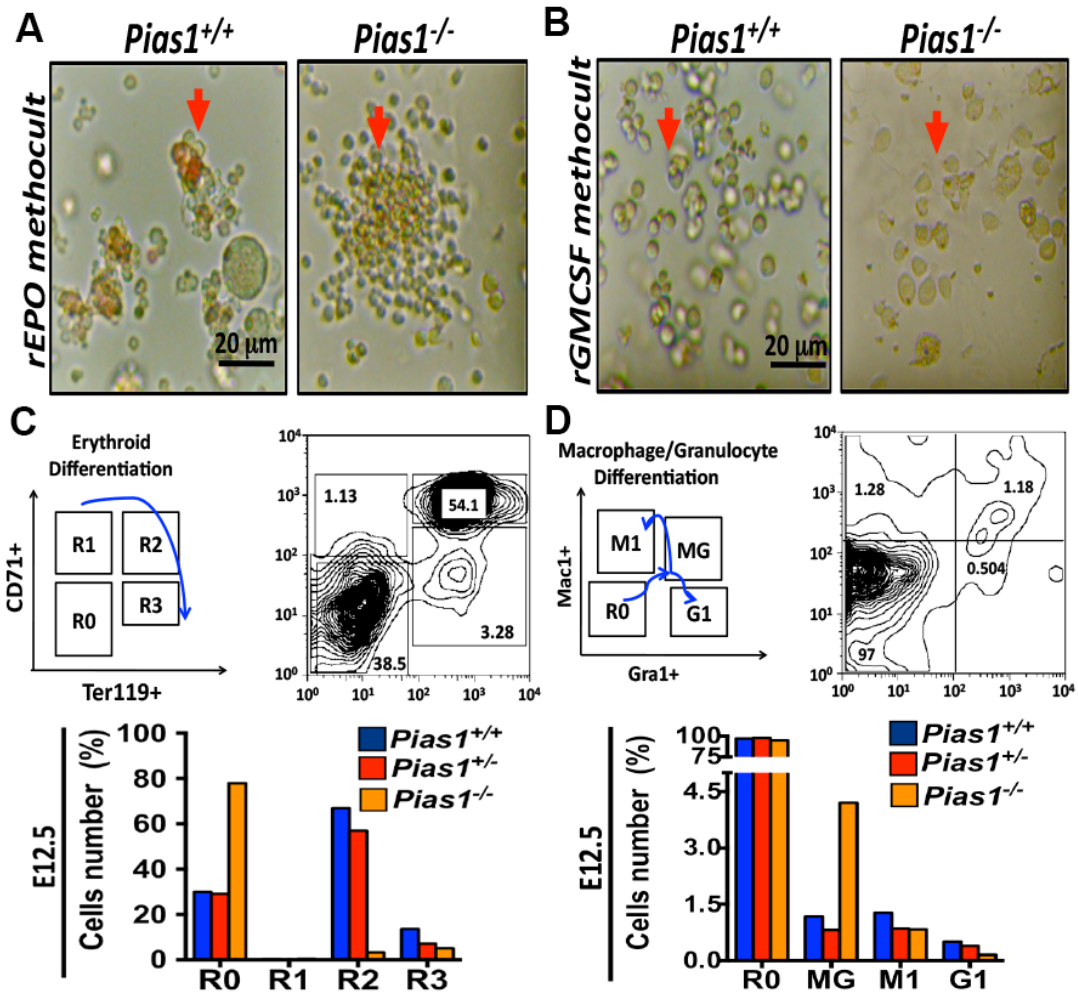

Figure 2.7 *Pias1* gene loss impairs erythrogenesis in the YS. A, Representative image of a Methocult™ differentiation assay of YS erythroid precursors obtained from *Pias1*$^{+/+}$ and *Pias1*$^{-/-}$ embryos using recombinant erythropoietin (rEPO). Note that *Pias1*$^{-/-}$ YS erythroid precursors are deficient at forming heme accumulating colonies *in vitro* (red arrows) compared to *Pias1*$^{+/+}$ controls (red arrows). **B**, Representative image of Methocult™ colonies from myeloid precursor cells of the indicated genotype treated with granulocyte and macrophage colony stimulating factor (rGMCSF). Note that *Pias1*$^{-/-}$ colonies show preferential differentiation toward the macrophage cell lineage (red arrows). Scale bar: A-B, 20 µm. **C**, Flow cytometry analysis of *Pias1*$^{+/+}$, *Pias1*$^{+/-}$ and *Pias1*$^{-/-}$ YS cells at E12.5, using CD71^{+} and Ter119^{+} erythroid differentiation markers. Histogram shows reduction in CD71^{+}Ter119^{+} double positive erythroid precursors (R2) and fully differentiated RBCs (R3) in *Pias1*$^{-/-}$ embryos. **D,** Flow cytometry analysis of *Pias1*$^{+/+}$, *Pias1*$^{+/-}$

and *Pias1*$^{-/-}$ YS cells using Mac1^{+} and Gr1^{+} differentiation markers. Histogram shows a fivefold increase in Mac1^{+}Gr1^{+} double positive cells in *Pias1*$^{-/-}$ YS as compared to *Pias1*$^{+/+}$ and *Pias1*$^{+/-}$.

We also determined changes in myeloid differentiation using the Macrophage-1 antigen (Mac1) and Granulocyte-1 (Gr1) antigen. This analysis identifies myeloid lineage committed cells at various stages of differentiation: Mac1^{+}Gr1^{-} (M1) polymorphonuclear leukocytes/macrophages, Mac1^{+}Gr1^{+} (MG) consists mostly of granulocytes, monocytes and macrophages and Mac1^{-}Gr1^{+} (G1) granulocytes/monocytes. We found a 5-fold increase in the amount of cells double positive for Mac1^{+}Gr1^{+} myeloid precursors, of the macrophage or granulocyte cell lineages (Figure 2.7D). Our results suggest that PIAS1 may be required for erythroid differentiation and for repression of granulocyte/macrophage cell lineage differentiation both *in vitro* and *in vivo*.

2.3.5 *Pias1* regulates YS vascular development and gene expression

The YS erythropoiesis and *de novo*-angiogenesis are interrelated processes during embryonic development. To compare the vascular density between *Pias1*$^{+/+}$ and *Pias1*$^{-/-}$ embryos, we performed whole mount IF of PIAS1, *Pecam* (CD31) and smooth muscle actin (SMA-1). We found blood vessel size and branching significantly reduced in *Pias1*$^{-/-}$ embryos (Figure 2.8A). E12.5 coincides with the onset of embryonic lethality in *Pias1* null embryos. Thus, we selected this time

point to determine how *Pias1* deficiency affects expression of genes involved in YS angiogenesis. We found that in *Pias1*$^{-/-}$embryos *Vcam-1* and *Angp2* were significantly reduced compared to *Pias1*$^{+/+}$ controls (* $P<0.05$) (Figure 2.8B).

To directly address the role of *PIAS1* in endothelial cell biology, we performed qPCR analysis of human umbilical vein endothelial cells (HUVECs), following *Pias1* ectopic expression. We analyzed expression of pro-angiogenic and anti-angiogenic genes reported to be responsible for endothelial cell proliferation, survival and migration (Dbouk et al., 2014; Meadows et al., 2013). We found that ectopic expression of *PIAS1* up-regulates *ZEB1, MMP28, WNK1* and *SEMA3A*, a group of genes that promote cell survival and migration. In contrast, ectopic expression of *PIAS1* repressed *THBS1* gene expression; an anti-angiogennic and anti-proliferative gene (Figure 2.8C).

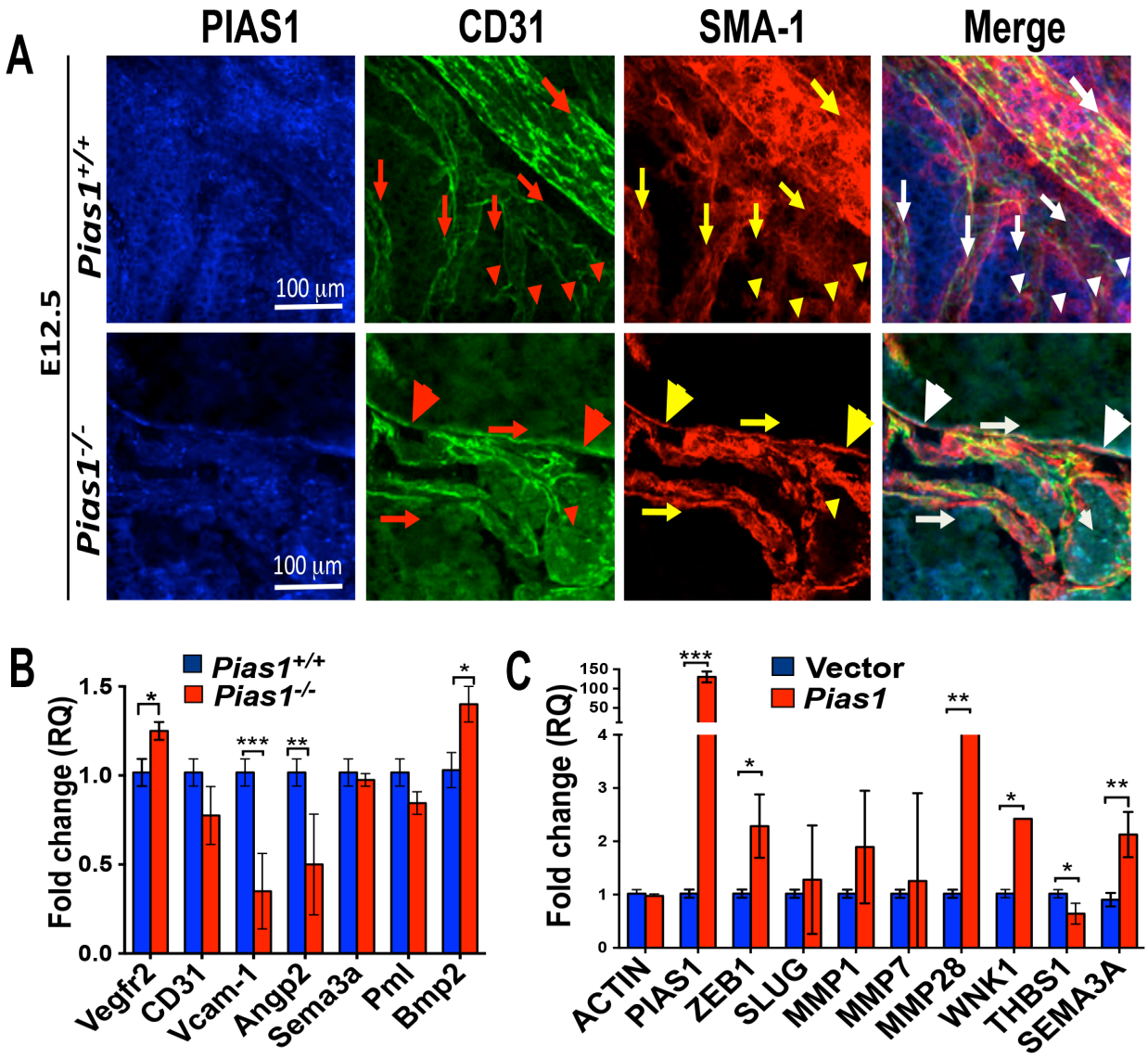

Figure 2.8 *Pias1* regulates YS angiogenesis and gene expression in the mouse embryo. A, Whole-mount IF and confocal micrograph of *Pias1*$^{+/+}$ and *Pias1*$^{-/-}$ embryos stained as indicated. Arrows indicate blood vessels, arrowheads capillaries and large arrowheads vessel occlusion. Scale bar: 100 µm. **B,** Histogram shows qPCR expression analysis of the indicated genes in *Pias1*$^{+/+}$ and *Pias1*$^{-/-}$ embryos at the onset of embryonic lethality (E12.5). Note the reduction in *Vcam-1* and *Angp2* gene expression in *Pias1*$^{-/-}$ embryos. n=3 (*: P<0.05). **C**, Histogram shows changes in mRNA levels for the indicated genes in HUVECs expressing either empty vector or *Pias1* cDNA.

HUVECs are a well-established cellular model used *in vitro* angiogenesis assays based on their ability to form three-dimensional capillary-like tubular structures, when cultured on Matrigel. During this assay, HUVECs migrate and polarize into tubular polygonal networks reminiscent of developing capillaries. Notably, we found that *PIAS1* silencing reduced the ability of HUVECs to form branching structures that mimic sprouting blood vessels when grown on Matrigel (Figure 2.9A-B). However, ectopic expression of *PIAS1* alone did not increase HUVEC branching and cord formation *in vitr*o (data not shown). We concluded that *PIAS1* promotes the survival of endothelial cells and their ability to form branching structures *in vitro*.

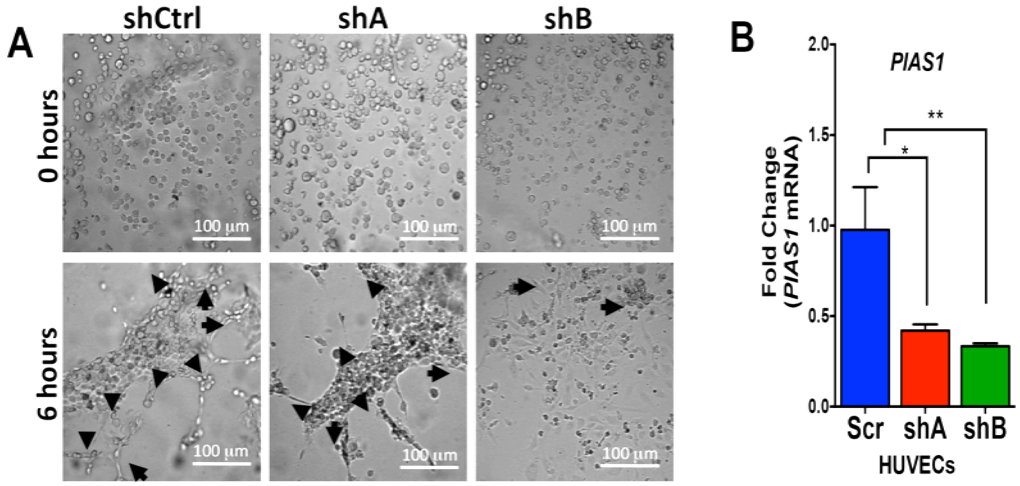

Figure 2.9 *PIAS1* silencing in endothelial cells impairs effective branch formation. A, Image shows branch formation assay of HUVECs cells treated with shRNA Control (shCtrl) or *PIAS1* targeting shRNA (shA; shB) at the indicated time points. Black arrows indicate branching points. **B**, Histogram shows knockdown efficiency of anti *PIAS1* shRNA in HUVECs.

2.3.6 *Pias1* inactivation impairs cardiac development in the mouse embryo

In addition to deterioration of the YS capillary plexus, we noticed that *Pias1*$^{-/-}$ embryos develop cardiomegaly between E9.5 and E12.5. At this stage of embryonic development *Pias1* is expressed predominantly in the neural tube, developing limb buds, gut and heart tissue (Figure 2.10A). We performed whole mount immunohistochemistry (IHC) for the endothelial marker CD31 in *Pias1*$^{+/+}$ and *Pias1*$^{-/-}$ embryos. Despite the increase in heart size in *Pias1* null embryos, CD31 was significantly reduced in comparison to *Pias1*$^{+/+}$ littermates (Figure 2.10B, magnification; arrowhead).

To test the relationship between *Pias1* and cardiovascular development we analyzed wild type embryonic hearts with qPCR at various stages of development. We found that CD31, *Vcam-1* and *Pias1* mRNA levels rise and fall together in developing heart tissue (Figure 2.10C). Next, we analyzed whether *Pias1* loss affects heart development by performing histological analysis and X-gal staining of heterozygous (*Pias1*$^{+/-}$) and null (*Pias1*$^{-/-}$) embryos at E9.5 and E11.5 (the latter time point immediately preceding embryonic death). At E9.5 we found that there were significantly fewer cells lining the myocardium wall of *Pias1*$^{-/-}$ hearts (Figure 2.10D). This phenotype worsens overtime as shown by a similar analysis using E11.5 embryos (Figure 2.10E, arrows).

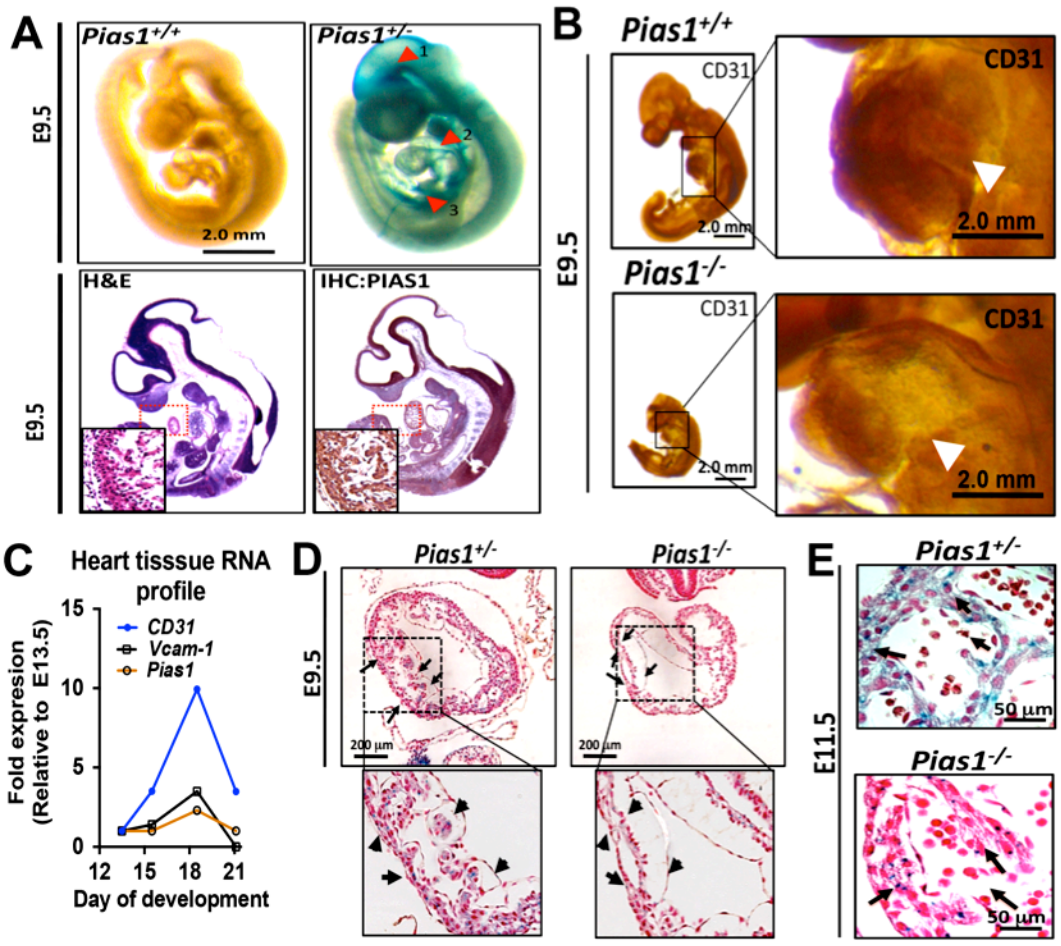

Figure 2.10 ***Pias1*** **gene loss impairs cardiac development. A**, Image shows activation of the *LacZ* reporter inserted into the *Pias1* promoter (upper panels, arrows indicate intense staining of the brain (1), heart (2) and umbilical cord (3) and H&E/IHC (lower panels) for PIAS1 protein in the developing embryo at E9.5. A magnification is provided of the developing heart. **B**, Whole mount IHC stain of the endothelial cell marker CD31 in *Pias1*$^{+/+}$ and *Pias1*$^{-/-}$ embryos. Note significantly decreased CD31 staining in *Pias1*$^{-/-}$ embryonic hearts compared to *Pias1*$^{+/+}$ littermates (white arrowhead). Scale bar: A-B, 2.0 mm. **C,** qPCR analysis of *CD31*, *Vcam-1* and *Pias1* gene expression at the indicated days of embryonic development. Graph shows a positive correlation between *CD31, Vcam-1* and *Pias1* gene expression in the heart. **D-E,** Histological analysis of embryonic hearts shows reduced cellularity in *Pias1*$^{-/-}$ embryos (black arrows), and decreased X-gal positive cells compared to *Pias1*$^{+/-}$ littermates at E9.5 and E11.5. Scale bar: D, 200 µm; E, 50 µm.

Previous reports have suggested a potential role for PIAS1 in cardiac gene regulation (Wang et al., 2004b; Wang et al., 2007). To gain insight into how *Pias1* may regulate cardiac development, we ectopically expressed *Pias1* in primary myoblasts obtained from E15.5 hearts (Berkes and Tapscott, 2005; Millay et al., 2013; Olson et al., 1991). After establishing short-term myoblast cultures in low serum conditions, we tested for changes in cardiac-specific gene expression. We found that *Pias1* expression in primary myoblasts promotes increase of CD31, *MyoD, Myogenin and Myomaker* mRNA, but has no direct effect on *Angp2* or *Vcam-1* genes (Figure 2.11A). Importantly, these changes in gene expression were not observed in primary MEFs under the same experimental conditions, suggesting that this is a cardiac specific phenotype (Figure 2.11B).

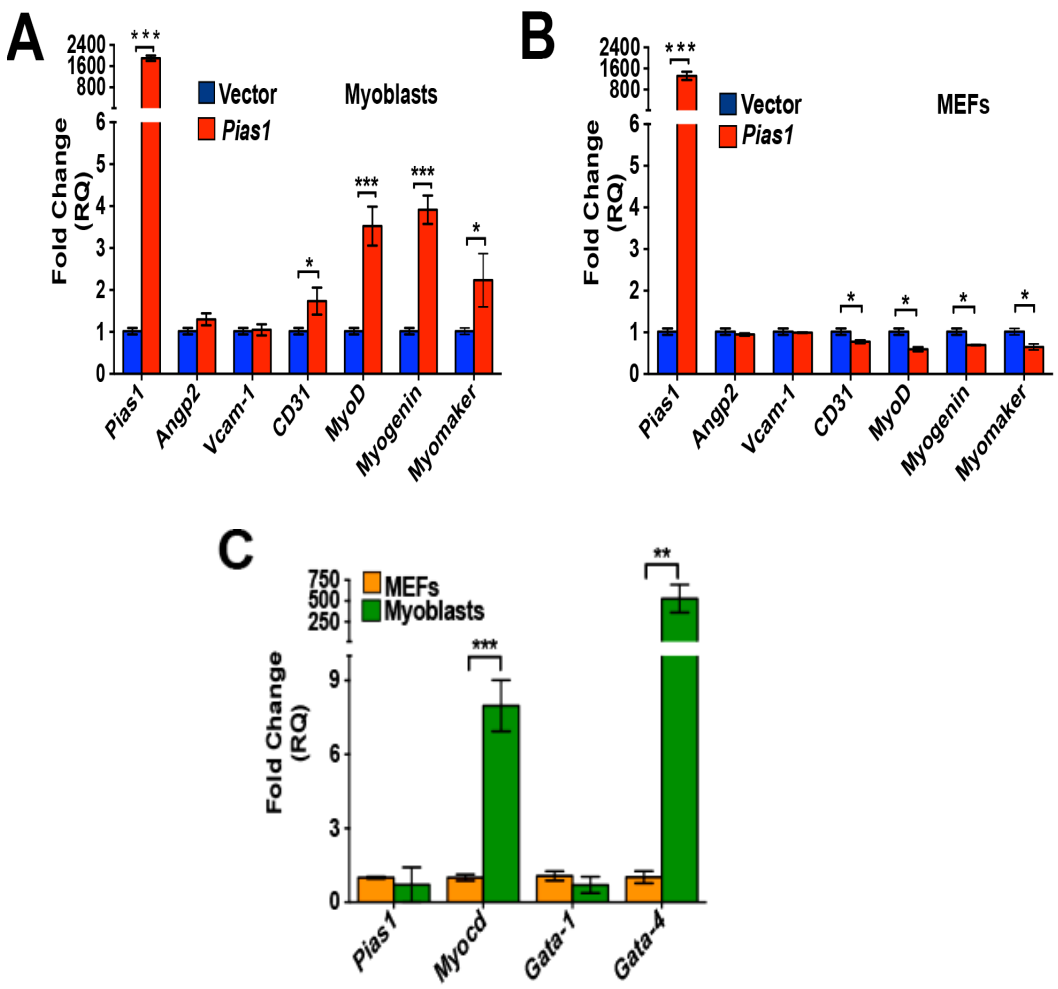

Figure 2.11 PIAS1 regulation of gene transcription is transcription factor dependent. A, qPCR analysis of cardiovascular genes *Angp2*, *Vcam-1*, *Pecam (CD31)*, *MyoD*, *Myogenin* and *Myomaker* in primary myoblasts expressing either empty vector or ectopic *Pias1*. Note significant upregulation of *Pecam*, *MyoD, Myogenin and Myomaker* in primary myoblasts expressing ectopic *Pias1* compared to empty vector**. B,** qPCR analysis in MEFs as performed in A. The cardiogenic profile observed in primary heart myoblast is not promoted in MEFs with addition of ectopic *Pias1*. **C**, qPCR comparing *Pias1*, *Myocd, Gata-1* and *Gata-4* mRNA levels between primary MEFs and primary myoblasts. There is comparable *Pias1* and *Gata-1* mRNA in MEFs and primary myoblast, but a significant enrichment in *Myocd* and *Gata-4* gene expression in primary myoblasts.

Since the progression towards a cardiac-specific developmental program in primary myoblasts is regulated by the expression of cardiac specific transcription factors, we compared *Pias1*, *Myocardin (Myocd)*, *Gata-1* and *Gata-4* gene expression between heart-derived myoblasts and mouse embryonic fibroblasts (MEFs). Even though we did not find differences in *Pias1* or *Gata-1* expression between primary myoblasts and MEFs, we found significant enrichment for *Myocd* and *Gata-4* mRNA in primary myoblasts (Figure 2.11C).

In view of these findings, we concluded that loss of the *Pias1* gene in the mouse embryo impairs cardiac development by affecting the structural development of the myocardium. Moreover, ectopic expression of *Pias1* in primary myoblasts promotes the cardiogenic differentiation program dependent of *Myocd* and/or *Gata-4* gene function.

2.3.7 *Pias1* inactivation in endothelial cells recapitulates YS erythroid and vascular phenotypes

Our findings indicate that *Pias1* inactivation results in failure of YS erythropoiesis, capillary plexus development and cardiac muscle defects. These findings prompted us to test whether deleting *Pias1* in endothelial cells would recapitulate the observed phenotypes. To achieve this, we crossed $Pias1^{f/f}$ (conditional) mice with a mouse strain that expressed the Cre under the endothelial-specific receptor tyrosine kinase Tie2 ($Tie2^{+/Cre}$) (Koni et al., 2001).

Consistent with our previous findings, the YS of *Pias1*$^{f/f}$*/Tie2*$^{+/Cre}$ embryos develop significantly fewer erythroid cells when compared to littermate controls (Figure 2.12A, black arrows). In addition, *Pias1*$^{f/f}$*/Tie2*$^{+/Cre}$ embryos showed reduced blood vessel density in the brain region (head vein) (Figure 2.12A, white arrow) and occlusion at the connecting stalk (CS), the structure that connects the YS to the embryonic blood vessels (Figure 2.12A, green arrow).

Despite aberrant distribution of blood, *Pias1*$^{f/f}$*/Tie2*$^{+/Cr}$ embryos showed no growth retardation and the heart and liver size appeared morphologically normal. We performed histological examination of heart and liver tissue to corroborate these findings. Upon close examination of the YS vascularity, we found a significantly reduced capillary plexus in *Pias1*$^{f/f}$*/Tie2*$^{+/Cre}$ embryos when compared to *Pias1*$^{f/+}$*/Tie2*$^{+/Cre}$ littermates (Figure 2.12B). Moreover, the endothelial cell layer and capillary lumens were significantly reduced contributing to the blockade of RBC circulation in the YS (Figure 2.12C). The myocardial wall of *Pias1*$^{f/f}$*/Tie2*$^{+/Cre}$ mice had reduced cell density as compared to their wild type littermates (Figure 2.12D). We found no significant differences in RBC or vascular content between the liver of *Pias1*$^{f/f}$*/Tie2*$^{+/Cre}$ and *Pias1*$^{+/+}$*/Tie2*$^{+/Cre}$ *Pias1*$^{f/+}$*/Tie2*$^{+/Cre}$ littermates (data not shown).

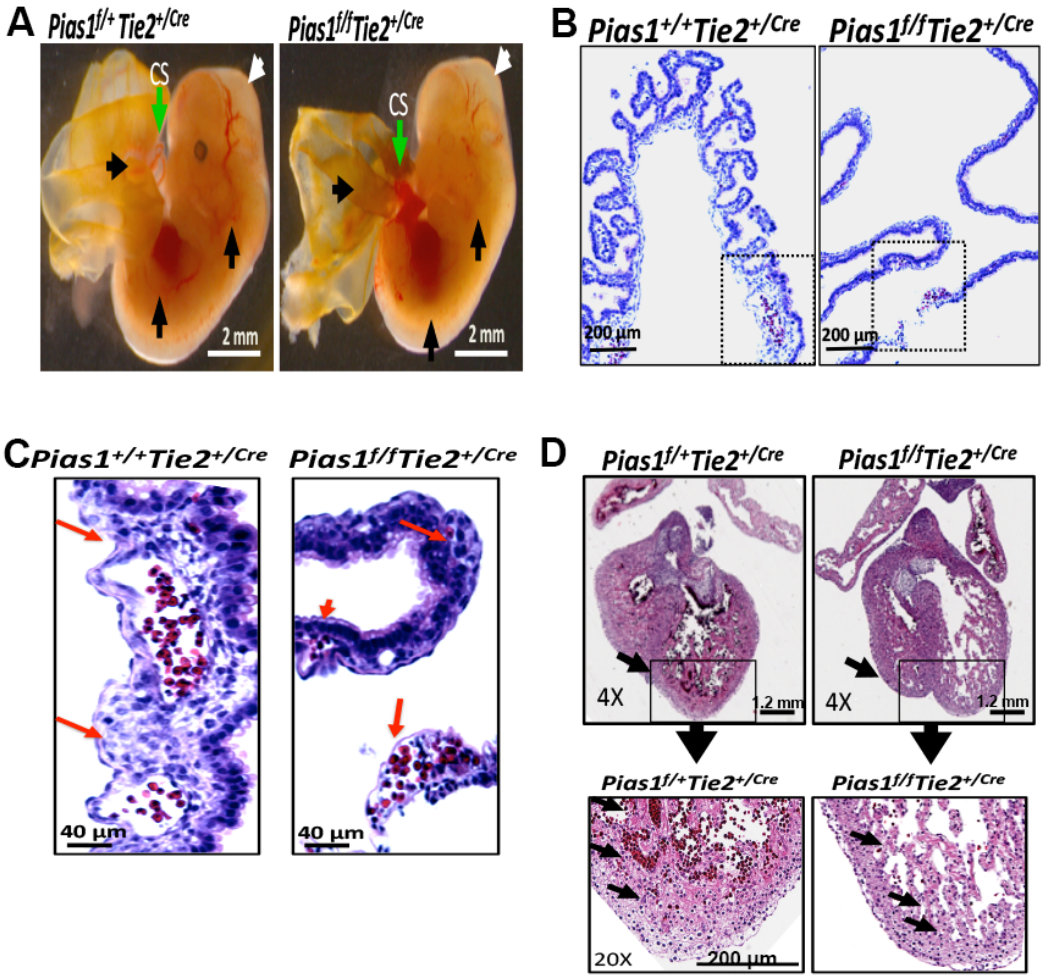

Figure 2.12. *Pias1* gene deletion in endothelial cells reduces YS erythropoiesis and capillary plexus formation. A, Comparison of *Pias1*$^{f/+}$/*Tie2*$^{+/Cre}$ and *Pias1*$^{f/f}$/*Tie2*$^{+/Cre}$ embryos at E12.5. Black arrows indicate reduced vascularity in the YS and embryo proper. White arrow indicates reduced vascularity into the developing brain region. Green arrow points to the connecting stalk (CS) of the umbilical cord indicating occlusion at YS interface. Scale bars: 2.0 mm. **B and C,** Histological analysis of YS from *Pias1*$^{+/+}$/ *Tie2*$^{+/Cre}$ and *Pias1*$^{f/f}$/*Tie2*$^{+/Cre}$ shows collapsed capillary beds and loss of capillary lumen integrity in *Pias1*$^{f/f}$/*Tie2*$^{+/Cre}$ embryos (red arrows). Scale bar: B, 200 µm; C, 40 µm. **D**, *Pias1*$^{f/+}$/*Tie2*$^{+/Cre}$ and *Pias1*$^{f/f}$/*Tie2*$^{+/Cre}$ embryos heart sections. Scale bar: 1.2 mm. Black arrows indicate sites of high tissue mass and RBC content in *Pias1*$^{f/+}$/*Tie2*$^{+/Cre}$ significantly reduced in *Pias1*$^{f/f}$/*Tie2*$^{+/Cre}$ mice. Scale bar: 1.2 mm and 200 µm.

In agreement with the results we obtained in *Pias1*$^{-/-}$ embryos, we found that CD71^{+} Ter119^{+} double positive cells were reduced in the YS of E9.5 and E11.5 *Pias1*$^{f/+}$*Tie2*$^{+/Cre}$ and *Pias1*$^{f/f}$/*Tie2*$^{+/Cre}$ embryos when compared to *Pias1*$^{+/+}$*Tie2*$^{+/Cre}$ controls (Figure 2.13A). In addition, we observed a twofold increase in Mac1^{+}Gr1^{+} double positive cells in *Pias1*$^{f/f}$*Tie2*$^{+/Cre}$ embryos when compared to *Pias1*$^{f/+}$*Tie2*$^{+/Cre}$ and *Pias1*$^{+/+}$*Tie2*$^{+/Cre}$ littermates at E9.5, which normalized at E11.5 (Figure 2.13B).

Together our results demonstrate that *Pias1* is required for the development of endothelial cells, those supporting erythropoiesis and angiogenesis. On the other hand, *Pias1* gene ablation in liver endothelium does not seem to grossly affect liver vascularity or RBC content.

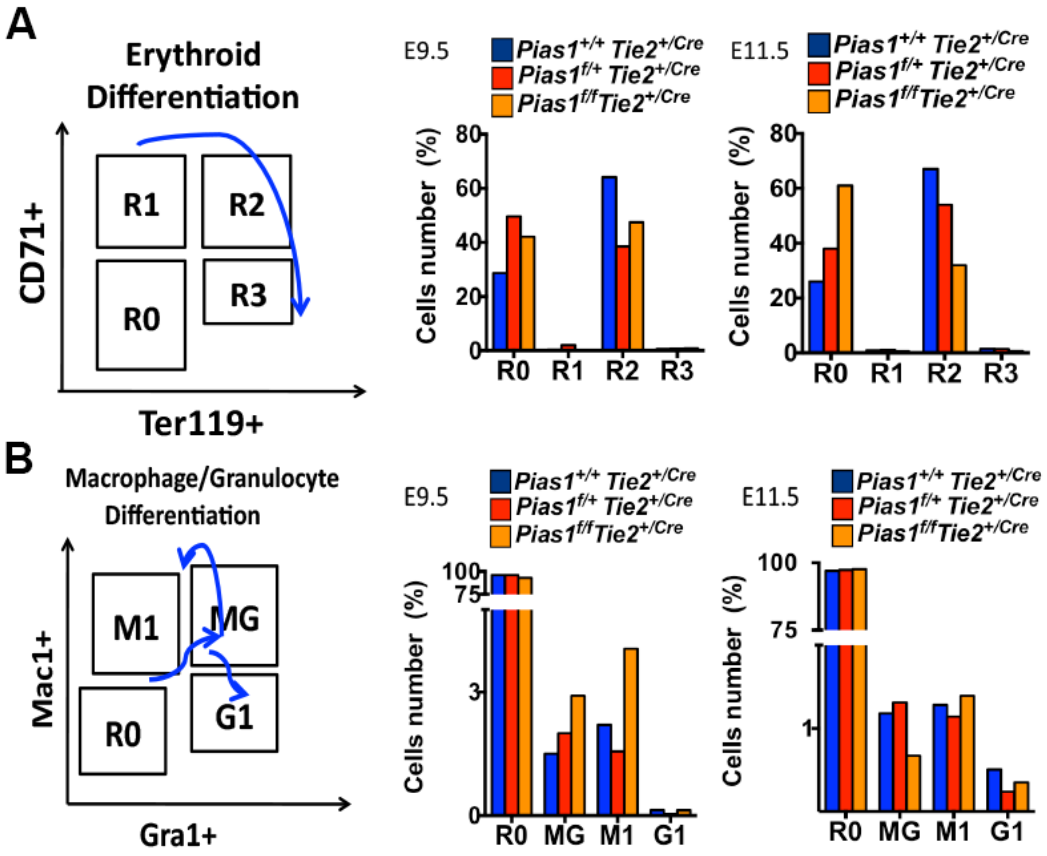

Figure 2.13 Endothelial specific inactivation of *Pias1* results in defective YS erythropoiesis and increases macrophage lineage differentiation. A, The diagram shows the expected immunophenotype of differentiating erythroid cells. The histogram shows the quantification of E9.5 YS subjected to flow cytometry analysis for $CD71^+$ and $Ter119^+$ erythroid differentiation markers in $Pias1^{+/+}/Tie2^{+/Cre}$, $Pias1^{+/f}/Tie2^{+/Cre}$ and $Pias1^{f/f}/Tie2^{+/Cre}$. We detected a 50% reduction, on average, in $CD71^+Ter119+$ double positive erythroid precursors in $Pias1^{+/f}$ $Tie2^{+/Cre}$ and $Pias1^{f/f}$ $Tie2^{+/Cre}$. **B,** The diagram shows the immunophenotype of myeloid precursor cells and the characterization of E9.5 YS cells by flow cytometry analysis for $Mac1^+$ and $Gr1^+$ markers in $Pias1^{+/+}/Tie2^{+/Cre}$, $Pias1^{+/f}/Tie2^{+/Cre}$ and $Pias1^{f/f}/Tie2^{+/Cre}$ YS. Histogram shows two-fold increase in $Mac1^+$ positive cells in $Pias1^{f/f}/Tie2^{+/Cre}$ compared to littermates at E9.5, but stabilizes at E11.5.

2.3.8 *Pias1* regulates survival and differentiation of endothelium derived stem cells

Our study suggests that *Pias1* is required for proper erythroid and vascular development by promoting cell differentiation and suppressing cell death mechanisms (Figure 2.14A). Specifically, we show that PIAS1 loss results in almost complete depletion of YS erythroid cells, failed YS angiogenesis and loss of heart muscle mass. We found a failure in erythroid differentiation following rEPO treatment *in vitro* and reduced $CD71^{+}$ $Ter119^{+}$ double positive erythro-myeloid progenitors (EMPs) cells *in vivo*. Our findings indicate deficient GATA-1 pathway activation, supported by our observation of GATA-1 loss in blood islands in *Pias1* null embryos. Moreover, analysis of erythroid and myeloid precursors *in vivo* demonstrate a substantial bias towards the macrophage and granulocyte lineages. In addition, heart structural development is impaired after PIAS1 loss and its ovexpression in primary heart myoblasts promotes cardiac gene differentiation, in a *Gata-4/Myocd* dependent manner. PIAS1 loss also results in a significant reduction of YS derived *Vcam-1* gene expression. However, *Pias1* expression alone did not promote *Vcam-1* gene transcription. This would suggest that PIAS1 is required for the survival or maintenance of *Vcam-1* expressing cells in the hemopoietic niche, not necessarily *Vcam-1* transcriptional regulation. Our findings support a model in which PIAS1 is essential for the maintenance and homeostasis of the hemopoietic niche in the YS; aiding endothelial cell survival and RBC

differentiation, while also suppressing the myeloid lineage in EMPs (Figure 2.14B).

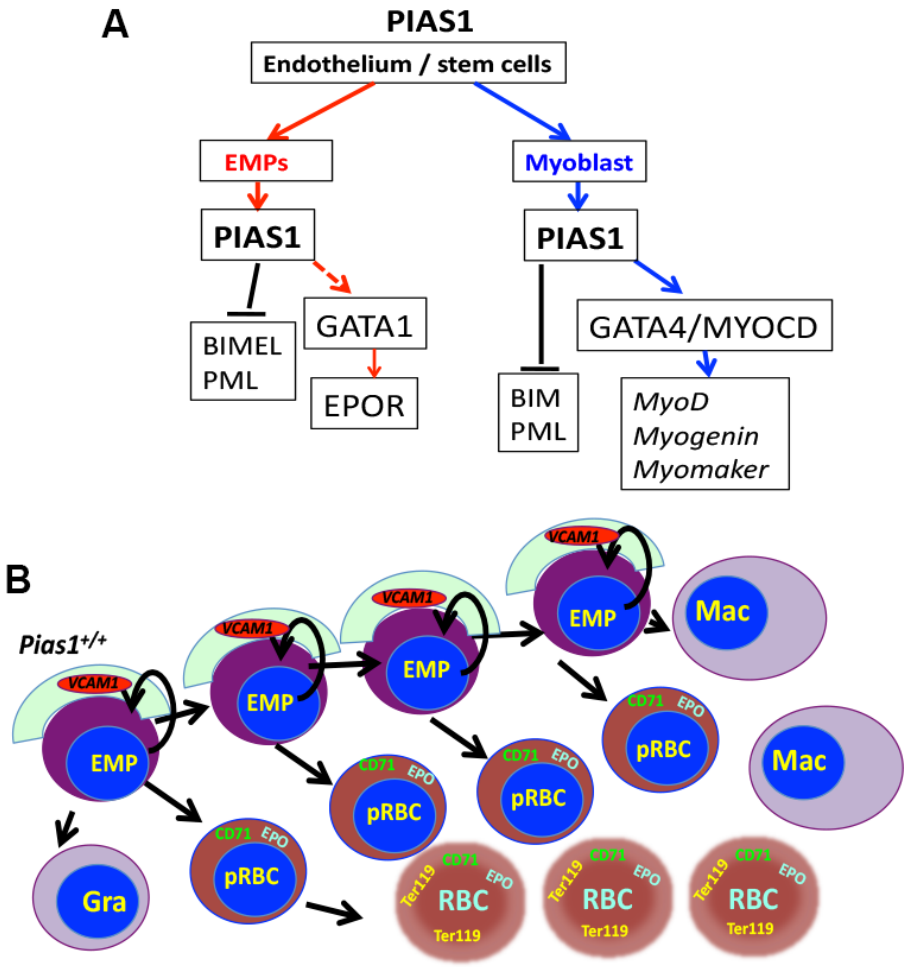

Figure 2.14 Proposed model for PIAS1 regulation of cell survival and differentiation during YS erythrogenesis and cardiovascular development. A, PIAS1 repression of PML and BIM proteins during embryogenesis protects ecto-mesoderm and erythromyeloid precursors (EMPs) from apoptosis during differentiation, potentially acting through GATA-1 and its downstream targets. On the other hand, PIAS1 enhances the transactivation of GATA-4 and MYOCD cardiac transcription factors during early heart development. **B**, Model illustrates the codependence of endothelium and EMPs of the YS for the maturation of RBC precursors (pRBC), macrophage (Mac) and Granulocytes (Gra) cells during YS early blood development.

2.4.0 Discussion

Several studies have investigated the function of *Pias1* in innate immunity, DNA repair and epigenetic regulation (Galanty et al., 2009; Liu et al., 2004; Liu et al., 2014b). However, the role of *Pias1* in embryonic development and tissue differentiation had not been previously studied. We report that *Pias1* loss in mouse embryos results in erythrogenic and angiogenic defects associated with ~90 % embryonic lethality. *Pias1* loss in early development results in deregulation of embryonic germ layer proliferation, severely decreasing the overall rate of embryonic growth. Furthermore, many tissues experience amplifying defects in cell survival and differentiation.

Others have shown that between E9.5 and E12.5 erythropoiesis is extremely important to support embryonic growth and survival (Maeda et al., 2009). We found that at this stage of embryonic development, erythroid cells are significantly depleted in the YS of *Pias1* null embryos. Furthermore, we demonstrated that *Pias1* loss is associated with a block of differentiation at the R2 stage of erythroid differentiation in the YS *in vivo*. Given the crosstalk between endothelial cells and erythroblasts, it is notable that our *in vitro* methyl cellulose assays indicate that *Pias1* null erythroid precursors have a concomitant cell autonomous defect.

The origin of YS erythroid cell populations, their relationship with the endothelium and contribution to definitive hemopoiesis is still under debate

(Auerbach et al., 1996; Lacaud et al., 2001; Myers and Krieg, 2013; Ueno and Weissman, 2006). Our *in vivo* experiments with *Tie2-cre* mice, which ablate *Pias1* in endothelial cells, indicate that *Pias1* is essential for the formation of the YS capillary plexus and blood islands, but has no obvious effect on liver erythropoiesis. A recent report has described the expansion of tissue resident macrophages originating from YS erythro-myeloid progenitors (EMPs), independently from definitive hematopoietic stem cells (HSCs) in the liver (Gomez Perdiguero et al., 2015). Constitutive and endothelial cell specific inactivation of *Pias1* gene in developing embryos results in a significant reduction of RBCs and higher number of macrophages in the YS. In light of our findings, we suggest that the EMP cell compartment within the YS may be regulated by PIAS1 through GATA-1 target genes to induce erythroid differentiation. However, previous reports disagree in whether SUMOylation repress or activates GATA-1 downstream gene transcription (Collavin et al., 2004; Lee et al., 2009; Liu et al., 2014b). In view of our findings, we propose that most likely PIAS1 is a positive regulator of GATA-1 during YS erythropoiesis. Further mechanisms underlying the function of PIAS1 in hematopoietic cells are likely related to the ability of PIAS1 to degrade the PML tumor suppressor, which exerts a well-known pro-apoptotic function (Bernardi and Pandolfi, 2003; Giorgi et al., 2010). Indeed, we found that *Pias1* loss is associated with upregulation of PML and BIM proteins both *in vitro* and *in vivo*.

In addition to YS erythroid deficiency, another important finding of our work is that in *Pias1*$^{-/-}$ embryos, the heart muscle mass is greatly reduced. Histological analysis and X-gal staining confirmed that *Pias1* gene loss results in reduced myocardial wall cellularity and negatively affects cardiac development. *In vitro* assays illustrate the involvement of PIAS1 in the regulation MYOCD and GATA-4 dependent transactivation of cardiac genes. Previous reports suggest that PIAS1 may play a role in cardiogenic transcription (Wang et al., 2004b; Wang et al., 2007; Wang et al., 2008). Thus, our results provide strong evidence for the requirement of PIAS1 in cardiac muscle development *in vivo,* and potentially for tissue regeneration following injury (Konstantinov et al., 2004; Tsai et al., 2011). We show that the lack of proper blood circulation and defective heart architecture promotes congestive heart failure in *Pias1*$^{-/-}$ embryos contributing to embryonic lethality at E12.5.

Together, our findings highlight PIAS1 as an essential regulator of YS erythrogenesis and cardiovascular development in the mouse embryo. We show that PIAS1 regulates erythroid and the macrophage cell lineage in the YS. Moreover, we show that *Pias1* is required for positive regulation of *MMP28*, *WNK1, SEMA3A genes* and inhibition of *TBSP1* in HUVEC endothelial cells. Moreover, inactivation of *Pias1* gene in embryonic endothelial cells *in vivo* recapitulates defective YS erythrogenesis and capillary plexus formation,

demonstrating the importance of this cell lineage for both erythroid and vascular development.

The identification of PIAS1 protein as a novel regulator of cardiovascular biology lays the foundation for future studies of *Pias1* gene function in normal biology and disease.

CHAPTER III

PIAS1-FAK interaction promote the survival and progression of non-small cell lung cancer cells

3.1.0 Introduction

PIAS1 was previously reported to be overexpressed in NSCLC and this correlates with the loss of the PML tumor suppressor, suggesting an involvement in tumor progression (Rabellino et al., 2012). Moreover, increase in PIAS1 protein levels has recently been linked to breast cancer tumorigenesis, albeit reports disagree as to the relevance of PIAS1 to tumorigenesis and metastasis (Dadakhujaev et al., 2014; Liu et al., 2014a). Thus we decided to characterize PIAS1 relevance to NSCLC tumor progression and metastasis. Moreover, we looked for PIAS1 downstream targets that could account for the discrepancy in phenotype and potentially serve as a therapeutic target of in NSCLC.

Lung cancer metastasis is an indicator of poor prognosis and a main determinant of cancer-related mortality. Consequently, targeting and prevention of cancer cell metastasis is among the biggest hurdles in clinical oncology to date (Frisch et al., 2013). During metastasis, cancer cells rely heavily on cell-extracellular matrix (ECM) interactions, cytoskeleton remodeling and gene transcription. An important player in these processes is focal adhesion kinase (FAK). FAK is a non-receptor tyrosine kinase that contributes to almost every aspect of metastasis; from ECM sensing, cytoskeleton remodeling to gene transcription (McKean et al., 2003; Pylayeva et al., 2009; Sieg et al., 1999; Wilson et al., 2014). The *FAK* gene is rarely mutated in human lung cancers, but

the *FAK* locus (chromosome 8q) is frequently amplified in lung, colon, breast and gastric tumors (Agochiya et al., 1999; Golubovskaya et al., 2009; Park et al., 2010; Rodenhuis et al., 1988).

FAK controls cytoskeleton remodeling by transducing signals from integrin receptors to ERK/MAPK, PI3K, RAC1 and RHOA (Carr et al., 2013; Chang et al., 2007; Konstantinidou et al., 2013; Pylayeva et al., 2009). Importantly, FAK promotes integrin β1 (ITGβ1) gene expression, which in turn, increases the survival of cancer cells (Eke et al., 2012). FAK has also been linked to transcriptional activation of *SNAIL*, *TWIST*, *ZEB1* and *ZEB2* genes, which are essential for epithelial to mesenchymal (EMT) reprogramming in epithelial cells (Chen et al., 2014a; Chen et al., 2014b; Li et al., 2012; Li et al., 2011). However, whether FAK is involved in transcriptional regulation is still a matter of debate because FAK resides mainly in the cytoplasm where it is associated with the plasma membrane. Nevertheless, FAK protein can relocate to the cell nucleus during cancer progression (Luo et al., 2009).

Despite several studies reporting FAK protein nuclear localization and involvement in gene transcription, no unifying mechanism exists to explain the nuclear accumulation of FAK and the potential implications of nuclear FAK for tumorigenesis and metastasis. Using single nucleotide polymorphism (SNPs) data, we discovered that *PIAS1* and *FAK* are frequently co-amplified in lung cancer

specimens. We found a positive correlation between increased gene copy number and FAK and PIAS1 protein levels in a subset of NSCLC cell lines *in vitro,* human lung tumor samples *in vivo* and in a mouse model of tumor metastasis. We report an interaction between FAK-PIAS1 that is crucial for the regulation of the turnover of focal adhesions and cell survival during oncogenic stress.

3.2.0 Materials and Methods

Gene copy number analysis. Single nucleotide polymorphism (SNP) was performed as previously described, (Rabellino et al., 2012). Briefly, SNP profile was obtained using Illumina DNA analysis Bead Chip (Illumina, Inc.). PIAS1 and FAK gene copy number was extrapolated from their relative probe intensity compared with diploid controls.

Histochemistry and antibodies. Formalin fixed, paraffin-embedded lung cancer specimens were obtained from the human tumor tissue bank at UTSW. Tissues were processed for IHC using standard protocols. Briefly, tissue slides were deparaffinized by placing slides in gradients of xylene, ethanol (100%; 90%; 75%), and water. Antigen retrieval and epitope unmasking was done boiling samples in 10mM Citrate pH 6.0 for 20min. Samples were cooled for 20 minutes and treated with 3% H2O2 for 1h to remove endogenous peroxidase activity. Endogenous antigens were blocked with 10% aquablock (East Coast Biologics,

No.: PP82-P0691) for 1h, incubated with 1:50 anti-PIAS1 (Abcam, No.: ab32219) or 1:50 anti-phospho-FAK (Y397) (Abcam, No.: ab39967) antibodies in 5% BSA/TBST overnight in wet chamber at 4°C. Tissues were washed four times with TBST for 5 minutes and incubated with HRP-conjugated secondary antibody for 2h at 4°C. Tissues were washed four times with TBST and signal detected with 3-3'-Diaminobenzydine (DAB) chromate system (Vector labs, No.: SK 4100).(Konstantinidou et al., 2013)

Cell lines and tissue culture. Human NSCLC cell lines HCC827, HCC44, 4006, H2228, H522, H460, H1299, H358, Calu-3, HCC95, H1993, H2073, H1395, H460, and HBEC3KT cells (HBEC3 normal epithelial cells, immortalized by introducing CDK4 and hTERT), were a gift from Dr. John Minna (UT Southwestern Medical Center). All these NSCLC have been fully characterized and authenticated by DNA barcode (Das et al., 2006; Phelps et al., 1996; Ramirez et al., 2004). Human cancer cells were cultured in RPMI supplemented with 5% serum and antibiotics. HBECS were grown in Keratinocyte growth media unless stated otherwise (Invitrogen, No.: 17005-042). Immortalized mouse fibroblast (NIH-3T3) cells were a gift from Dr. Laurence Lum (UT Southwestern Medical Center). NIH-3T3 cells were cultured in DMEM supplemented with 5% serum and antibiotics. All cells were maintained in humidified incubator with 5% C02 at 37°C.

RNAi interference. Stable PIAS1 knockdown was performed with pGIPZ vectors containing shRNA against PIAS1 (5'-CCGGATCATTCTAGAGCTTTA-3' No.: TRCN0000231898); (5'-TTTGCTGGGCTTTGCTATTTC-3'; No.: TRCN0000231555) and non-targeting scramble shRNA controls (Open biosystems, No.: RHS4346). Lentiviral particles were generated by transfection of HEK-293T cells with pGIPZ and helper plasmids (Addgene, No.: 84545; 8455). 4ug/mL Polybrene (SIGMA, No.: H9268) was used with viral supernatant to enhance transduction efficiency. siRNA (siGenome) against PIAS1, or non-targeting siRNA control were purchased from Dharmacon (Thermo Scientific) (Rabellino et al., 2012).

Western blotting. Cellular lysate was prepared with radioimmunoprecipitation assay buffer (RIPA buffer); 150 mM NaCl, 1.0% NP-40, 1.0% sodium deoxycholate, 0.1% SDS, 10 mM Tris, pH7.5, with protease and phosphatase inhibitors. Cells were lysed on ice, spun down to remove cell debris and protein concentration was measured using Bradford Assay (Biorad, No.: 500-0006). Proteins were resolved on 8% SDS-PAGE gel, transferred to nitrocellulose membrane, blocked for 1 hour in 5% non-FAT milk and incubated with primary antibody overnight. Finally, Blot was washed three times for 5 minutes in TBST with gentle agitation, probed with HRP-conjugated secondary antibody for 2

hours, washed three times for 5 minutes in TBST with gentle agitation and signal detected with West Pico Chemiluminescent substrate (Thermo Scientific, No.: 34080).

Subcellular fractionation protocol. Cellular fractionation was carried out as previously described (Gil del Alcazar et al., 2014); (Ramson H., et al AJPCP. 2013). Briefly, cells were scraped with ice-cold PBS, pellet by centrifugation at 600xg for 5 minutes, resuspended in hypotonic lysis buffer (10 mM Tris-base pH 7.5, 10 mM KCl, 1.5 mM MgCl2) with protease/phosphatase inhibitors and incubated for 10 minutes. Cells were lysed by Dounce homogenization and centrifuged at 3000xg to separate cytoplasmic (supernatant) from nuclear (pellet) fractions. To extract nuclear protein from the DNA rich fraction, a high salt buffer was used (50 mM Tris-base, pH 7.9, 0.5 M NaCl) 2 mM EDTA, 10% sucrose, 10% glycerol) with protease and phosphatase inhibitors. Finally, nuclear cellular fractions were dialyzed against TM buffer (50 mM Tris-base pH 7.5; 10 mM MgCl2; 2 mM EDTA; 20% glycerol; 100 mM KCl), spun down at 13000xg for 15 minutes to clarify lysate. Proteins concentration was measured with Bradford assay and resolved with SDS-PAGE.

Immunoprecipitation (IP). Whole cell lysate was prepared on ice using "IP-lysis buffer" (15 mM Tris-base pH7.5, 150 mM NaCl, 5 mM EDTA and 1.0

% NP40) with protease, phosphatase inhibitors. 1.0-1.5 mg of protein was incubated with Protein-A/G Sepharose beads (Invitrogen, No.: 101242) overnight with or without anti PIAS1 or anti-FAK antibodies. Beads were washed three times with IP-lysis buffer, boiled in 1:1 SDS/loading buffer and ran on SDS-PAGE gel. Western blotting was performed as described before(Konstantinidou et al., 2013).

Immunofluorescence. Cells were grown on top of round glass coverslips overnight, fixed in 4% PFA for 20 minutes, washed with cold PBS and incubated for 15 minutes in 30 mM NH4Cl. Cells were permeabilized with 0.1% Triton X-100 in PBS for 5 minutes, blocked in 0.02% sodium azide/20% Aquablock- PBS (East Coast Biologics, No.: PP82-P0691) for 1 hour. Cells were then incubated with anti-PIAS1 (Invitrogen, No.: 39-6600) and anti-FAK (Abcam, No.: ab39967) primary antibodies diluted 1:200 in 1% BSA/TBST overnight in wet chamber at 4°C. Cells were washed twice with cold PBS, incubated with alexa fluor488/568-conjugated secondary antibodies (1:500) and 4',6-diamidino-2-phenylindole (DAPI) (1:800) for 1 hour. Coverslips were washed twice in cold PBS and mounted with a drop of fluomount onto glass slides (Southern Biotech, No.: 0100-01). 40x magnification pictures were taken on a Leica DMI6000 inverted fluorescence microscope.

Live cell microscopy Live microscopy of green fluorescent protein-labeled FAK (GFP-FAK) and transient transfection of blue fluorescent protein-labeled PIAS1 (BFP-PIAS1) was performed by stable viral-transduction into HBECs. Cells were grown on serum free media for 16 hours then pulsed with 10nM recombinant EGF or serum media and imaged using Andor Spinning Disc confocal microscope at with 63x magnification objective.

Soft agar Colony formation assays. Anchorage-independent growth of NSCLC cells in soft-agar were performed following standard protocols. Briefly, A 0.5% agar base was prepared by mixing 1.0% agarose solution in 1xPBS with 1 volume of RPMI-1640 containing 10% FBS and 2x antibiotics. We used a 60-mm dish to make the bottom gel. Approximately, 2x104 Cells were mixed 2:1 with 1.0% agarose suspension solution at a final concentration of 0.3%, which was then layered onto the bottom agar. After 30-60 days incubation, pictures of the colonies were taken and colonies with more than 50 cells/colony in triplicate plates.

Transwell migration assays. Analysis of in vitro cell migration was done using Transwell inserts on 24 well/plates (Fisher, No.: 07-200-147) following recombinant EGF and or serum stimulation. Briefly, 5x104 cells were seeded into each insert of the 24-well plate and incubated at 37 °C overnight. Cells were

washed once with 1xPBS, fixed with 10% Formalin and stained with crystal violet. Following removal of the cells on the upper side of the 8.0um membrane with cotton-swabs, pictures of invading cells on the lower membrane were taken. Three random fields of these images were quantified and plotted per each insert.(Zhang et al., 2015)

Scratch assays. Cell migration upon scratch assay was conducted following standard protocols (Sieg et al., 1999).

Mouse xenografts. Briefly after stable knockdown-of PIAS1 protein, cell suspensions of shRNA scramble and shRNA-PIAS1 treated cells were prepared at concentration of 4x107 cells/mL. 100µL cell suspension (4x106 cells) was injected into 6-7 weeks old NOD-SCID mice. For this experiment 7-mice/ group/ cell line were used. Tumor growth was measured using a standard caliper. Tumor volume was determined by the equation: V = (L x W x H) x 0.5, where L is length, W is the width and H is the height of the tumor in mm3. Mice were sacrificed when tumors reached ~2.0 cm3 or developed sign of distress (Konstantinidou et al., 2009).

Complete Antibodies list:

1. 4'-,6-diamidino-2-phenylindole (DAPI); Life technologies, No.: D1306 (1:800).

2. GADPDH; Santa Cruz, No.: sc-32233 (1:2000)

3. BIM; Cell signaling, No.: 2933 (1:1000)

4. ACTIN; SIGMA, No.: A2066 (1:2000)

5. PIAS1; Cell signaling No.: 3350 (1:1000)

6. PIAS1; Abcam No.: Ab32219 (1:100)

7. FAK; Cell signaling No.: 3285 (1:1000)

8. FAK; Abcam No.: Ab40794 (1:1000)

9. Lamin B; Santa Cruz.: SC 6216 (1:1000)

10. RAB11; Cell signaling No.: 5589 (1:200-1000)

11. RAC1; Cell signaling No.: 2465 (1:1000)

12. Calpain Millipore No.: MAB3104 (1:1000)

13.LAMP1; Cell signaling No.: 9091 (1:200-1000)

14 Calnexin Cell signaling No.: 2679 (1:1000)

15. mCherry; Abcam no.: Ab125096 (1:200-1000)

16. GFP; SIGMA No.: G1544 (1:2000)

17. ROCK1; Cell signaling No.: 4035 (1:1000)

3.3.0 Results

***3.3.1 FAK* and *PIAS1* genes are frequently co-amplified in a subset of NSCLCs**

Using single nucleotide polymorphism (SNPs) gene copy number analysis we looked for novel genomic cooperating alterations in a panel of over 100 non-

small cell lung cancer (NSCLC) cells. This analysis revealed that approximately 8% of NSCLC cells had amplification of the *FAK* and/or *PIAS1* genes (Figure 3.1A).

To investigate the relationship between gene copy number gain and gene expression we detected FAK and PIAS1 by immunoblot in cell lines representative of our larger panel of NSCLC cells. We found that changes in protein amounts were concordant with gene copy number variations (Figure 3.1B). Since gene amplification/deletions may result from adaptive responses to selective pressures of tissue culture, we tested primary NSCLC specimens for FAK and PIAS1 proteins using immunohistochemistry (IHC). We found that primary NSCLC samples exhibited elevated total FAK (tot-FAK), phospho-FAK (p-FAK; Y397) and PIAS1 positivity compared to normal surrounding tissue (Figure 3.1C, arrowhead).

Using lung tumor tissue microarrays we further confirmed that samples with high tot-FAK positivity score had a concomitant increase in PIAS1 positivity, but not p-FAK positivity (Figure 3.1D). Because FAK has previously been associated with metastatic cancer progression (Luo et al., 2009), we also tested several paired primary and metastatic human NSCLC samples for FAK and PIAS1 protein levels. As observed in primary lung tumor samples, we found a

positive correlation with FAK and PIAS1 protein levels in lymph node metastasis (Figure 3.1E and 3.1F).

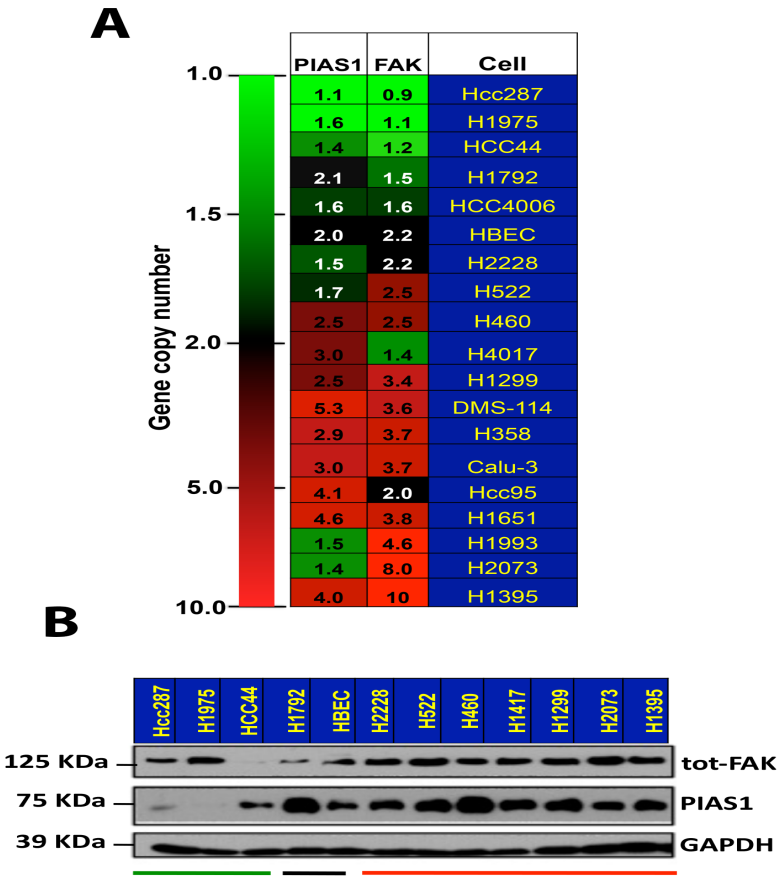

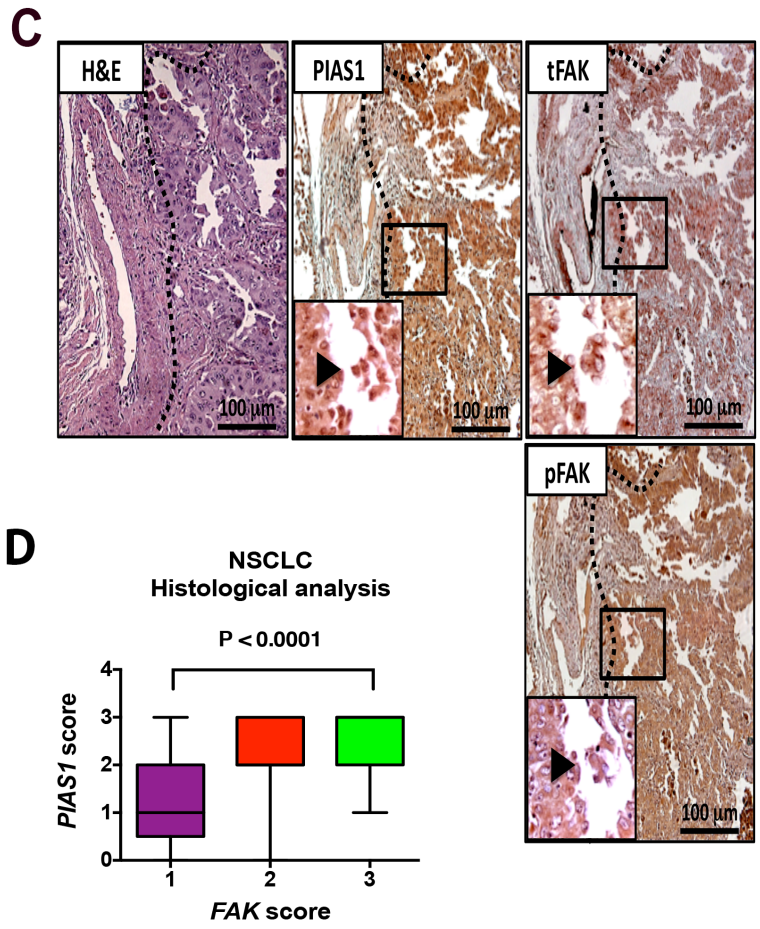
C
H&E
PIAS1
tFAK
pFAK
100 µm
D
NSCLC
Histological analysis
P < 0.0001
PIAS1 score
FAK score
0
1
2
3
4

E

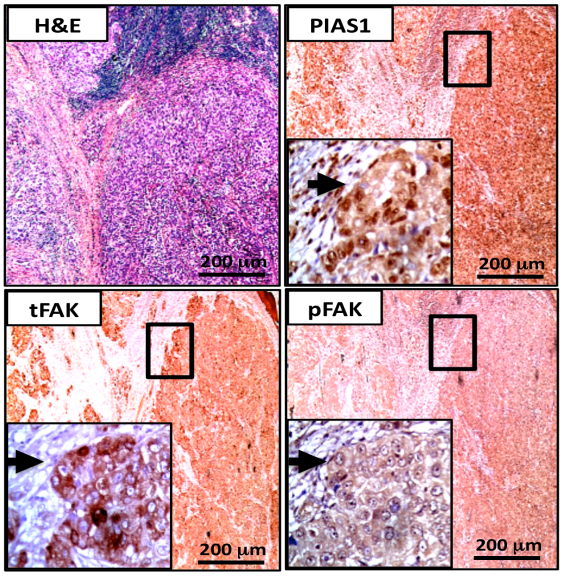

F

n= 16 lung adenocarcinomas

Tumor type	PIAS1 Positive	FAK Positive	Double positive
Primary	9/16 56%	5/16 30%	4/16 25%
Metastasis	9/10 90%	6/10 60%	5/10 50%

Figure 3.1 FAK and PIAS1 protein levels are correlated in NSCLC. **A**, Heat map shows single nucleotide polymorphism (SNPs) gene copy number analysis for *FAK* and *PIAS1* genes in the indicated lung cancer cell lines. Green, black and red indicate copy number loss, no change or gene copy number gain, respectively. **B**, Immunoblot confirms increment in FAK and PIAS1 at the proteins in a representative panel of cells with gene amplification. Green, black and red horizontal lines indicate NSCLC cells with loss, neutral and gain of *PIAS1* and *FAK*. **C**, Hematoxylin and eosin (H&E) and IHC stain of PIAS1, phospho-FAK (pFAK) and total FAK in primary NSCLC samples. Insert shows cytoplasmic and nuclear positivity for both proteins (black arrowheads). Scale bar: 100 μm. **D**, IHC positivity score analysis of FAK and PIAS1 in human NSCLC tumor tissue microarrays samples (n=330). Graph shows positive correlation between increase

positivity in FAK stain and PIAS1. Score=1 low intensity; 2= moderate intensity; 3 high intensity. Statistical analysis was done using a Mann-Whitney U test. **E**, H&E and IHC stain of PIAS1, phospho-FAK (pFAK) and total FAK in metastatic NSCLC. Insert shows positivity for cytoplasmic and nuclear stain for both proteins. Scale bar: 200 μm. **F,** Contingency table shows positive correlation between FAK and PIAS1 IHC stain positivity in primary *vs* metastatic samples. The number of samples is indicated.

The $Kras^{G12D}/p53^{R172H}$ mouse model (KP hereafter) faithfully recapitulates aggressive human lung adenocarcinoma, developing advanced lung tumors that are highly metastatic (Zheng et al., 2007; Gibbons et al., 2009). Metastatic lung tumors in this mouse model have been fully characterized and show elevated expression of the *ZEB1* transcription factor and activation of Notch1 and Jagged2 signaling pathways, recapitulating the EMT profiles associated with human metastatic NSCLC (Yang et al., 2014; Yang et al., 2011b). As in human NSCLC, we found that KP lung tumors are positive for total-FAK and PIAS1, but not for p-FAK (Figure 3.2A). Next we took advantage of 393P and 344SQ lung cancer lines, which are a pair of lung cancer cell lines derived from a KP lung specimen. 393P cells, were derived from a primary lung tumor, are epithelial and have low metastatic potential; while 344SQ cells were derived from a metastatic KP lung tumor, are mesenchymal and are highly metastatic (Gibbons et al., 2009). In this experimental system we found that PIAS1 is significantly unregulated *in vivo* and metastatic cell line 344SQ (Figure 3.2B).

In view of these findings, we concluded that co-amplification of *FAK* and *PIAS1* genes occurs in a subset of primary NSCLC samples. Moreover, subsets of primary and metastatic NSCLC samples have elevated tot-FAK and PIAS1 protein levels.

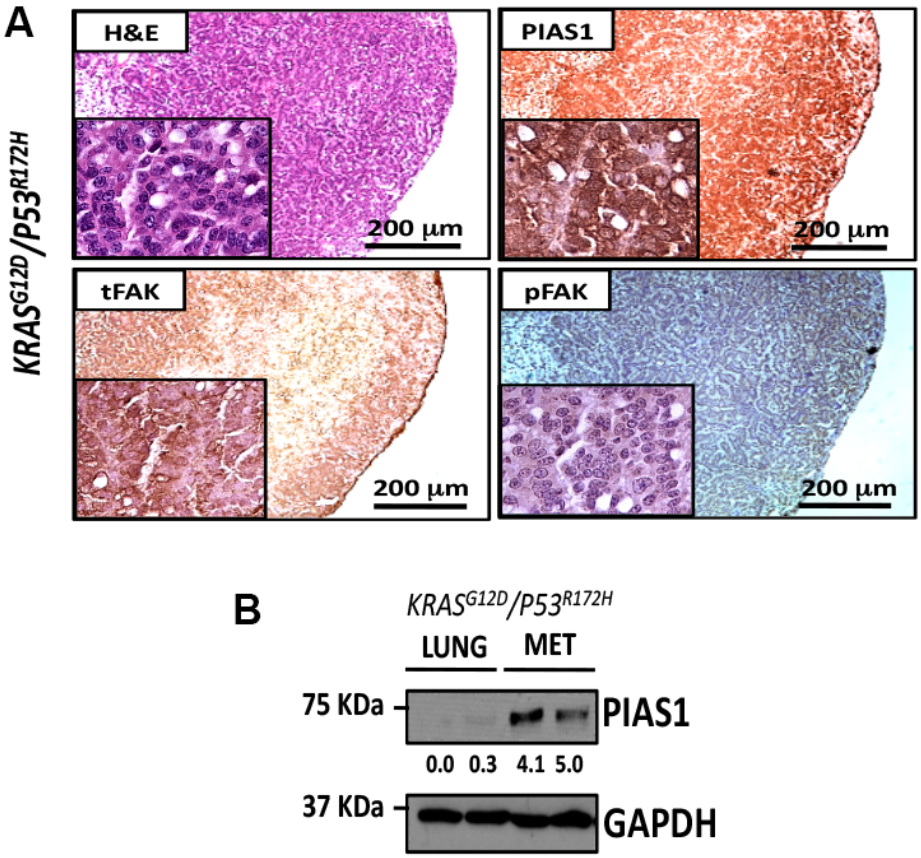

Figure 3.2 Activation of oncogenic *KRAS*^{G12D} in *p53R*^{172H} (KP) mice promotes an increase in FAK and PIAS1s. **A**, H&E and IHC analysis of lung tumors samples of KP mice stained as indicated. Insert shows area magnified. **B**, Immunoblot for PIAS1 in established cell lines from the KP mouse tumors. Blot shows over four-fold increase total PIAS1 protein in metastatic cell lines. Lung:

393P, non-metastatic lung cancer cells; 344SQ metastatic lung cancer cells, both derived from KP mice lung tumors.

3.3.2 PIAS1 and FAK proteins interact in NSCLC

We tested whether FAK and PIAS1 physically interact with co-IP assays using NIH-3T3 cells transiently transfected with *FAK or PIAS1* cDNAs. We co-immunoprecipitated FAK with PIAS1 from transfected NIH-3T3 cells (Figure 3.3 A). Furthermore, we co-immunoprecipitated endogenous FAK and PIAS1 proteins in several NSCLC cells, which co-amplify *FAK* and *PIAS1* genes (Figure 3.3B).

To gain insights into the location and stimulus required for FAK and PIAS1 interaction, we performed cellular co-fractionation of endogenous proteins during serum starvation, apoptosis or mitogenic stimulation. To our surprise, we discovered that FAK and PIAS1 mostly co-purified in the cytosolic fractions, when cells were treated with protein kinase C inhibitor (PKCi; Calphostin-C, a proapoptotic agent), or serum for 2-4 hours post starvation, but not after stimulation with epithelial growth factor (EGF) (Figure 3.3C lanes 5, 7 and 10). This finding suggests that pro-apoptotic and mitogenic stimuli promote FAK and PIAS1 protein interaction. Using immunofluorescence (IF) and confocal microscopy we found significant co-localization of endogenous FAK and PIAS1 at the nuclear periphery of serum treated cells (Figure 3.3D). We subsequently

performed immunoblot and confocal co-localization studies with well-characterized organelle markers following serum stimulation. Although partial localization of PIAS1 and FAK can be seen with the endoplasmic reticulum protein Calnexin, the dominant sites of interaction contain the RAB11 and LAMP1, endosome associated proteins (Figure 3.3E-G). These findings suggest that downstream activation of growth factor receptors promote the association of FAK and PIAS1 proteins in endosomes localized in the cytoplasm and nuclear periphery.

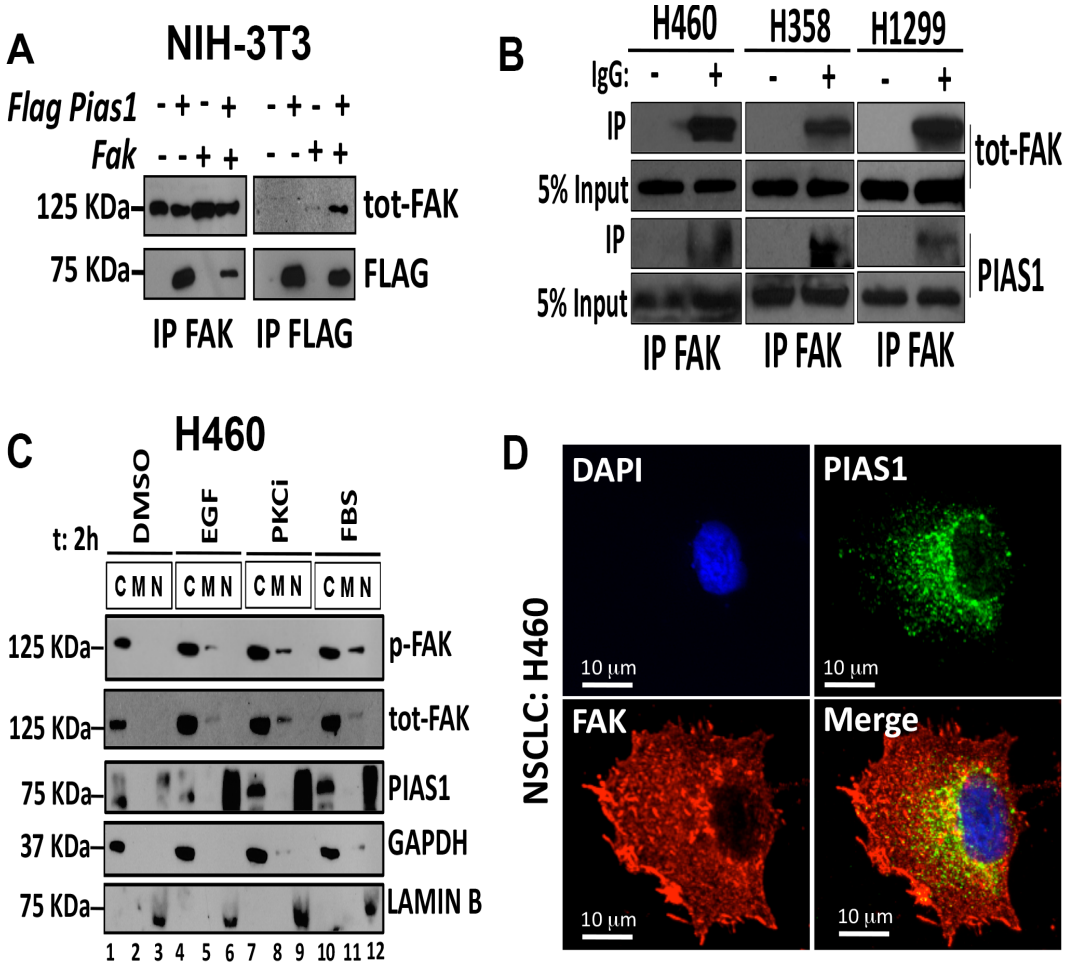
A
NIH-3T3
Flag Pias1 - + - + - + - +
Fak - - + + - - + +
125 KDa
tot-FAK
75 KDa
FLAG
IP FAK IP FLAG
B
H460 H358 H1299
IgG: - + - + - +
IP
tot-FAK
5% Input
IP
PIAS1
5% Input
IP FAK IP FAK IP FAK
C
H460
t: 2h
DMSO EGF PKCi FBS
C M N C M N C M N C M N
125 KDa
p-FAK
125 KDa
tot-FAK
75 KDa
PIAS1
37 KDa
GAPDH
75 KDa
LAMIN B
1 2 3 4 5 6 7 8 9 10 11 12
D
NSCLC: H460
DAPI
PIAS1
FAK
Merge
10 μm

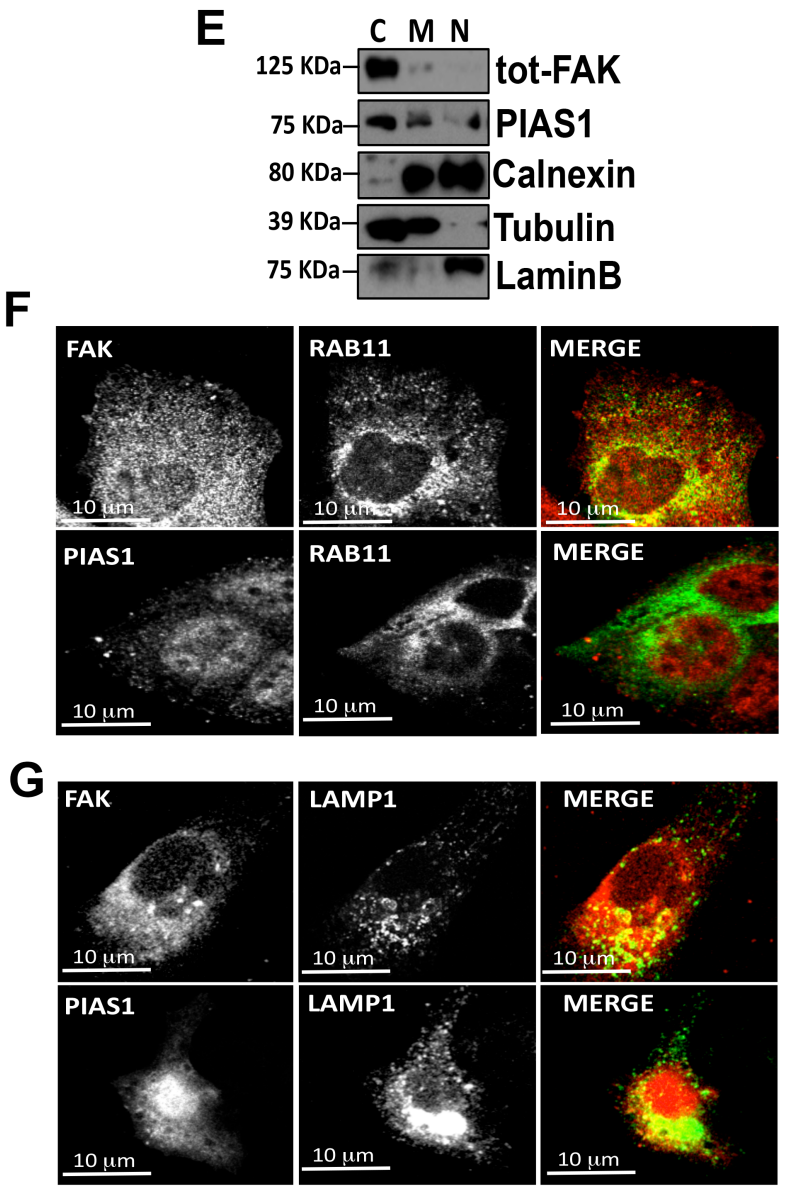
E
C M N
125 KDa
tot-FAK
75 KDa
PIAS1
80 KDa
Calnexin
39 KDa
Tubulin
75 KDa
LaminB
F
FAK
RAB11
MERGE
PIAS1
RAB11
MERGE
G
FAK
LAMP1
MERGE
PIAS1
LAMP1
MERGE
10 µm

Figure 3.3 PIAS1 and FAK physically interact in human NSCLC cell lines. **A**, NIH 3T3 cells were transiently transfected with the indicated plasmids and FAK and PIAS1 protein interaction was analyzed by co-IP followed by immunoblotting. **B**, Immunoblot showing endogenous PIAS1 and FAK protein co-IP in the indicated NSCLC cell lines. **C**, Subcellular fractionation and immunoblotting of endogenous FAK and PIAS1 proteins was performed in serum starved lung cancer cells H460 following treatment with: DMSO; EGF; protein kinase C inhibitor Calphostin (PKCi) and 10% FBS. Fractions: C; cytosolic; M; matrix; N: nuclear. Note significant cytoplasmic accumulation in PKCi and serum treatment, but not with EGF. **D**, IF and confocal micrograph of FAK (red) and PIAS1 (green) localization at nuclear periphery in H460 NSCLC cells. Scale bar: 10um. **E**, Immunoblot shows co-fractionation of tot-FAK and PIAS1 with endoplasmic reticulum resident protein Calnexin, Tubulin and nuclear membrane protein Lamin B. **F**, Confocal microscopy of H460 NSCLC stained with the indicated antibodies. Note the co-localization of FAK and PIAS1 with the late endosome protein RAB11. **G**, Confocal microscopy of H460 NSCLC stained with the indicated antibodies. Note the co-localization of FAK and PIAS1 with the late endosome protein Lamp1.

To begin testing the biological significance of the interaction between FAK and PIAS1, we determined the effects of *Flag-Pias1* and or SUMO overexpression on FAK protein using non-transformed mouse fibroblasts. We found that overexpression of *Flag-Pias1* or SUMO-1 did not promote a significant change in tot-FAK or p-FAK (Figure 3.4A). However, expression of *Flag-Pias1* or the combination of *Flag-Pias1* and SUMO1 resulted in the appearance of a lower molecular weight species of FAK (Figure 3.4A arrowheads). FAK was previously reported to undergo proteolytic cleavage by Calpain proteases on its C-terminus to allow disengagement from focal adhesions (Chan et al., 2010). Indeed, we found that in *Flag-Pias1* overexpressing cells FAK-Calpain interaction is significantly increased (Figure 3.4B). To test whether

PIAS1 contributes to FAK C-terminal cleavage we used a mutant (Fak^{V744G}) that abolishes FAK protein C-terminal cleavage. Indeed, we found that the Fak^{V744G} is resistant to PIAS1-induced FAK C-terminal proteolysis (Figure 3.4C).

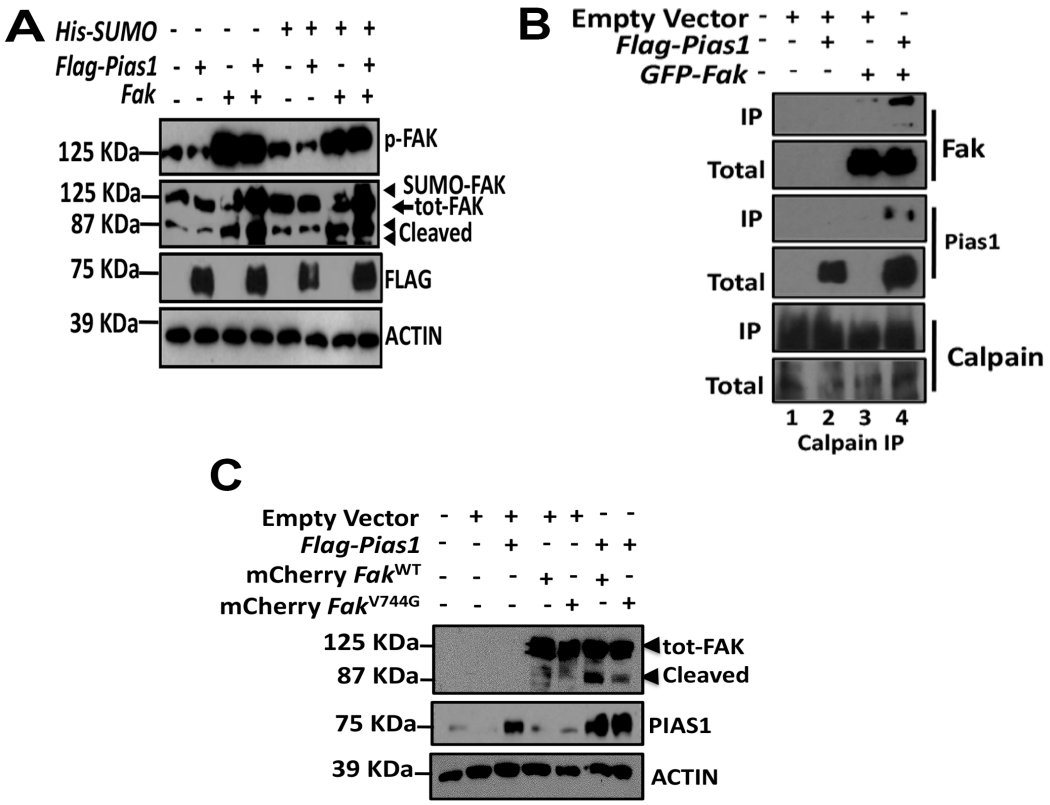

Figure 3.4 PIAS1 promotes FAK-Calpain interaction and FAK c-terminal proteolysis. **A,** Immunoblot following *Flag-Pias1* and *Fak* overexpression in NIH-3T3. Blot shows no change in total FAK or pFAK (Y397), but note the appearance of low and higher molecular weight species of FAK protein in cells overexpressing *Flag-Pias1* or *Flag-Pias1-SUMO1* overexpression, which correspond to SUMOylated-FAK and cleaved FAK. **B**, IP against Calpain protein

in cells over expressing *Flag-Pias1, GFP-Fak or the* combination. Note the increase in *GFP-Fak* co-purifying with Calpain in *Flag-Pias1* overexpressing cells. **C**, Cells were transfected with *mCherry-Fak*^{wt} or mCherry-*FAK*^{V744}, a cleavage resistant mutation, in combination with *Flag*-Pias1 and analyzed with immunoblot as indicated. Note that *Flag-Pias1* promotes the cleavage of *mCherry-Fak*^{wt} as expected, but cleavage of C-terminus mutant *FAK*^{V744G} is impaired.

Thus, we concluded that mitogenic signaling promotes FAK and PIAS1 physical interaction, which correlates with PIAS1-induced FAK C-terminal cleavage. Importantly, this phenotype is rescued by using a *FAK* mutant resistant to proteolytic cleavage.

3.3.4 PIAS1-FAK interaction regulates focal adhesion dynamics

We found that in primary human NSCLC endogenous PIAS1 is mostly nuclear, but can also be found scattered in the cytoplasm of lung cancer cells *in vivo* and *in vitro*. We hypothesized that PIAS1-FAK interaction may affect focal adhesion dynamics and how cells integrate extracellular signaling. To test this hypothesis, we used RNAi to determine how *PIAS1* affects F-Actin stress fiber formation. We found that *PIAS1* silencing in lung cancer cells destabilizes F-Actin fibers and reduces Vinculin (VCL) localization to focal adhesions (Figure

3.5A). Then we tested if the opposite was true using human bronchoalveolar epithelial cells (HBECs), which are immortalized, but not transformed, by transduction of CDK4 and human Telomerase Reverse Transcriptase (hTERT) (Ramirez et al., 2004). Indeed, we found that ectopic expression of *PIAS1* (*Flag-Pias1*) in HBECs increases VCL puncta at focal adhesions, while also promoting the nuclear localization of GFP-FAK (*GFP-Fak*) (Figure 3.5B). We tested for changes in VCL puncta formation in live cells using mCherry labeled VCL (*mCherry-VCL*). We measured the formation, duration and turnover of mCherry-VCL focal adhesion, as inverse correlation to FAK-dependent turnover of focal adhesions (Chan et al., 2010; Sieg et al., 1999). Compared to control shRNA, *PIAS1* silencing increased the turnover of mCherry-VCL puncta; along the leading and lagging edge of cells (Figure 3.5C-F). Furthermore, we found that *Flag-Pias1* gene expression induces membrane ruffle formation in NIH-3T3 fibroblasts and rescues endogenous VCL puncta loss in *GFP-Fak* expressing cells (Figure 3.6A). Interestingly, induction of membrane ruffles by PIAS1 correlates with increases in Rac1-GTPase and ROCK-1 protein levels without an increase in pFAK levels (Figure 3.6C).

In view of these findings we concluded that PIAS1 regulates focal adhesion dynamics, promotes FAK nuclear localization and facilitates cell motility.

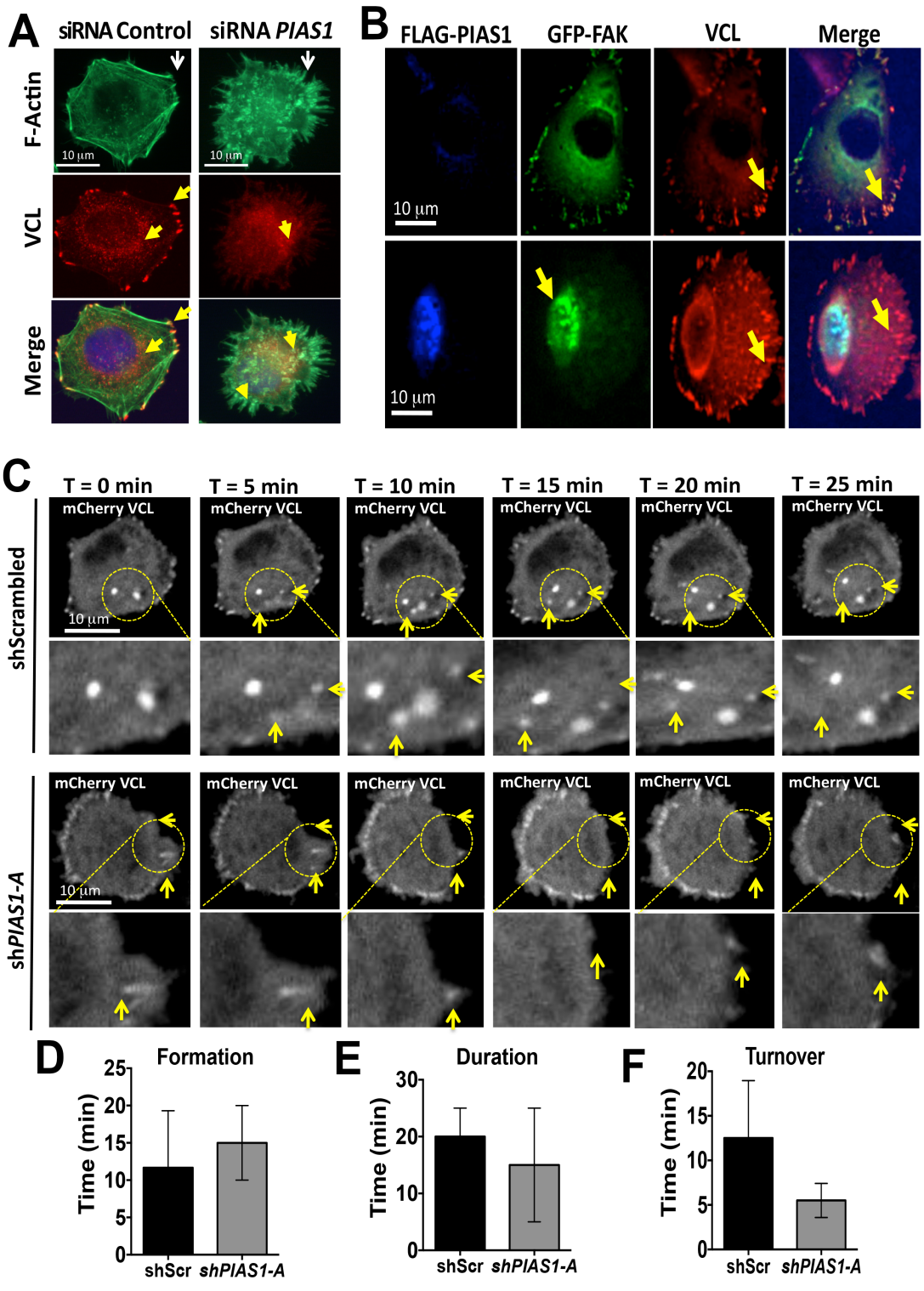
A
siRNA Control
siRNA PIAS1
F-Actin
VCL
Merge
10 μm
B
FLAG-PIAS1
GFP-FAK
VCL
Merge
10 μm
C
T = 0 min
T = 5 min
T = 10 min
T = 15 min
T = 20 min
T = 25 min
shScrambled
shPIAS1-A
mCherry VCL
10 μm
D
Formation
Time (min)
shScr
shPIAS1-A
E
Duration
Time (min)
shScr
shPIAS1-A
F
Turnover
Time (min)
shScr
shPIAS1-A

Figure 3.5 *PIAS1* silencing reduces stable stress fiber formation. A, IF image of filamentous Actin (F-Actin) fiber formation in H460 NSCLC cells. White arrows indicate F-Actin fibers in control siRNA treated cells (Ctrl siRNA) or following *PIAS1* gene silencing; yellow arrows indicates Vinculin (VCL) protein localization to F-Actin fibers, which is lost in cells with *PIAS1* silencing. Scale bar: 10 μm. **B**, IF image of VCL and GFP-FAK co-localization at F-Actin fibers in HBECs cells following ectopic *Flag-Pias1* expression. Top row shows HBECs cells expressing ectopic *GFP-Fak* and endogenous *VCL*. Bottom row image shows HBECs expressing ectopically expressed *Flag-Pias1* and GFP-FAK stained as indicated. Note FAK nuclear accumulation and increase in VCL puncta at focal adhesions (yellow arrows). Pink arrows indicate co-localization of GFP-FAK and VCL proteins. Scale bar: 10 μm. **C**, Confocal live imaging of H460 NSCLC cells examining *mCherry-VCL* puncta formation dynamics in cells expressing the indicated shRNA. Yellow arrows indicate sites of rapid focal adhesion turnover over a time lapse of 25 minutes. **D-F**, Histograms show the average time for *mCherry-VCL* puncta formation, duration and turnover. Values represent an average of n=3 cells.

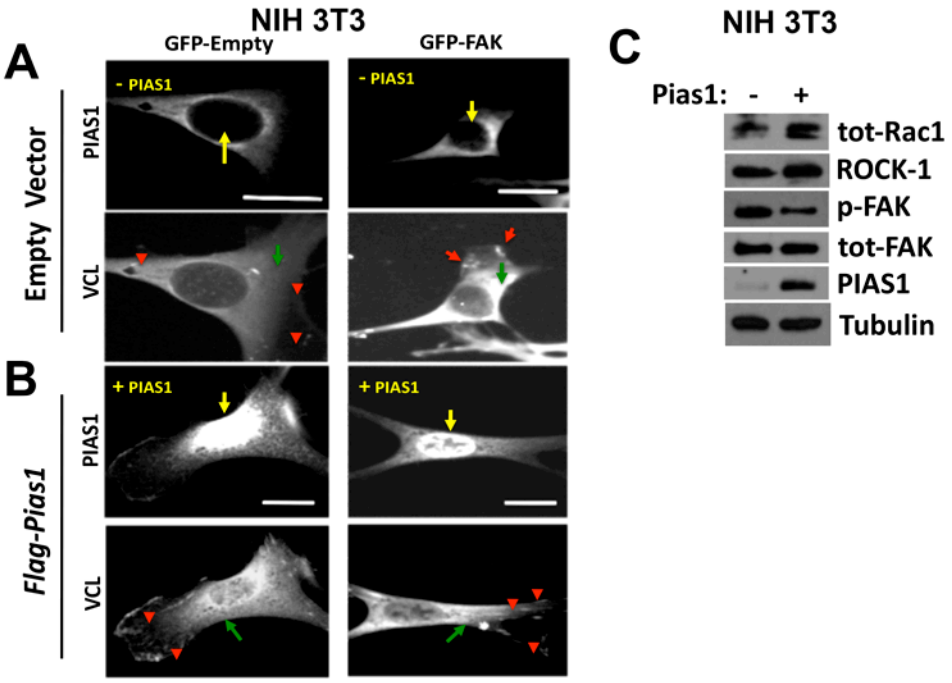

Figure 3.6 *PIAS1* expression promotes lamellipodia formation in NIH-3T3 fibroblast. A, IF image of NIH-3T3 cells stably transduced with the indicated retroviral vectors. Yellow arrows indicate FLAG-PIAS1, red arrows show VCL at focal adhesions and green arrow indicate internalized VCL. **B**, IF image of NIH-3T3 cells stably transduced with the indicated retroviral vectors. Yellow arrows indicate FLAG-PIAS1, red arrows show VCL at focal adhesions and green arrow indicate internalized VCL. **C**, Immunoblot of NIH-3T3 transiently transfected with empty vector or Flag-*Pias1* shows increase in integrin downstream effector proteins Rac1-GTPase and ROCK-1, with a modest decrease in p-FAK protein.

3.3.5 PIAS1 silencing impairs the ability of NSCLC cells to form colonies on soft agar and reduce directional migration in vitro

To elucidate how PIAS1-FAK interaction can modulate lung cancer progression we tested the effect of *PIAS1* inhibition on cell proliferation and survival. We found that *PIAS1* silencing with a short hairpin RNA (shRNA) had a modest effect on cell growth on plastic for most NSCLC cell lines (Figure 3.7A). Because FAK activity has been associated with the ability of cells to grow in an anchorage independent manner, we examined how *PIAS1* inhibition would affect growth of NSCLC cells in soft agar. Indeed, following *PIAS1* inhibition, we observed a marked reduction in colony formation in soft agar assays (Figure 3.7B-D). Next we tested whether *PIAS1* inhibition may result in defective p-FAK activation, which could explain the inability of NSCLC cells with silenced *PIAS1* to establish colonies in soft agar assays. Surprisingly, p-FAK levels did not correlate with soft agar growth impairment in lung cancer cells (Figure 3.7E). However, *PIAS1* silencing promotes increase baseline levels of pro-apoptotic protein BIM in several lung cancer cells including: H2228 and H1395 (Figure 3.7F). This finding suggests that *PIAS1* silencing lowers the threshold for apoptosis in NSCLC cells.

Our analysis of human NSCLC samples suggested that PIAS1 and FAK proteins are elevated in a subset of highly invasive tumors. Thus, we tested whether *PIAS1* silencing affects NSCLC cell invasion and migration potential *in*

vitro. To do this, we performed Transwell migration and scratch assays in NSCLC cells with gene amplification of *FAK* and *PIAS1* (Chen et al., 2014b; Zhang et al., 2015). In Transwell assays, H460 cells expressing the control shRNA completed migration after 16 hours (16h), whereas cells expressing a shRNA targeting *PIAS1* showed reduced migration through Transwell membranes (Figure 3.7G-H). These findings were replicated in H1395 cells, a NSCLC cell line with gene amplification of *FAK* and *PIAS1* (Figure 3.7I-J). These results suggest that *PIAS*1 suppression significantly reduce the migration capacity of NSCLC cells. Thus, we performed scratch migration assays using NSCLC cells: H1792, H522 and H460 as representative examples of NSCLC cells from our panel. We found that *PIAS1* suppression did not have an effect on H1972, which has a loss of *FAK* gene copy number, but reduced the migration of H522 and H460, which have substantially higher levels of FAK and PIAS1 protein (Figure 3.8A-F). We assessed for changes in the cytoskeleton following scratch formation in H460 cells by staining for F-Actin and cells polarity with the GM130 Golgi maker. After 8 hours, cells transfected with the siRNA control were oriented towards the scratch site, whereas cells with *PIAS1* silencing were not, suggesting reduced ability to polarize towards the stimulus (Figure 3.8G-H).

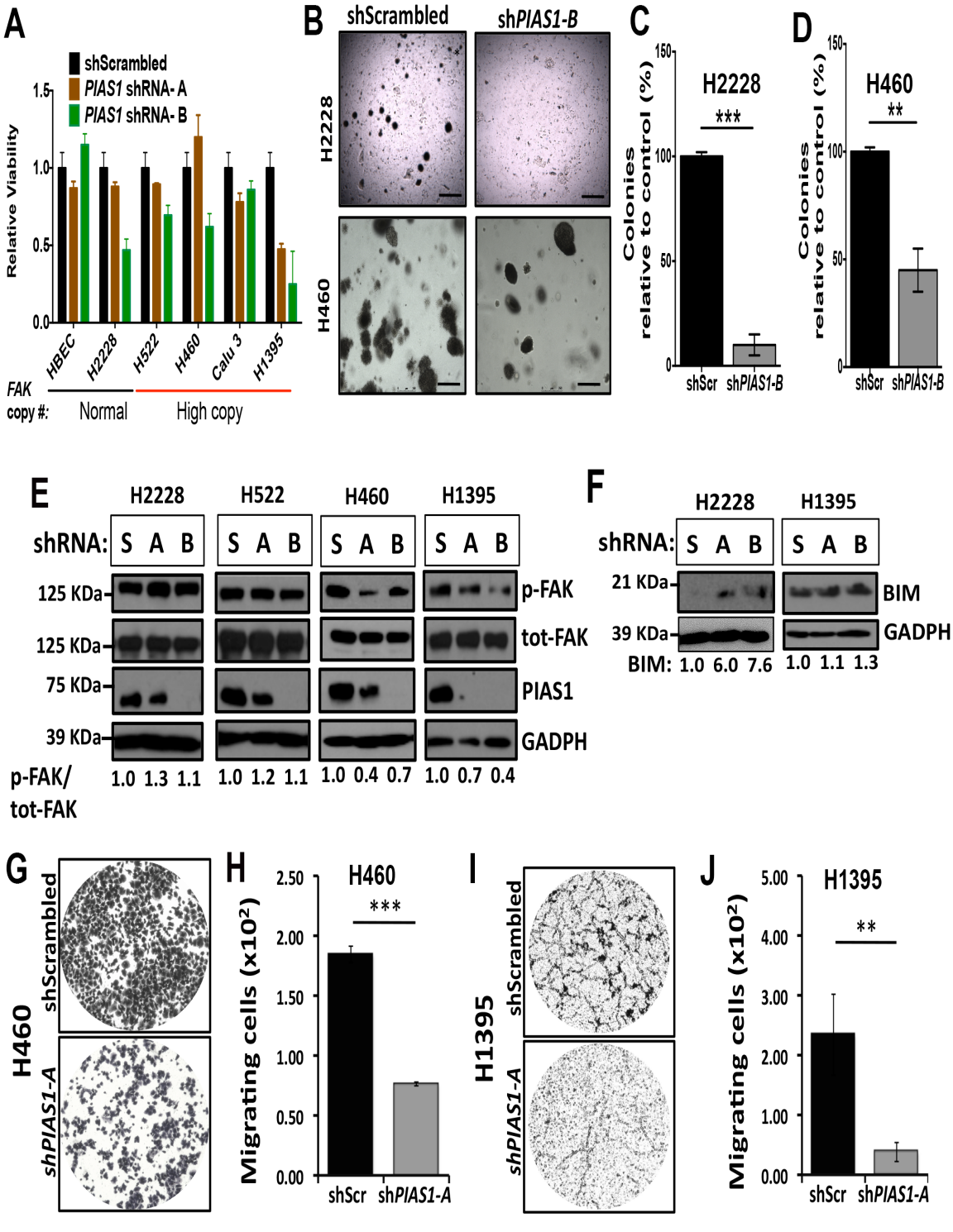
A
shScrambled
PIAS1 shRNA-A
PIAS1 shRNA-B
Relative Viability
1.5
1.0
0.5
0.0
HBEC
H2228
H522
H460
Calu 3
H1395
FAK copy #:
Normal
High copy
B
shScrambled
shPIAS1-B
H2228
H460
C
H2228
***
Colonies relative to control (%)
150
100
50
0
shScr
shPIAS1-B
D
H460
**
Colonies relative to control (%)
150
100
50
0
shScr
shPIAS1-B
E
H2228
H522
H460
H1395
shRNA: S A B S A B S A B S A B
125 KDa
125 KDa
75 KDa
39 KDa
p-FAK
tot-FAK
PIAS1
GADPH
p-FAK/ tot-FAK
1.0 1.3 1.1
1.0 1.2 1.1
1.0 0.4 0.7
1.0 0.7 0.4
F
H2228
H1395
shRNA: S A B S A B
21 KDa
39 KDa
BIM
GADPH
BIM: 1.0 6.0 7.6
1.0 1.1 1.3
G
H460
shScrambled
shPIAS1-A
H
H460
***
Migrating cells (x10²)
2.50
2.00
1.50
1.00
0.50
0.00
shScr
shPIAS1-A
I
H1395
shScrambled
shPIAS1-A
J
H1395
**
Migrating cells (x10²)
5.00
4.00
3.00
2.00
1.00
0.00
shScr
shPIAS1-A

Figure 3.7 *PIAS1* silencing impairs tumor progression in NSCLC cells with *FAK* gene amplification. **A**, Histogram shows cell viability following *PIAS1* gene silencing. *FAK* gene copy number status is also indicated. **B**, Representative soft agar colonies formation of NSCLC cells expressing the indicated shRNA. Scale bar: 500 μm. **C**, Quantification of soft agar colonies of H2228 NSCLC cells 3 weeks post plating. **D**, Quantification of soft agar colonies of H460 NSCLC cells 10 days post plating. **E**, H2228, H522, H460 and H1395 NSCLC cells were treated with the indicated shRNA and analyzed by Immunoblot with the indicated antibodies. **F**, Immunoblot following *PIAS1* shRNA knockdown in H2228, H460 and H1395 NSCLC cells shows BIM pro-apoptotic protein upregulation. **G**, Representative image of a Transwell migration assay performed with H460 cells expressing the indicated shRNA. **H**, Histogram shows the absolute number of migrating cells in triplicate wells following PIAS1 knockdown in lung cancer cell line H460. Student's t-test = ***P<0.001. **I**, Representative image of a Transwell migration assay performed with H1395 cells expressing the indicated shRNA. **J**, Histogram shows the absolute number of migrating cells in triplicate wells following *PIAS1* knockdown in H1395 cells. Student's t-test = **P<0.01.

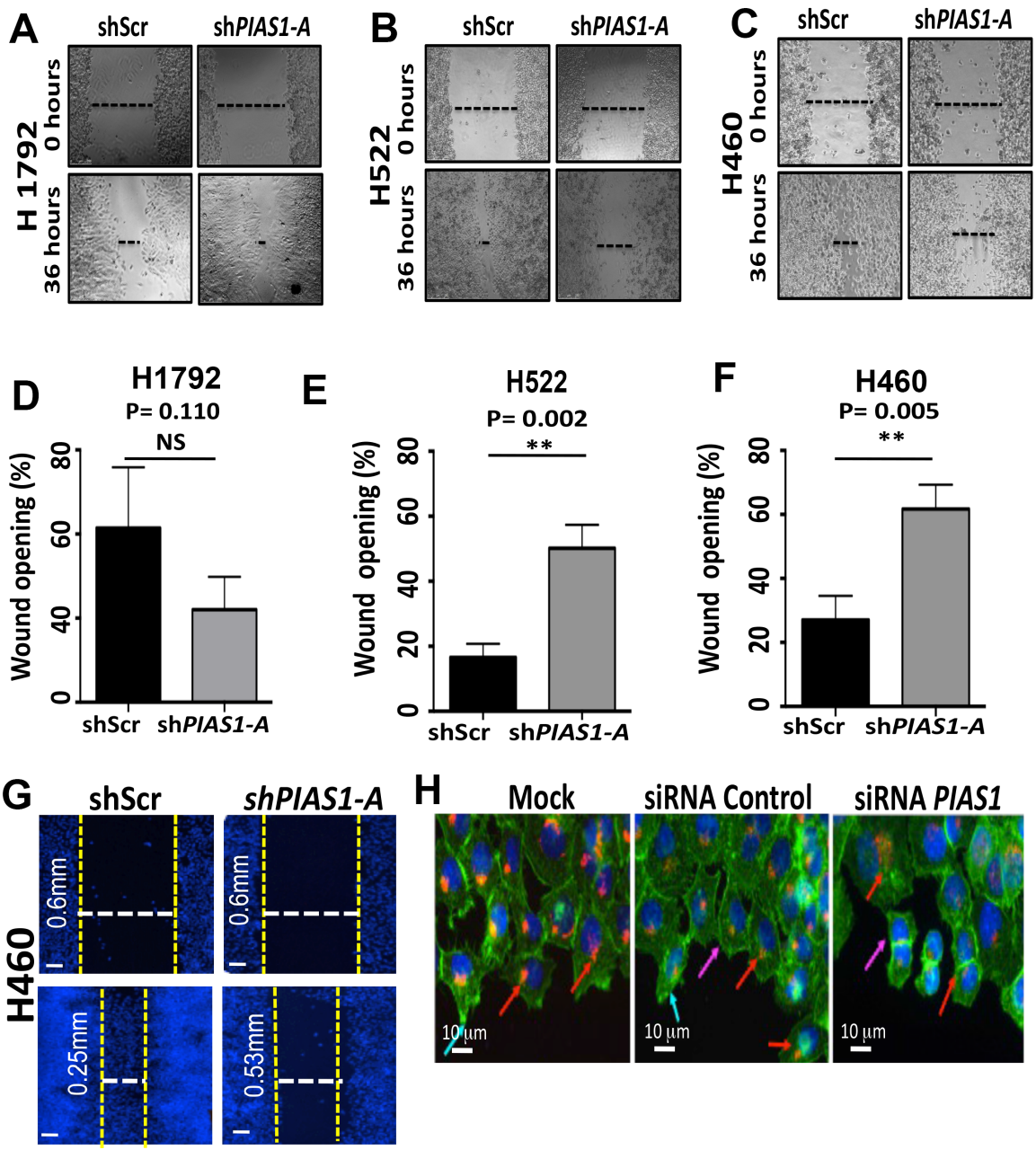

Figure 3.8 *PIAS1* silencing in NSCLC cells reduces migration efficiency in scratch assays. A-C, Phase contrast micrograph of NSCLC cell lines H1792, H522 and H460 at 0 hours post scratch wound formation and end point of 36 or 16 hours. **D-F**, Histogram shows the quantification of migrating cells as the

percentage of remaining wound opening area. **G-H**, Scratch assay and IF from H460 cells at 0 hours post scratch wound formation and end point of 16 hours. Note that approximately 50% of wound opening remain in anti-PIAS1 shRNA treated cells. Yellow arrows indicate PIAS1 protein, red arrows indicate VCL at focal adhesion and green arrows indicate vesicular VCL.

In view of our findings we conclude that *PIAS1* suppression is associated with reduced anchorage-independent growth. In addition, *PIAS1* silencing reduces cell polarization during stimulus-driven migration in NSCLC cells with *FAK* and *PIAS1* gene amplification.

3.3.6 PIAS1 silencing is detrimental for xenograft tumor growth *in vivo*

We examined whether *PIAS1* was required for tumor engraftment *in vivo* by performing xenograft experiments. We compared H460 cells growth rate *in vivo* following stable viral transduction of control shRNA or a *PIAS1* shRNA. Xenografts expressing *PIAS1* shRNA showed a significant reduction in growth 15 days post implantation as compared to controls ($P<0.05$) (Figure 3.9A). Furthermore, mice in the control group were euthanized on average after 37-days due to tumor burden; whereas the survival of mice in the PIAS1 shRNA group averaged 55 days (Figure 3.9B). We performed postmortem histological analysis of xenograft tumors and found no significant difference in cell morphology or vascularity (Figure 3.9C). We then examined the contribution of shRNA harboring cells to the xenograft using the GFP reporter in the shRNA vector

backbone and discovered a significant underrepresentation of GFP positive cells in the *PIAS1-shRNA* treatment group as compared to shRNA controls ($P < 0.05$) (Figure3.9D)

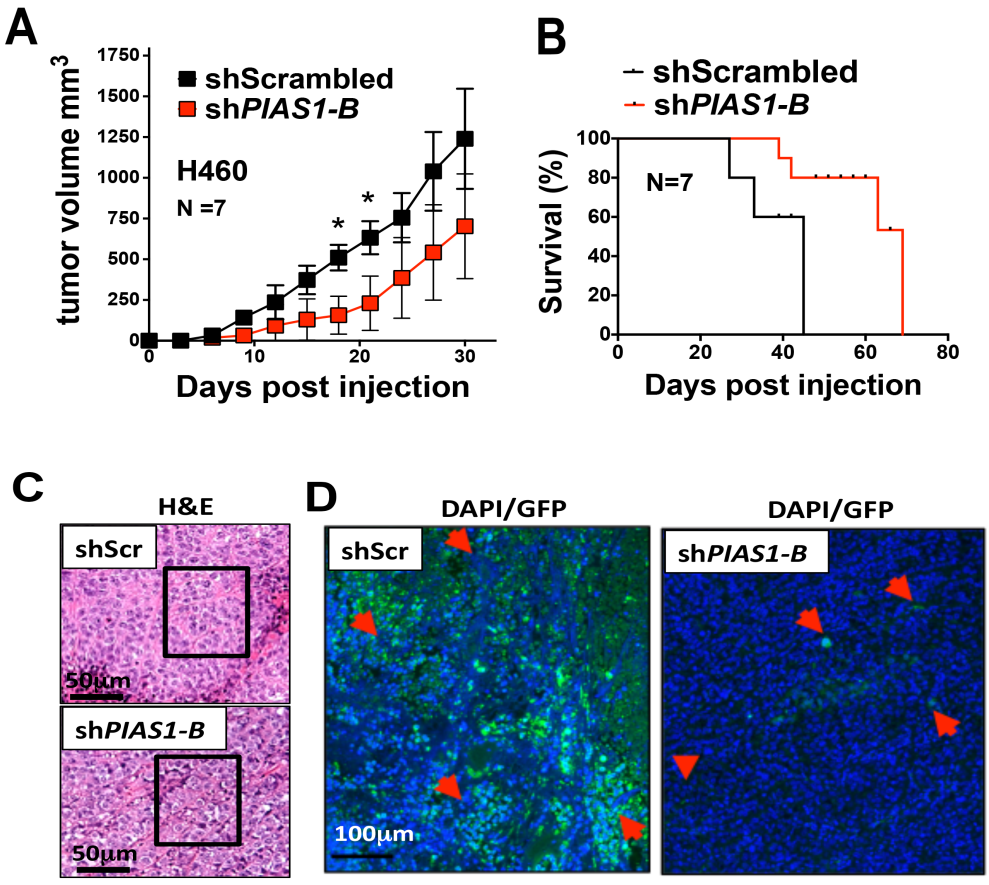

Figure 3.9 *PIAS1* gene silencing impairs xenograft tumor growth *in vivo*. A, The histogram shows the volume of xenografts from H460 cells grown subcutaneously in NOD-SCID mice following transduction with scrambled shRNA (shScr; black line) or *PIAS1* shRNA (*shPIAS1*; red line). Mice per group N=7. **B**, Kaplan–Meier curve of mice carrying xenografts shown in panel A. Mice were sacrificed when the tumors reached 2000 mm^3. **C**, H&E histological analysis of xenografts expressing Scr or *PIAS1* shRNA at the end point of the experiment. Squares indicate the sections analyzed for the GFP reporter in the shRNA construct. **D**. Anti-GFP IF shows loss of GFP positive cells in the PIAS1 shRNA xenograft group compared to the scramble shRNA group.

In view of these findings, we concluded that *PIAS1* is required for the growth of tumor xenografts *in vivo*. Furthermore, *PIAS1* inhibition is selected against during tumor growth as demonstrated by the underrepresentation of *PIAS1* shRNA expressing cells at the experiment endpoint.

3.4.0 Discussion

Metastasis accounts for more than 90% of cancer related deaths worldwide (Cho et al., 2015; Gibbons et al., 2009; Guan, 2015; Zheng et al., 2007). Consequently, identification of novel biomarkers and potential therapeutic targets is of paramount importance. FAK nuclear localization has been reported to be important for disease progression in various cancer types and a requirement during embryogenesis and tissue homeostasis (Albasri et al., 2014; Lim et al., 2012; Ward et al., 2013). However, the mechanism that mediates FAK relocation to the cell nucleus and if and how this enhances cell survival, metastasis and tissue development has remained unclear (Lim et al., 2008; Serrels et al., 2015).

Using single nucleotide polymorphism (SNPs) data, we discovered that the SUMO-E3 ligase *PIAS1* and *FAK* genes are co-amplified in a subset of NSCLC specimens. Furthermore, we show a positive correlation between gene copy number gain and increase in total FAK and PIAS1 protein levels, using NSCLC cell lines *in vitro* and human lung tumor samples *in vivo*. Interestingly, we found that FAK and PIAS1 protein are elevated in a subset of primary and

invasive human lung tissues and in a *bona fide* mouse model of NSCLC metastasis (Zheng et al., 2007).

It was previously reported that FAK and PIAS1 protein interact in a yeast two-hybrid screen and in transfected HEK-293T cells. In this setting PIAS1 promotes FAK phosphorylation at Y397 (pFAK), a key event for FAK activation (Kadare et al., 2003). We confirmed that endogenous PIAS1 and FAK interact in NSCLC cells and this interaction is observed at the nuclear periphery or within the cell nucleus. However, our findings indicate that *PIAS1* expression does not increase pFAK protein levels in NSCLC cells. *PIAS1* expression, or the combined expression of *PIAS1* and *SUMO-1*, results in the appearance of a ~87 KDa form of FAK, previously reported as a Calpain-mediated FAK cleavage product (Chang et al., 2007). Indeed we found that using a point mutant form of FAK protein (Fak^{V744G}), that renders FAK resistant to Calpain proteolysis, the ~87KDa form of FAK was significantly reduced. Because FAK cleavage is part of its negative regulation at focal adhesions, we argue that PIAS1 may be involved in the regulation of FAK and focal adhesion dynamics.

Recently, *PIAS1* inhibition was found to reduce breast cancer tumorigenesis by increasing genomic instability and loss of stem cell potential (Liu et al., 2014a). Silencing of *PIAS1* in a subset of NSCLC cells with *FAK* amplification results in deregulated F-Actin formation and increase in focal

adhesion turnover. We found that *PIAS1* expression can promote GFP-FAK nuclear accumulation and rescues the accumulation of VCL puncta at focal adhesions. The latter correlates with an increase in the activation of integrin downstream targets (RAC-1 and ROCK-1), but not pFAK activation, as it is no longer at the cell membrane.

Although FAK is widely associated with metastasis (Pylayeva et al., 2009; Sieg et al., 1999; Serrels et al., 2015), it is still unclear whether PIAS1 negates or contributes to tumor progression (Hoefer et al., 2012; Netherton and Bonni, 2010). PIAS1 was reported to repress TGF-β and reduced EMT transition in breast cancer cells by repression of *N-cadherin* (Dadakhujaev et al., 2014). However, other reports suggest that PIAS1 is necessary for breast cancer progression via activation of WNT5A, regulation of the estrogen receptor (ER) signaling and promoting tumor growth *in vivo* (Liu et al., 2014a). In our study, we found that *PIAS1* silencing in NSCLC did not have an effect on EMT genes including *N-Cadherin or E-Cadherin* (JDC and PPS, unpublished data). However, *PIAS1* silencing in NSCLC reduced cell polarization and migration, suggesting that PIAS1 contributes to NSCLC stimulus-driven migration. Specifically, we observed deficient lamellipodia formation and GM130 leading edge orientation following migration stimulus *in vitro*, which may have contributed to cells inability to integrate extracellular signaling and properly migrate. We propose that

FAK recruitment to the nucleus by means of increase interaction with PIAS1, allows for focal adhesion maturation and increase integrin signaling, as demonstrated by the appearance of lamellipodia projections in *Flag-Pias1* expressing cells. In contrast, lamellipodia are decreased or absent in migrating cells after *PIAS1* knockdown. *PIAS1* gene silencing in NSCLC cells also reduced cell viability, independently of pFAK activation. Interestingly, following *PIAS1* gene silencing we observed a concomitant increase in BIM protein levels. In addition, we also observed a significant decrease in soft agar colony growth following *PIAS1* knockdown.

An unexpected result in our study was that PIAS1-induced FAK nuclear recruitment promotes DNA repair transcription program. Because FAK deletion led to DNA-damage hypersensitivity, shown by γH2AX and pCHK2 activation, we speculate that the co-amplification of *FAK* and *PIAS1* promotes DNA damage repair, providing a survival advantage to genomically unstable cancers. In fact, FAK was found to be a negative regulator of p53 tumor suppressor in immortalized fibroblasts, and FAK inhibition radiozensitizes head and neck carcinomas (Eke et al., 2012; Hehlgans et al., 2012; Lim et al., 2008). Work is already in progress to characterize in better detail the involvement FAK in DNA damage repair and possible applications for NSCLC radiotherapy. Another unexpected finding was that silencing of *FAK* is associated with decrease of

oxygen consumption and ATP production, an observation that underscores the importance of FAK in the maintenance of FAK-dependent NSCLC cells.

In agreement with previous findings in breast cancer, *PIAS1* silencing affects NSCLC cells growth in soft agar *in vitro* and tumor xenograft growth *in vivo*. Future studies will be necessary to determine the mechanisms of cell death that contribute to this antitumor response. We speculate DNA damage regulation in NSCLC may provide the prosurvival signaling required for tumor progression in cancers with *PIAS1/FAK* gene amplification. It will be of interest to identify the transcriptional modulators interacting with FAK while in the nucleus, as they represent potential tumor biomarkers or therapeutic targets.

Finally, our results show that a subset of NSCLCs has co-amplification of *FAK* and *PIAS1* and that their protein is enriched in metastatic NSCLC. We show that PIAS1 expression promotes FAK nuclear accumulation, integrin signaling activation and DNA damage repair. We conclude that the FAK-PIAS1 signaling axis is a novel regulator of NSCLC progression, integrating extracellular cues that regulate cell survival, migration and the DNA damage response. We propose that FAK-PIAS1 status would serve as a biomarker for the selection of patients undergoing personalized cancer treatment protocols likely to respond to FAK inhibitors.

CHAPTER IV

PIAS1 and FAK in DNA damage: therapeutic applications of FAK inhibition

4.1.0 Introduction

FAK is amplified or overexpressed in several cancer types including ovarian, colon, breast and lung cancer (Cerami et al., 2012; Pylayeva et al., 2009). Importantly, FAK inhibition is detrimental to breast and lung cancer cells: where disruption of FAK is associated with alterations in the cytoskeleton or induction of senescence and activation of DNA damage pathways, respectively (Konstantinidou et al., 2013; Pylayeva et al., 2009). However, the mechanisms underlying senescence induction following FAK inhibition and the functional consequences of this event in cancer cells remain unexplored.

In the previous chapter we discussed that *FAK* and *PIAS1* genes are co-amplified in a subset of non-small cell lung cancers (NSCLC) and this interaction results in FAK C-terminal cleavage by the calcium-dependent protease Calpain (Figure 3.4). More importantly, PIAS1 expression is associated with FAK nuclear accumulation with potential implication for gene transcription and epigenetic mechanisms.

In this section of the study, we characterized the effects of FAK nuclear translocation on gene expression and epigenetic mechanisms. Moreover, we characterize in detail the effect of FAK suppression in a large panel of NSCLC cells with representative cancer associated mutations in order to identify synthetic lethal vulnerabilities.

Interestingly we found that FAK nuclear localization is associated with DNA damage, metabolism and oncogenic signatures. Moreover, we discovered that FAK depletion leads to γ-H2AX activation and that FAK inhibition invariably reduced the viability of mutant *KRAS* NSCLC cells. In this genetic context, suppression or inhibition of FAK was also accompanied by baseline DNA damage. In addition, we demonstrate that FAK suppression synergizes with radiation therapy both *in vivo* and *in vitro*. We propose that combination therapy with FAK inhibition and ionizing radiation (IR) may lead to important clinical benefits in the treatment of NSCLC.

4.2.0 Materials and methods

Cell cultures and reagents. Human NSCLC cell lines and human bronchoalveolar cells were provided by Dr. John Minna (UT Southwestern Medical Center) and cultured as described (Phelps et al., 1996; Ramirez et al., 2004). All cells were mycoplasma free. FAK inhibitor PF-562,271 was obtained from Verastem, Inc. FAK inhibitor was added to mid-log phase cell cultures at the indicated concentrations. Control cells were incubated with medium containing DMSO at a concentration corresponding to the highest dose used in inhibitor-treated cells. All other chemicals were purchased from Sigma-Aldrich.

Expression profiling. Gene expression profiles were obtained from exponentially growing HBEC cells. For total RNA extraction we used total RNA

isolation kit (SIGMA) followed by DNase digestion and cleanup according to the manufacturer's instructions. We processed 100 ng of total RNA with the Ambion TotalPrep Kit for Illumina arrays and hybridized the product to human HT12v4.0 Expression BeadChips according to the manufacturer's instructions. We used R/Bioconductor package MBCB with default parameters to process raw data, background subtraction and quantile normalization. We used a We used the Database for Annotation, Visualization and Integrated Discovery (DAVID) tool (http://david.abcc.ncifcrf.gov/) to determine functional enrichment between experimental groups. The selected enriched groups where further analyzed for gene sets by Ingenuity Gene Set Enrichment Analysis (IGSEA). Data is deposited online and accessible thought NCBI GEO accession ID GSE73280.

Gene editing with CRISPR/CAS9. We followed the methods described previously (Wang et al 2014) to ablate FAK from NSCLC H460. First, cells were transduced with the inducible Lentiviral expression vector pCW-Cas9 (Addgene plasmid 50661), which allows Puromycin selection of transduced cells and expression of SpCas9 upon Doxycycline addition to the culture medium. Puromycin resistant cells were subsequently transduced with Lentiviral particles generated with vector pLX-sgRNA (Addgene plasmid 50662) that constitutively expresses the sgRNA guide GGUGAACCTCCUCTGACCGC - pairing with a DNA target in FAK exon 4 - and the scaffold RNA. We selected transduced cells with Blasticidin. Double-drug-resistant single clones were amplified and kept in

selection medium or added with Doxycycline, and tested for lack of FAK by sequencing and lack of FAK protein by Western blot. See also: Tang et al. 2015.

Immunofluorescence. Immunofluorescence was performed as described previously using γ-H2AX (Millipore) and TP53BP1 (Bethyl) antibodies. (Boothman et al., 1987).

Flow cytometry. Cells were allowed to adhere overnight. When indicated, cells were treated with PF-562,271 and/or IR (2 Gy). Analysis of the cell cycle and percentage of cells stained with propidium iodide (PI, Sigma-Aldrich) and γ-H2AX (Millipore) were performed following a standard procedure with a FC500 Beckman Coulter flow cytometer using the WinMDI V2.8 software (Huang and Darzynkiewicz, 2006; Nicoletti et al., 1991).

Clonogenic survival assays after exposure to ionizing radiations. Clonogenic assays were performed as described previously (Franken et al., 2006). Surviving fractions (SF) were derived using the number of colonies formed after treatment, divided by the number of cells seeded multiplied by plating efficiency. Cells were plated in triplicate onto 60-mm dishes 14-16 hours prior to irradiation. We added PF-562,271 at indicated concentrations to the cells four hours before irradiation (Roberts et al., 2008). Drug-containing medium was replaced with drug-free medium after 48 hours. Cells were irradiated with a Mark I cesium irradiator (1.31 Gy/min). Plates were fixed and stained with 0.1% crystal violet

12-30 days after treatment. We scored colonies of >50 normal-appearing cells and graphed the SF versus dose of IR (Gy).

Mouse xenograft. Using *FAK* wild type (FAK^+) and *FAK* null (FAK^-) H460 NSCLC cells were performed by subcutaneous inoculation of cells into 6-week-old female athymic nude mice. Mice with xenograft tumors of 300 mm^3 (7 mice/group) were treated with IR. Mice were irradiated with five 4 Gy fractions every other day for 10 days using an X-RAD 320 irradiator (Precision X-Ray, Inc., North Branford, CT) to deliver local irradiation to the flank or thigh of lead-shielded mice. Tumor volumes were calculated every other day using the formula: (length × $width^2$) /2. All studies were performed according to the guidelines of the UT Southwestern Institutional Animal Care and Use Committee.

Complete Antibodies list:

1. 4'-,6-diamidino-2-phenylindole (DAPI); Life technologies, No.: D1306 (1:800).
2. GADPDH; Santa Cruz, No.: sc-32233 (1:2000)
3. ACTIN; SIGMA, No.: A2066 (1:3000)
4. PIAS1; Cell signaling No.: 3350 (1:1000)
5. PIAS1; Abcam No.: Ab32219 (1:100)
6. t-FAK; Cell signaling No.: 3285 (1:1000)
7. p-FAK; Cell signaling No.: 8556 (1:1000)
8. FAK (histology); AbcamNo.: Ab40794 (1:100)

9. pH2AX; Millipore No.: 16-202A (1:1000)

10. Chk2; Cell signaling No.: 6394 (1:1000)

11. pChk2; Cell signaling No.: 2197 (1:1000)

12. Tubulin: SIGMA, No.: T6199 (1:4000)

4.3.0 Results

4.3.1 PIAS1-FAK interaction and FAK nuclear localization: effect on gene transcription

We determined that *PIAS1* promotes focal adhesion maturation and FAK protein nuclear accumulation. This phenotype was conserved in NSCLC cells, NIH-3T3 fibroblasts and HBECs (Figure 4.1A-B). GFP-FAK nuclear accumulation also occurs in HBECs cells harboring the oncogenic $KRAS^{G12D}$ mutation and *p53* knockdown, suggesting a positive correlation with lung cancer progression (Figure 4.1B). To test whether PIAS1-FAK interaction and FAK nuclear accumulation are directly associated with a pro-tumorigenic gene transcription program, we analyzed HBECs ectopically expressing *GFP-Fak and Flag-Pias1*. We analyzed mRNA-transcript linearized data with the Benjamini-Hochberg statistics (log ratio 0.6; and p value < 0.3) and subtracted values obtained from HBECs expressing *GFP-Fak* alone or *Flag-Pias1* alone to obtain transcripts that change only when both genes are co-expressed. We identified 473

differentially up/down-regulated transcripts, which we used for further characterization (GEO accession ID: GSE73280). Using gene ontology analysis we uncovered that co-expression of *GFP-FAK* and *PIAS1* correlates with activation of several transcriptional programs that include DNA damage repair genes, oxidative phosphorylation genes, nuclear receptors and a pancreatic adenocarcinoma signature (Figure 4.1D).

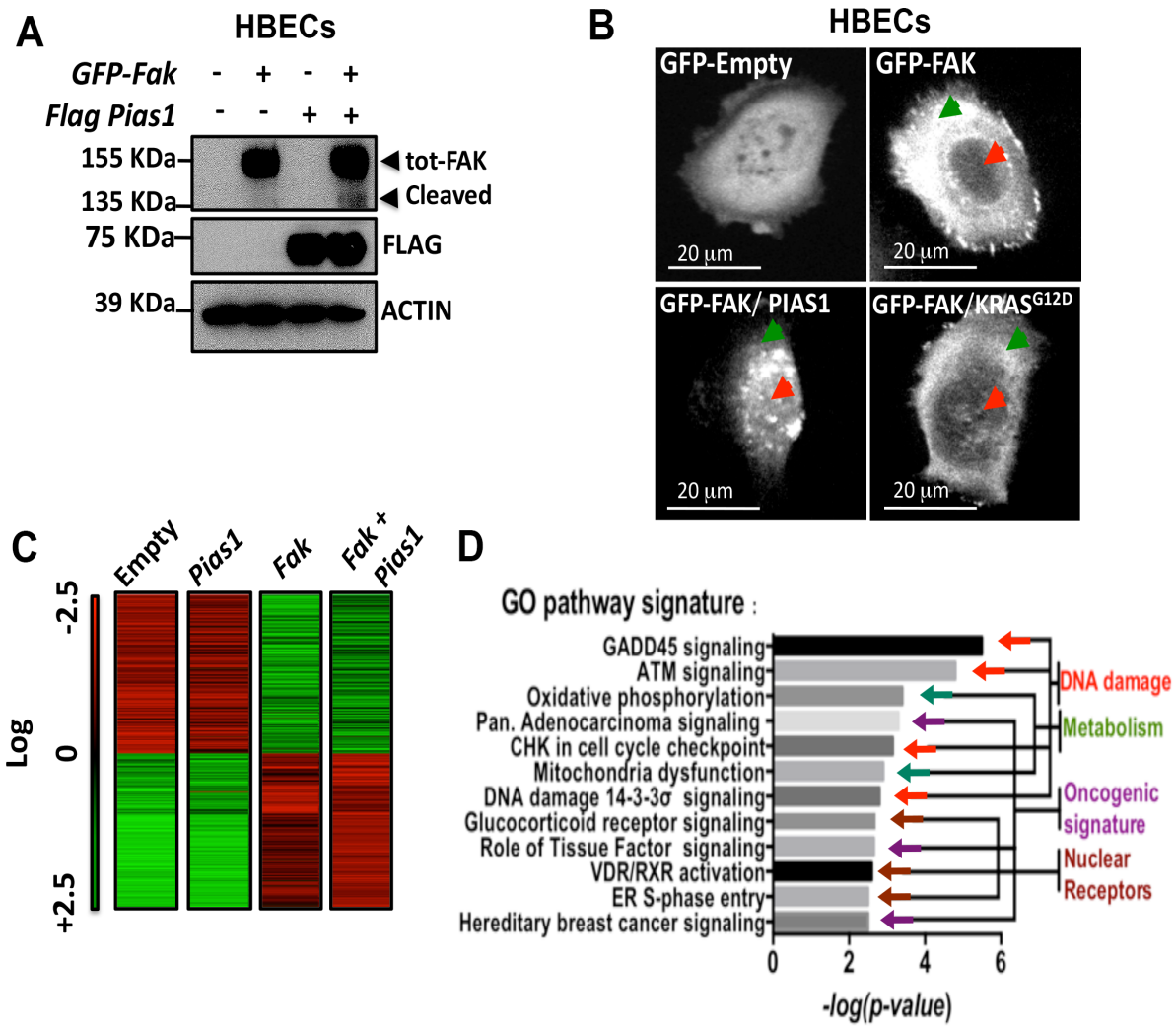

Figure 4.1 PIAS1 promotes FAK protein nuclear localization and gene transcription. A, Immunoblot of immortalized HBECs transduced/transfected with the indicated plasmids. Arrow indicates cleaved FAK. **B**, Confocal microscopy of HBECs transduced as indicated. Note the nuclear relocation of GFP-FAK after ectopic *Flag-Pias1* overexpression in HBECs cells harboring $KRAS^{G12D}$ mutations (green and red arrows indicate cytoplasmic and nuclear FAK, respectively). Scale bar: 20 µm. **C-D**, Heat map and gene ontology analysis of HBECs expressing *GFP-Fak* alone or in combination with *Flag-Pias1*.

Our finding suggests that nuclear FAK may participate in DNA repair and cell cycle progression, a hypothesis consistent with the known function of PIAS1 in these processes (Galanty et al., 2009; Hoefer et al., 2012).

To confirm whether *FAK* is involved in DNA repair or mitochondrial function, we targeted its deletion in NSCLC cells by CRISPR/Cas9 gene editing. First, we tested for changes in γ-H2AX and pCHK2, which are well-known DNA damage response genes (Camacho et al., 2010; Gil del Alcazar et al., 2014). We found that in addition to having baseline activation of γ-H2AX and phospho-Chk2 (pCHK2), surrogate markers of DNA damage, *FAK* null (*FAK*$^-$) H460 NSCLC cells were hypersensitive to ionizing radiation (IR) (Figure 4.2 A).

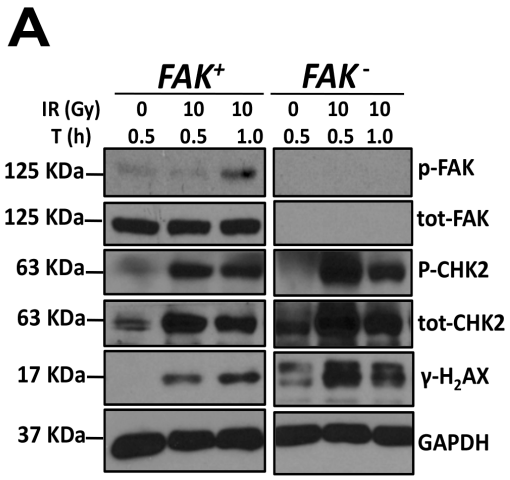

Figure 4.2 *FAK* gene deletion leads to activation of the DNA damage response in NSCLC. A, Immunoblot of *FAK* wild type (*FAK*$^+$*)* or *FAK* deleted (*FAK*$^-$) H460 NSCLC cells treated with IR and harvested at the indicated time points. Note upregulation of p-CHK2 and γ-H2AX in null cells, indicating DNA damage hypersensitivity following *FAK* loss.

This result suggests a direct link between FAK nuclear localization and DNA damage response in NSCLC cells. We also tested the effect of *FAK* loss on oxidative phosphorylation by assessing ATP production and mitochondria respiration. We found that in accordance with the perturbation in oxidative phosphorylation signatures during *PIAS1-FAK* overexpression, FAK protein depletion by CRISPR/Cas9 led to a reduced mitochondria ATP production and oxygen consumption rates, cross-validating our findings from the expression profiling (Figure 4.3 A, B).

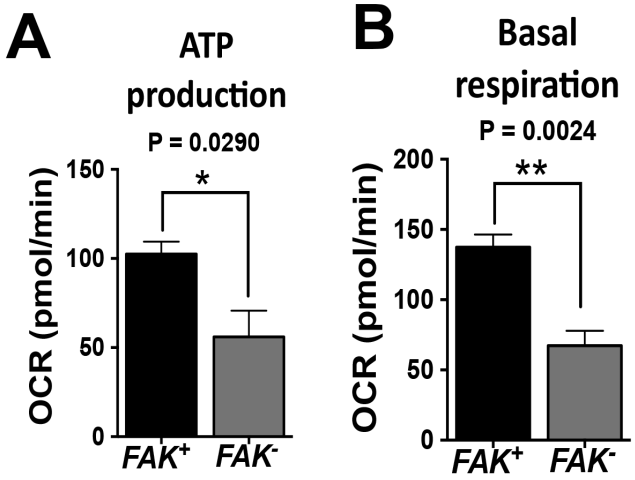

Figure 4.3 *FAK* gene deletion reduces mitochondria energy production. **A-B**, Histogram shows ATP production and basal mitochondria respiration in NSCLC H460 following *FAK* deletion.

Taken together these results suggest that PIAS1, by promoting FAK nuclear localization, promotes tumor progression by engaging transcriptional programs that regulate DNA damage repair and oxidative phosphorylation.

4.3.2 Suppression of FAK leads to activation of the DNA damage response in mutant *KRAS* NSCLC

To directly address whether nuclear FAK and DNA damage repair is clinically relevant, we tested how pharmacological inhibition of FAK affects baseline activation of γ-H2AX and whether it negatively affects cell survival. Indeed, we found that pharmacologic inhibition of *FAK* with PF-562,271 let to upregulation of γ-H2AX in mutant *KRAS* NSCLC A549 and H460 cells but not in wild type *KRAS* NSCLC H522 and H596 cells (Figure 4.4 A). Importantly, we found that NSCLC carrying mutant *KRAS* are sensitized to the deleterious effects of ionizing radiation (IR) upon FAK kinase inhibition (Figure 4.5 A-D)

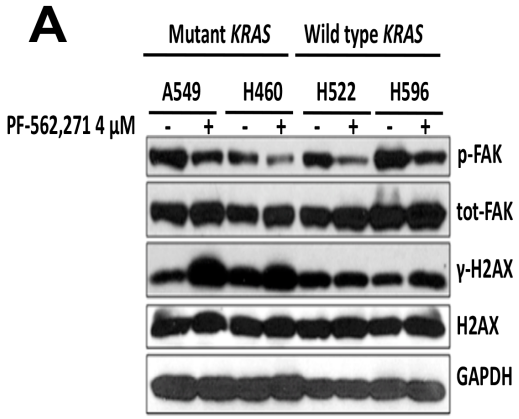

Figure 4.4. Suppression of FAK promotes a DNA damage response. A, WB analysis of NSCLC cells treated with FAKi as indicated. Note upregulation of γ-H2AX in mutant, but not in wild type, *KRAS* NSCLC cells treated with FAKi.

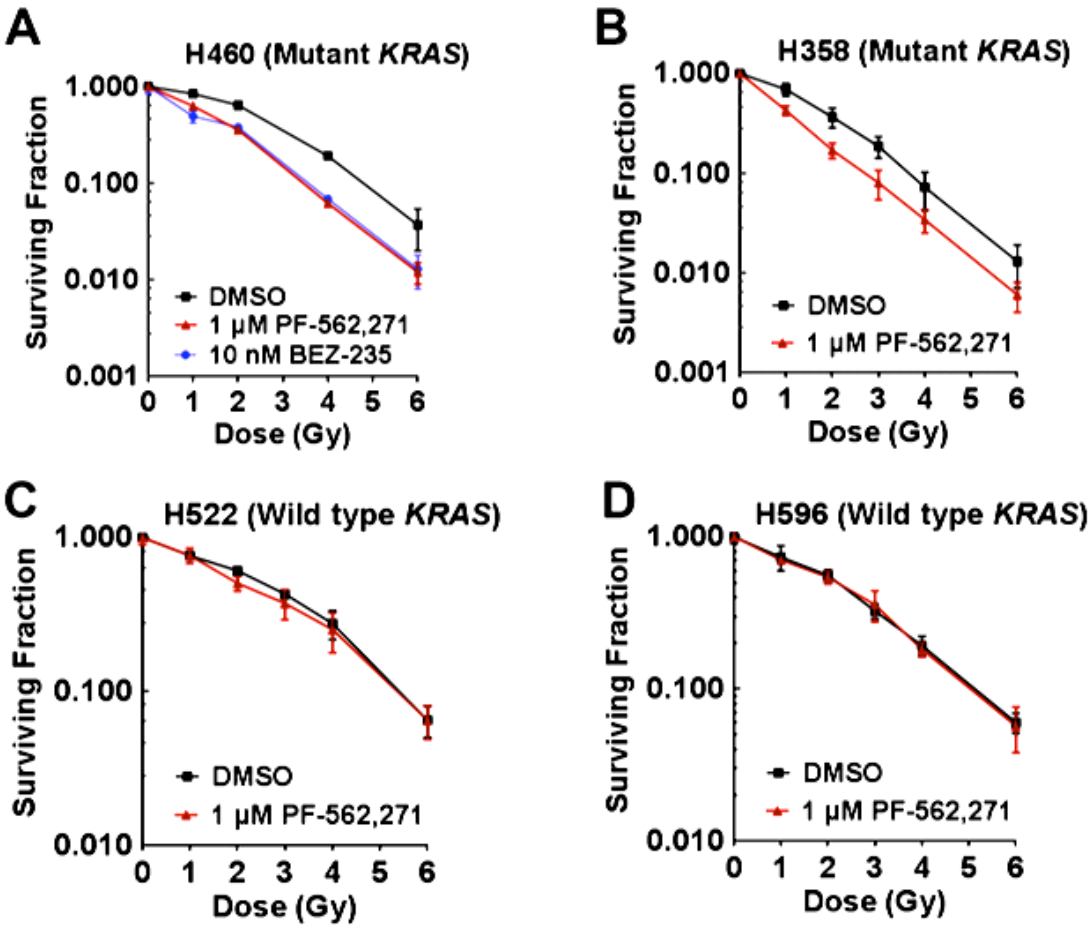

Figure 4.5 FAK blockade sensitizes mutant *KRAS* NSCLC cells to the effects of ionizing radiations. A-D. Clonogenic survival assays of NSCLC cells treated with PF-562,271 and IR as indicated.

Taken together, our data support the conclusion that loss of the *FAK* gene or its pharmacological inhibition leads to a DNA damage response in NSCLC cells driven by oncogenic *KRAS*.

4.3.3 Radiosensitization induced by FAK blockade or loss is accompanied by persistent DNA damage micro foci

Our data suggest that inhibition of FAK facilitates the cytotoxic effects of IR by promoting increased or unresolved DNA damage. Thus, we examined whether PF-562,271 affects induction and repair of DNA breaks after IR exposure in H460 cells. We determined that resolution of γ-H2AX foci, a well-known marker of DNA double-strand break damage and repair (when foci decrease), occurred rapidly after treatment with IR (2 Gy). In contrast, treatment with FAK inhibitor PF-562, 271 in combination with IR (2 Gy) led to a striking persistence of γ-H2AX foci at 24 hours post-IR administration compared with exposure with IR alone (Figure 4.6 A). We obtained equivalent results when we determined the induction and resolution of γ-H2AX and TP53BP1 foci, as readout of DNA damage, in CRISPR/CAS9 H460 FAK^{+} and H460 FAK^{-} cells (Figure. 4.6 B). In addition, we found that mutant *KRAS* H460 cells treated with FAKi in combination with IR display a significant increase in the percentage of cells in the G_2 phase of the cell cycle at 4 and 24 hours after treatment as compared to H460 cells treated with IR alone, which would suggest arrest in a G_2-phase-induced checkpoint (Figure 4.6 C).

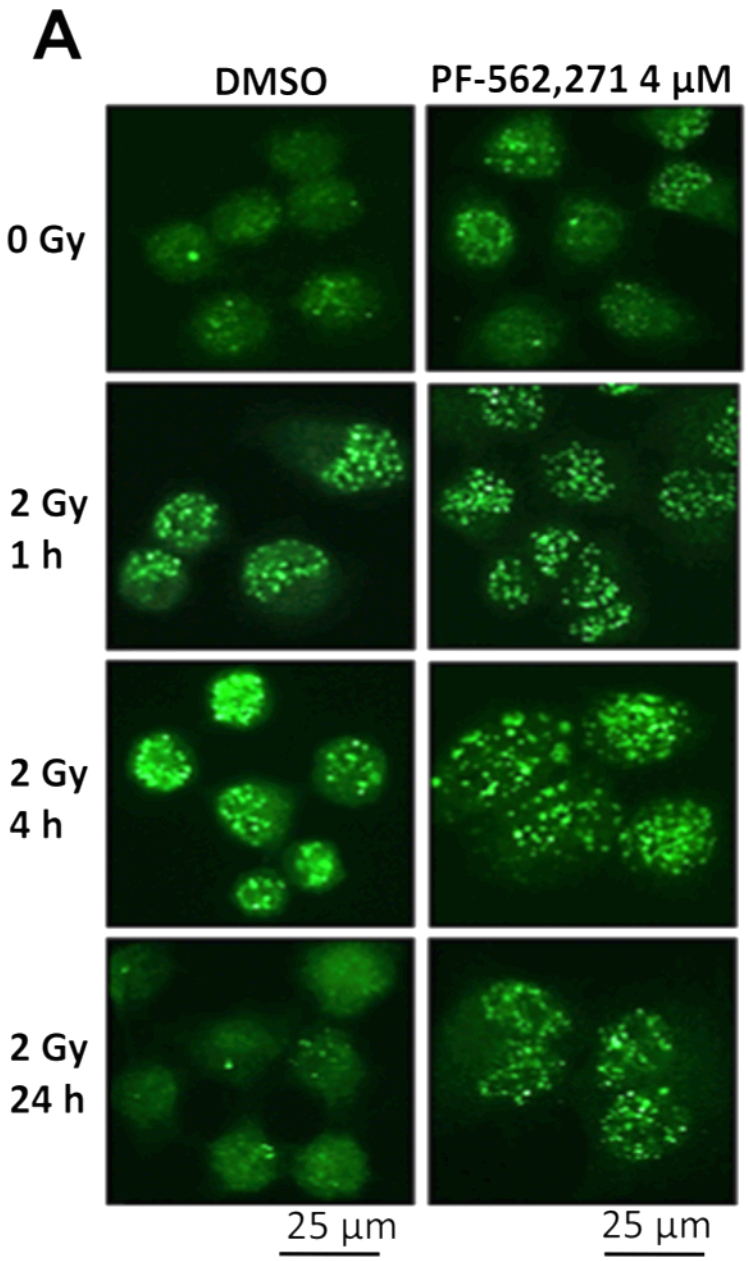
A
DMSO
PF-562,271 4 µM
0 Gy
2 Gy
1 h
2 Gy
4 h
2 Gy
24 h
25 µm
25 µm

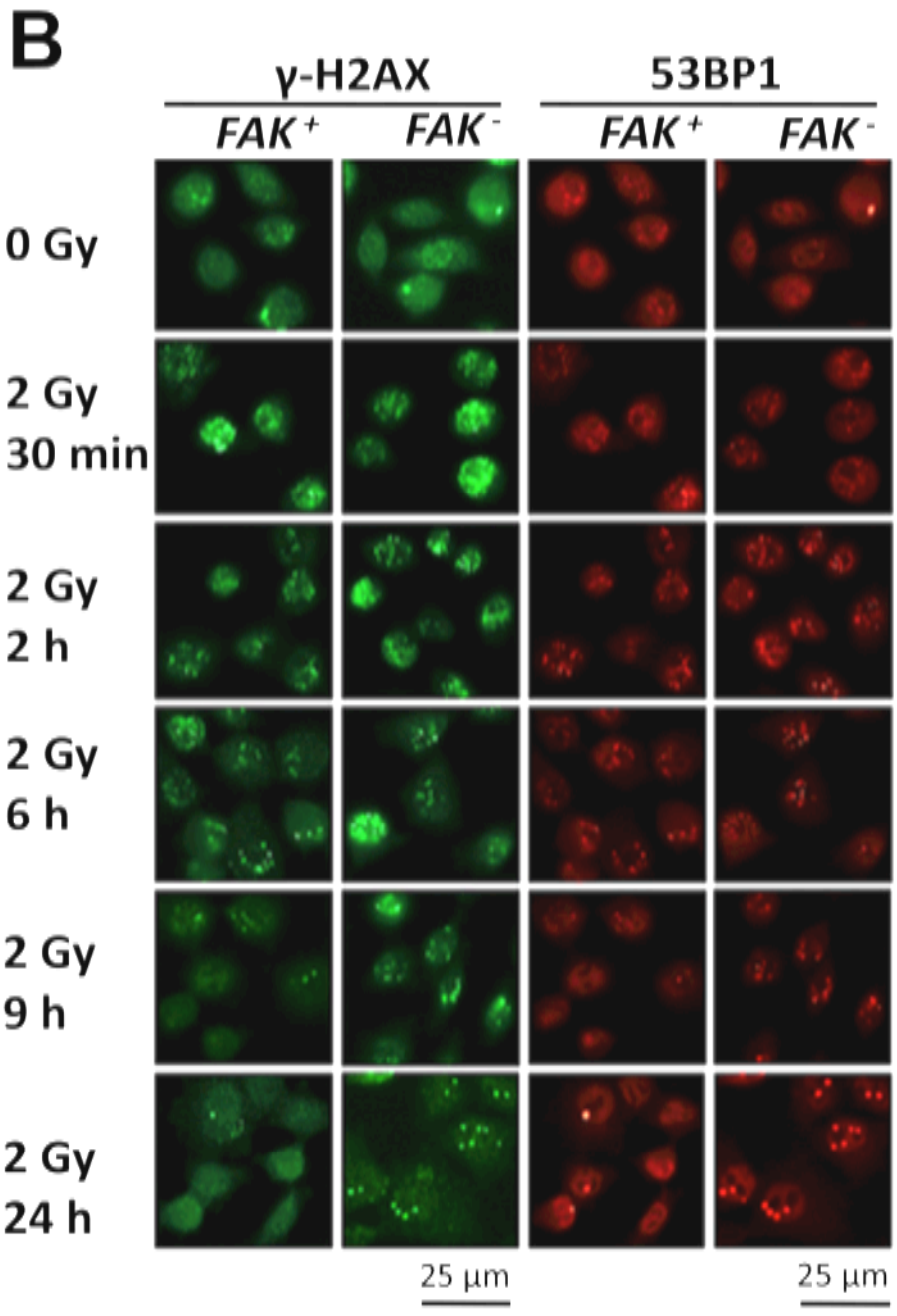
B
γ-H2AX
53BP1
FAK+
FAK-
FAK+
FAK-
0 Gy
2 Gy
30 min
2 Gy
2 h
2 Gy
6 h
2 Gy
9 h
2 Gy
24 h
25 μm
25 μm

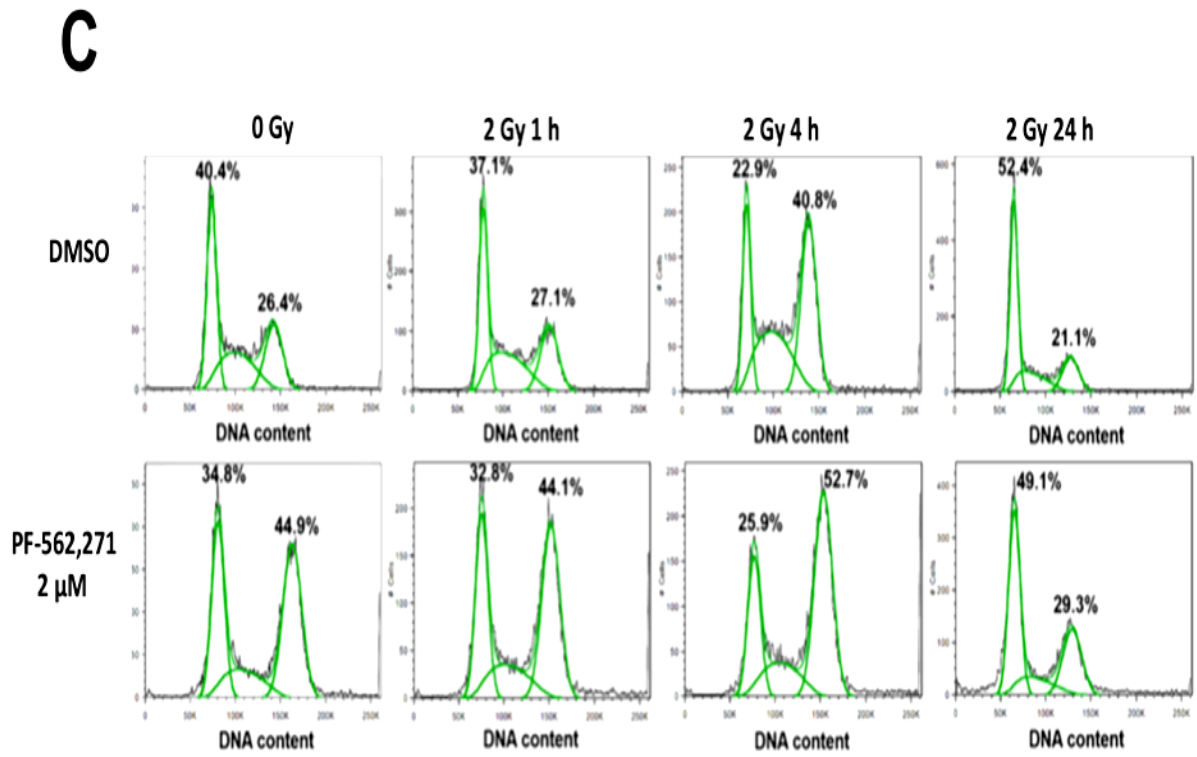

Figure 4.6 Radiosensitization induced by FAK blockade is accompanied by persistence of DNA damage foci. A. Detection by immunofluorescence of γ-H2AX foci in H460 cells treated with DMSO, PF-562,271 or BEZ-235 followed by 2 Gy of IR. Foci were detected at the indicated time points. Note striking increase in the number of foci 24 hours after treatment with PF-562,271 and BEZ-235 (a known radiosensitizing drug) in combination with IR. Bar, 25 µm. B. Detection by immunofluorescence of γ-H2AX foci in *FAK*+ and *FAK* - H460 cells after treatment with 2 Gy of IR. Foci were detected at the indicated time points. Note striking increase in the number of foci at 9 and 24 h after IR. Bar, 25 µm. C. Cell cycle analysis of H460 cells treated as indicated. The percentage of cells in each phase of the cell cycle is indicated. Note a significant increase in the percentage of G_2 cells after combination treatment with FAKi and IR.

Taken together these data suggest that inhibition/suppression of FAK results in persistent DNA damage in NSCLC cells because of inhibition of DNA repair or augmentation of damage by cell cycle checkpoint abrogation, which occur without affecting the activation and recruitment to sites of DNA damage of the DNA damage sensing machinery. These observations also suggest that IR therapy could be exploited to sensitize cancer cells to therapy with FAK inhibitors.

4.3.4 Combination of FAK inhibition and radiation is an effective antitumor strategy *in vitro* and *in vivo*

We tested the anti-tumor effects of FAK inactivation mediated by CRISP/CAS9 editing in combination with IR in H460 NSCLC xenografts, a well-established model of aggressive NSCLC and a representative example of the cells we used in tissue culture experiments.

We generated 4 cohorts of 7 athymic nude mice bearing xenografts of H460 FAK^{+} and H460 FAK^{-} cells of 300 mm^3 average size. Mice were either mock treated or treated with five 4 Gy fractions every other day for 10 days. We delivered local irradiation to the flank or thigh of lead-shielded mice using a fractionated dose to limit overall tissue toxicity and mimic the administration modality used in the clinic (Fairchild et al., 2008). Notably, this xenograft volume

and IR dose is comparable with previous studies involving H460 xenografts (Iwasa et al., 2008; Konstantinidou et al., 2009).

As expected FAK ablation impaired xenograft growth compared to the parental H460 cells. However, we noticed that growth of H460 FAK^- H460 cells accelerated after two weeks (Figure 4.7 A). The median survivals of mock treated mice carrying H460 FAK^+ and FAK^- cells were 19 days and 24 days, respectively ($P = 0.0467$) (Figure 4.7 B). IR treatment of H460 FAK^- cells resulted in a greater than 75% reduction in xenograft volume as compared to H460 FAK^+ cells 30 days after the first dose of IR ($P < 0.001$) (Figure 4.7 C, D). All irradiated mice carrying xenografts from H460 FAK^- cells were alive 40 days after the initiation of IR treatment, in contrast five out of seven mice carrying of H460 FAK^+ cells were sacrificed between days 34 and 38 post-radiation due to excessive tumor burden (Figure 4.7 E). IR treatment was well tolerated in xenograft bearing mice and we did not observe any drop in body weight or other signs of toxicity in both groups (data not shown).

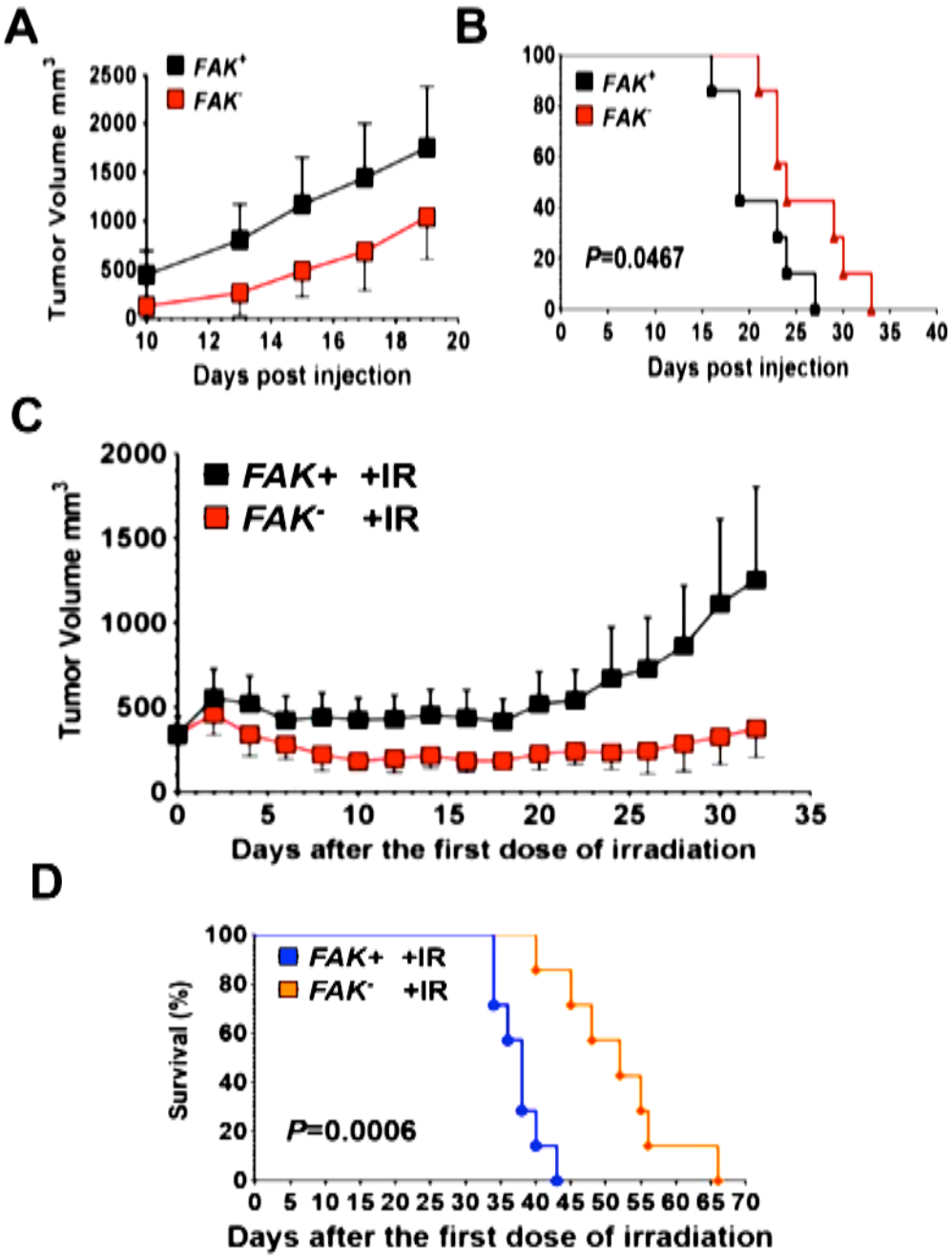
A
Tumor Volume mm3
FAK+
FAK-
2500
2000
1500
1000
500
0
10 12 14 16 18 20
Days post injection
B
100
80
60
40
20
0
FAK+
FAK-
P=0.0467
0 5 10 15 20 25 30 35 40
Days post injection
C
Tumor Volume mm3
FAK+ +IR
FAK- +IR
2000
1500
1000
500
0
0 5 10 15 20 25 30 35
Days after the first dose of irradiation
D
Survival (%)
100
80
60
40
20
0
FAK+ +IR
FAK- +IR
P=0.0006
0 5 10 15 20 25 30 35 40 45 50 55 60 65 70
Days after the first dose of irradiation

E

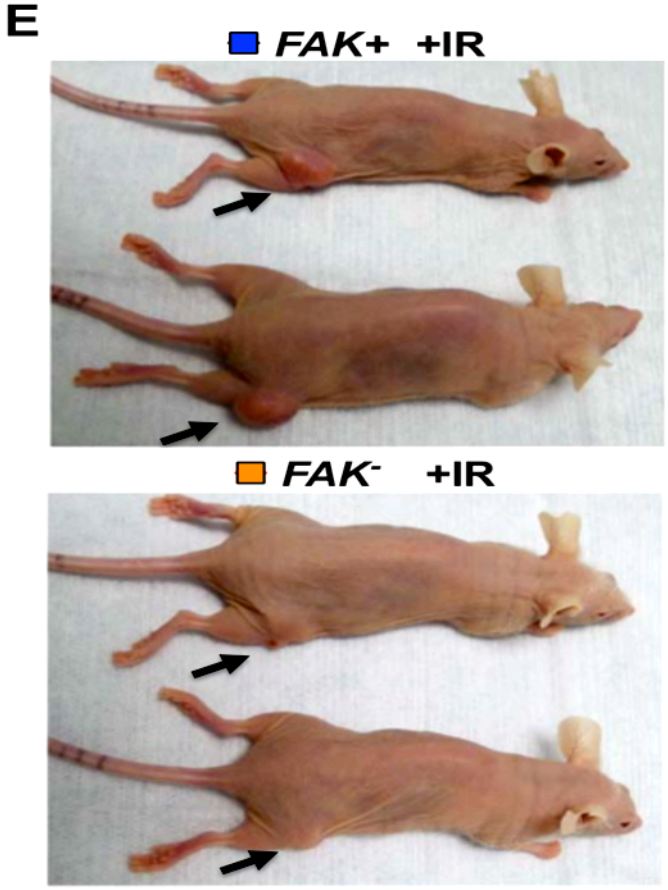

Figure 4.7 FAK inhibition is radiosensitizing in a xenograft tumor model of NSCLC. A. Xenograft growth of H460 FAK^+ and FAK^- cells in nude mice treated as indicated. The graph shows xenograft volumes. Points represent the mean of tumor volume (mm^3) at each time point. **B.** Kaplan-Meyer curve of xenografts of H460 FAK^+ and FAK^- cells. $P = 0.0467$. **C.** Xenograft growth of H460 FAK^+ and FAK^- cells in nude mice treated with IR as indicated. **D.** Tumor burden in representative mice carrying xenografts of the indicated genotype 20 days after initiation of IR treatment. **E.** Kaplan-Meyer curve of xenografts of H460 FAK^+ and FAK^- cells treated with IR as indicated. $P = 0.007$. Number of mice = 7/group; Mice were sacrificed when tumor volume reached 2,000 mm^3; bars, SE; *p* value is indicated.

These final results demonstrate that the ablation of FAK leads to significant radiosensitizing effects, which in turn led to significant anti-tumor effects *in vivo*.

4.4.0 Discussion

NSCLC remains a significant clinical challenge due to the fact that few medical treatments are effective in this disease. It is well known that NSCLC displays either primary or acquired resistance to chemotherapy and targeted therapy. Our work reveals several important conclusions relevant for the treatment of NSCLC: not only is FAK recruited to the nucleus by its interaction

with PIAS1, a known DNA damage repair protein, but it can affect gene expression regulating DNA damage and metabolism.

Moreover, *FAK* gene deletion or its pharmacological inhibition in NSCLC leads to persistent DNA damage observed in the form of γ-H2AX activation. I noted for the first time that IR activates FAK and that *FAK* depletion promotes the hyperactivation of checkpoint kinase CHK2, a known downstream target of ATM/ATR and G_2/M effectors of cell cycle arrest or apoptosis in response to DNA damage.

FAK deficient cells have a decreased clonogenic capacity, which may be caused by growth arrest or impaired cell proliferation. It is likely that the effects of FAK inhibition/suppression are mediated by loss of G_2 checkpoint control that, in turn, leads to an inherent loss of DNA repair capacity. Alternatively, these effects could be caused by inhibition of a DSB repair protein (such as ATM, ATR or DNA-PKcs) that affects DSB repair and cell cycle checkpoint control. In the future, it will be of interest to differentiate between these two possibilities. It is noteworthy that it was reported that FAK loss in murine breast cancer cells and primary fibroblast is associated with induction of replicative senescence even though the mechanism underlying this outcome is yet to be defined (Pylayeva et al., 2009).

Even though we tested NSCLC cells carrying oncogenotypes other than mutant *KRAS*, we did not find anti-proliferative responses consistently in wild type *KRAS* NSCLC cells. Thus we conclude that the dependency on FAK may be a specific feature of mutant *KRAS* driven NSCLCs.

Finally our work provides preclinical data useful for the design of therapeutic protocols using FAK inhibitors (FAKi). We propose that mutant *KRAS* should represent a biomarker for the enrolment of patients in clinical trials using FAKi in NSCLC. Furthermore, we suggest that the clinical testing of combined therapy using FAKi and IR should be prioritized. In the future, it will be of interest to determine the mechanistic underpinning of the role of FAK in DNA damage repair to optimize the use of FAKi in cancer patients, identify biomarkers that predict clinical response and test FAKi in other tumor types that harbor mutant *KRAS*.

CHAPTER V

Conclusions and future directions

5.0.0 Conclusion and future directions

Small ubiquitin like modifier (SUMO) is a posttranslational modification used to alter the biochemical properties of a target protein. SUMOylation is a hierarchical process in which SUMO proteins are added onto substrates by the stepwise transfer of SUMO from activating enzyme E1, cargo enzyme E2 and finally onto conjugating enzyme E3 ligase (Palvimo, 2007; Rytinki et al., 2009). PIAS1 is one of the few known SUMO E3 ligases and has been involved in processes as diverse as DNA damage repair, inflammation, transcription factor regulation and cancer development (Galanty et al., 2009; Liu et al., 1998; Liu et al., 2007). Being involved in many diverse cellular processes allows PIAS1 to take center stage not only in normal tissue biology but also during disease processes. Thus, PIAS1 is a valuable candidate for studying SUMO E3 ligases function.

The goal of our research study was to uncover novel PIAS1 targets or signaling pathways that depend on SUMO E3 ligases to properly operate within a multicellular organism and/or individual cells during disease progression. Also, we wanted to leverage this knowledge to investigate PIAS1 requirement during lung cancer progression and survival. Another major goal of this work was to assess the clinical relevance of targeting one of PIAS1 downstream targets, the non-receptor tyrosine kinase FAK, for the treatment of NSCLC. FAK is of great interest because it contributes to tumor progression by engaging in cytoskeleton

remodeling during cell migration and activation of the PI3K/mTOR, MEK1/2/ERK1/2, RHOA-FAK and TBK1 signaling networks (Barbie et al., 2009; Chien et al., 2006; Konstantinidou et al., 2013; Pylayeva-Gupta et al., 2011). Since SUMOylation of target proteins can affect their localization within the cell or their recognition by interacting partners, we hypothesized that PIAS1 could affect FAK function by either altering its location or binding partner recognition.

To our knowledge, this is the first attempt to describe the function of PIAS1 in embryogenesis and lung cancer progression, specifically its regulation of FAK function.

5.1.0 PIAS1 in embryogenesis

With our work, we discovered that PIAS1 is essential for the proper development of mouse embryos, especially through regulation of yolk sac (YS) erythropoiesis and angiogenesis. In absence of PIAS1, blood island resident red blood cells (RBCs) are significantly depleted and the surrounding capillary plexus is not properly formed (Figure 2.3). Previous reports suggest that deletion of genes important for blood or vascular development ultimately result in embryonic lethality before E12.5 due to lack of proper blood circulation to the embryo (Beliakoff et al., 2008; Maeda et al., 2009). Indeed, PIAS1 deficient embryos show growth retardation and anemia right before the onset of death between E9.5

and E12.5. Importantly, *in vitro* differentiation assays shows deficient erythroid differentiation accompanied by the low heme content. Molecularly, cell surface presentation of the transferring receptor (CD71) and the erythropoietin (EPO) receptor (Ter119) were underrepresented in hematopoietic precursor cells from *Pias1* null embryos. Although, future studies are needed to determine the nature of CD71 and Ter119 loss in hematopoietic precursors. We propose that PIAS1 interaction with the GATA-1 transcription factor may regulate expression of CD71 and Ter119 in hematopoietic cells (Collavin et al., 2004; Lee et al., 2009; Liu et al., 2014b; Yu et al., 2010), may play a role in their gene expression. In addition, future studies should investigate what other cell lineages are affected by PIAS1 loss and whether it corresponds to epigenetic or transcription factor dependent mechanisms.

Accompanying hematopoietic and angiogenic defects, we found a concomitant alteration of the vascular transcript profile in the YS corresponding to blood flow associated genes in *Pias1* null embryos. These include, vascular cell adhesion molecule 1 (*Vcam-1*), platelet endothelial cell adhesion molecule (*Pecam or CD31*), Angiopoietin 2 (Angp2) and Semaphorin 3A (Sema 3A). However, only *Pecam* and Sema3A mRNA levels positively correlate with *Pias1* expression, suggesting a direct association in their gene regulation. Moreover, lack of proper circulation also led to improper heart development with a characteristic loss of myocardium muscle mass. These events occur rather early in

the embryo and significantly worsen prior to embryonic death. We argue that lack of functional blood flow and potentially cell autonomous mechanism are responsible for increased susceptibility to apoptosis in the developing heart. Studies on ischemic heart injury and regeneration suggest a role for the SUMO pathway during heart tissue death and regeneration (Knight et al., 2012). Future studies should determine the contribution of *Pias1* during heart regeneration to better understand *Pias1* function in cardiac development and myocardial cell survival.

Given that the primary erythrogenic defect lie within the YS and the capillary plexus is significantly under developed, we used endothelial cell specific Cre-recombinase ($Tie2^{+/Cre}$) to ablate *Pias1* ($Pias1^{f/f}$) specifically in endothelial and hematopoietic cells of the YS. Inactivation of *Pias1* in endothelial cells recapitulates erythropoiesis deficiency in the YS, but not growth retardation defects or loss of liver hematopoiesis. This would indicate that YS erythropoiesis is dependent on endothelial cell expression of *Pias1*, while liver hematopoietic cells do not require *Pias1* for erythropoiesis. Although the origin of YS erythrogenesis is still contentious, recent reports suggest that hematopoiesis from the YS arises from erythromyeloid precursors (EMPs) independent from liver hematopoietic stem cells (HSC) (Gomez Perdiguero et al., 2015). Future studies using lineage tracing of $Rosa26^{+/GFP}$-labeled $Pias1^{f/f}$ deficient EMPs or HSC will be required to determine their contribution to erythroid cell formation in the

embryo and to discard the possibility of incomplete excision of the *Pias1* alleles in the *Tie2*$^{+/Cre}$ that could compensate for the initial loss in erythropoiesis.

5.2.0 PIAS1 in NSCLC tumor progression

In addition, to learning about PIAS1 requirement during embryogenesis we sought to determine whether human cancers where PIAS1 protein is elevated have a selective advantage during tumor progression. Thus, we examined NSCLC with gene amplification for PIAS1 and discovered a concurrent amplification of the FAK gene. Accordingly, we used this subgroup of NSCLC cell lines that concomitantly express high levels of both *PIAS1* and *FAK* genes and characterized their tumorigenic potential following *PIAS1* silencing.

We found that gene amplification of *PIAS1* and *FAK* genes result in increased amounts of both proteins in this subgroup of NSCLCs. This was of interest to us because in transformation assays (unpublished data) we found that sustained increase in PIAS1 levels is only achieved during viral infection with adenoviral protein E1A. This suggested that a continuous drive for proliferation and abrogation of the retinoblastoma (RB) checkpoint, as it is usually attained with Adenoviral infection, was required to sustain PIAS1 expression. We speculate that the combination of *FAK* and *PIAS1* amplification was a characteristic of cells with extensive genomic abnormalities, an aggressive phenotype and poor prognosis. Indeed, most of the cells in our panel were

obtained from either pleural effusions or lymph node metastasis (Gazdar et al., 2010; Ramirez et al., 2004) and have been deemed highly aggressive.

We also confirmed that the increase in PIAS1 and FAK protein levels observed in our panel of cells lines also occurs in primary human tissue samples, suggesting that high levels of these two proteins is not simply a tissue culture artifact. An interesting observation was that only the total levels of FAK protein (tot-FAK) show a correlative increase with PIAS1, not the phosphorylated form of FAK (p-FAK). This observation was also true in a cohort of metastatic NSCLCs. Of note, PIAS1 protein was notably increased in a mouse model of NSCLC metastasis harboring $KRAS^{G12D}$ in $p53^{R172H}$ (KP mice).

When we proceeded to characterize the significance of *PIAS1* and *FAK* expression in human NSCLC, we discovered that not only the two proteins interact in the cytoplasm of cancer cells, but it seems to correlate with mitogenic stimulation. PIAS1 interaction with FAK in the cytoplasm appears to be part of a negative feedback loop regulation on FAK turnover of focal adhesions. While *PIAS1* silencing led to rapid turnover of focal adhesions, which has been reported as one of the putative functions of active p-FAK (Chan et al., 2010; Mierke, 2013), *PIAS1* expression promoted focal adhesion maturation and FAK nuclear accumulation. While focal adhesion turnover is a requirement during cell migration, it can reduce cells interaction with the extracellular matrix and make them susceptible to apoptosis. As a consequence, cells with *PIAS1* silencing show

a lower threshold for apoptosis and when challenged to grow in suspension they form less colonies than controls.

Another important function of FAK is to receive external cues during cell motility and/or changes in extracellular substrate (Ezratty et al., 2005; Wang et al., 2001). Thus we wanted to determine how *PIAS1* inhibition would affect this property of focal adhesions in cells with *FAK* amplification. We found that cells treated with *PIAS1* shRNA were less efficient migrating through porous membranes compared to scrambled shRNA. These very cells showed a defect in polarization characterized by mislocalized Golgi marker (GM130), at the lagging-end instead of leading edge of migration, and reduced lamellipodia projections. Lamellipodia projections have been previously attributed to Rac1GTPase activation in various cell types and Rac1GTPase was found to be significantly increased in cells expressing PIAS3 (Lao et al., 2015; Son et al., 2015). In agreement with this observation, we find that *PIAS1* expression alone is sufficient to induce lamellipodia like projections, with a concomitant increase in Rac1-GTPase protein levels. Thus, it will be interesting to explore the relationship between PIAS1 and Rac1-GTPase, in order to better understand PIAS1 role in migration and NSCLC metastasis. We speculate that PIAS1/3 may promote Rac1-GTPase stabilization at the protein level and therefore increase the abundance of Rac1-associated lamellipodia.

5.3.0 Clinical relevance of PIAS1-FAK interaction

An unexpected result of this work was that PIAS1 would promote FAK nuclear accumulation in NSCLC. FAK nuclear localization has been reported to be important for disease progression in various cancer types and a requirement during embryogenesis and tissue homeostasis (Albasri et al., 2014; Lim et al., 2012; Ward et al., 2013). Recent reports have also showed the colocalization of FAK and PIAS1 in the nucleus (Kadare et al., 2003), but the significance of these findings were never studied.

We performed a transcriptome analysis to determine how FAK nuclear accumulation influences global mRNA levels. We found that FAK nuclear localization mostly correlated with DNA damage repair and mitochondria dysfunction signatures (Figure 4.1-4.3). Interestingly, FAK inhibition or CRISPR/CAS9 deletion results in pronounced activation of p-CHK2 and γ-H2AX, validated markers of DNA damage (Camacho et al., 2010; Gil del Alcazar et al., 2014; Lim et al., 2008). Is important to note that p-CHK2 is a downstream target of pATM and G_2/M effector of cell cycle arrest. Moreover, FAK inhibition has previously been associated with γ-H2AX activation in breast cancer cells and activation of p53/p21 tumor suppressors in primary fibroblast (Lim et al., 2008). We also found that pharmacological inhibition or CRISPR/CAS9 deletion of FAK also led to a DNA damage signature in mutant *KRAS*, but not in wild type *KRAS* NSCLC cell lines (Figure 4.4). This finding was of interest to us because

therapeutic options are still limited for NSCLC patients with mutant *KRAS* (Gysin et al., 2011). In the future it will be important to characterize the remnants of tumor suppressive functions as synthetic lethality opportunities or as part of personalized therapy.

KRAS belongs to a family of small guanosine triphosphatases (GTPase). Tumor-associated mutations lock *KRAS* in a constitutively active state (i.e. oncogenic *KRAS*) (Pylayeva-Gupta et al., 2011; Rodenhuis et al., 1988). When bound to GTP, KRAS activates several critical cell proliferation and survival signals, including the PI3K/mTOR, MEK1/2/ERK1/2, RHOA-FAK and TBK1 signaling networks (Barbie et al., 2009; Chien et al., 2006; Konstantinidou et al., 2013; Pylayeva-Gupta et al., 2011). Oncogenic *KRAS* also stimulates the production of reactive oxygen species (ROS), promoting DNA damage and genomic instability, which in turn would activate the p53 tumor suppressor (Abulaiti et al., 2006; Weinberg et al., 2010). The later could explain why mostly *KRAS* mutant NSCLCs show marked activation of DNA damage associated proteins (p-CHK2 and γ-H2AX) upon FAK inhibition. In addition, p53 mutations in human cancers render it deficient at transcribing tumor suppressor gene such as p21. However p53 may still retain some of the non-transcriptional tumor suppressive functions that could be exploited in the treatment of NSCLC (Chipuk et al., 2003; Erster et al., 2004; Marchenko et al., 2000). These findings raise a very important question regarding whether p53 function can be restored to induce

tumor regression. Proof of principle studies have shown striking tumor regression in transgenic mice of NSCLC with reactivation of wild type p53 protein at selective stages of tumorigenesis (Feldser et al., 2010). Future studies are still needed to better characterize these remnant functions of p53 for their potential clinical application in personalized therapy. Alternatively, recent findings suggest that dehydroascorbate (DHA: Vitamin C) treatment of mutant *KRAS/CRAF* driven colon cancers can lead to oxidative stress and can potentially be leveraged as a therapeutic against mutant *KRAS* (Yun et al., 2015).

Our findings support the hypothesis that PIAS1 mediated FAK nuclear localization protects mutant *KRAS* driven cancers from oncogenic-induced DNA damage. We tested this hypothesis by using NSCLC H460 and H358, which are mutant *KRAS vs* NSCLC H522 and H596, which are wild type for *KRAS*. In clonogenic survival assays we found that H460 and H358 cells were sensitized to the deleterious effects of ionizing radiation (IR) following FAK inhibition with PF-562,271, whereas H522 and H596 were not sensitized. After treatment with FAK inhibitor PF-562,271, *KRAS* mutant H460 cells showed the formation of γ-H2AX foci, indicator of DNA damage. γ-H2AX foci formation in H460 cells is a direct consequence of FAK inhibition. Given that *FAK* null H460 (*FAK*$^{-}$) cells also show increase in γ-H2AX and also 53BP1 foci, another validated indicator of DNA damage (Asaithamby and Chen, 2009). Thus it is not surprising that FAK inhibitors alone or in combination with IR causes cell arrest in the G_2/M phase of

the cell cycle. Our findings show a strong link between FAK and the regulation of DNA repair. However future studies are needed to determine whether homologous recombination (HR) or non-homologous end joining (NHEJ) pathways are involved in FAK regulatory network.

An emerging question from our findings was whether a combination therapy of FAK inhibitors and radiation therapy could be sufficient to induce tumor regression *in vivo*. We found that in KRAS mutant H460 cells *FAK* deletion alone was not sufficient to fully inhibit the xenograft tumor growth *in vivo* and *FAK* deleted clones were able to start growing back again. However the combination of *FAK* deletion and IR therapy regimens was able to debulk the initial tumors and prevented further xenograft tumor growth without any evident toxicity to tumor bearing mice.

Future studies are needed to more fully characterize FAK involvement in DNA damage repair and how this can be exploited as an intrinsic cancer vulnerability. Also, we will need to optimize FAKi use in lung cancer patients, identify biomarkers that predict clinical responses and test FAKi in other tumor types that harbor mutant *KRAS*. Given that PIAS1-FAK protein levels correlates with genomic instability, FAK nuclear localization and DNA damage repair, our findings open the possibility of using PIAS1-FAK protein levels as indicators of susceptibility to radiation therapy in oncogenic *KRAS* bearing tumors.

BIBLIOGRAPHY

1. Abulaiti, A., Fikaris, A. J., Tsygankova, O. M., and Meinkoth, J. L. (2006). Ras induces chromosome instability and abrogation of the DNA damage response. Cancer research *66*, 10505-10512.

2. Agochiya, M., Brunton, V. G., Owens, D. W., Parkinson, E. K., Paraskeva, C., Keith, W. N., and Frame, M. C. (1999). Increased dosage and amplification of the focal adhesion kinase gene in human cancer cells. Oncogene *18*, 5646-5653.

3. Albasri, A., Fadhil, W., Scholefield, J. H., Durrant, L. G., and Ilyas, M. (2014). Nuclear expression of phosphorylated focal adhesion kinase is associated with poor prognosis in human colorectal cancer. Anticancer research *34*, 3969-3974.

4. Arora, T., Liu, B., He, H., Kim, J., Murphy, T. L., Murphy, K. M., Modlin, R. L., and Shuai, K. (2003). PIASx is a transcriptional co-repressor of signal transducer and activator of transcription 4. The Journal of biological chemistry *278*, 21327-21330.

5. Asaithamby, A., and Chen, D. J. (2009). Cellular responses to DNA double-strand breaks after low-dose gamma-irradiation. Nucleic acids research *37*, 3912-3923.

6. Aslanukov, A., Bhowmick, R., Guruju, M., Oswald, J., Raz, D., Bush, R. A., Sieving, P. A., Lu, X., Bock, C. B., and Ferreira, P. A. (2006). RanBP2 modulates Cox11 and hexokinase I activities and haploinsufficiency of RanBP2 causes deficits in glucose metabolism. PLoS genetics *2*, e177.

7. Auerbach, R., Huang, H., and Lu, L. (1996). Hematopoietic stem cells in the mouse embryonic yolk sac. Stem cells *14*, 269-280.

8. Bailey, D., and O'Hare, P. (2004). Characterization of the localization and proteolytic activity of the SUMO-specific protease, SENP1. The Journal of biological chemistry *279*, 692-703.

9. Barbie, D. A., Tamayo, P., Boehm, J. S., Kim, S. Y., Moody, S. E., Dunn, I. F., Schinzel, A. C., Sandy, P., Meylan, E., Scholl, C.*, et al.* (2009). Systematic RNA interference reveals that oncogenic KRAS-driven cancers require TBK1. Nature *462*, 108-112.

10. Baudino, T. A., McKay, C., Pendeville-Samain, H., Nilsson, J. A., Maclean, K. H., White, E. L., Davis, A. C., Ihle, J. N., and Cleveland, J. L. (2002). c-Myc is essential for vasculogenesis and angiogenesis during development and tumor progression. Genes & development *16*, 2530-2543.

11. Beliakoff, J., Lee, J., Ueno, H., Aiyer, A., Weissman, I. L., Barsh, G. S., Cardiff, R. D., and Sun, Z. (2008). The PIAS-like protein Zimp10 is essential for

embryonic viability and proper vascular development. Molecular and cellular biology *28*, 282-292.
12. Berkes, C. A., and Tapscott, S. J. (2005). MyoD and the transcriptional control of myogenesis. Seminars in cell & developmental biology *16*, 585-595.
13. Bernardi, R., and Pandolfi, P. P. (2003). Role of PML and the PML-nuclear body in the control of programmed cell death. Oncogene *22*, 9048-9057.
14. Boddy, M. N., Howe, K., Etkin, L. D., Solomon, E., and Freemont, P. S. (1996). PIC 1, a novel ubiquitin-like protein which interacts with the PML component of a multiprotein complex that is disrupted in acute promyelocytic leukaemia. Oncogene *13*, 971-982.
15. Bolhy, S., Bouhlel, I., Dultz, E., Nayak, T., Zuccolo, M., Gatti, X., Vallee, R., Ellenberg, J., and Doye, V. (2011). A Nup133-dependent NPC-anchored network tethers centrosomes to the nuclear envelope in prophase. The Journal of cell biology *192*, 855-871.
16. Boothman, D. A., Greer, S., and Pardee, A. B. (1987). Potentiation of halogenated pyrimidine radiosensitizers in human carcinoma cells by beta-lapachone (3,4-dihydro-2,2-dimethyl-2H-naphtho[1,2-b]pyran- 5,6-dione), a novel DNA repair inhibitor. Cancer research *47*, 5361-5366.
17. Brien, G. L., Healy, E., Jerman, E., Conway, E., Fadda, E., O'Donovan, D., Krivtsov, A. V., Rice, A. M., Kearney, C. J., Flaus, A.*, et al.* (2015). A chromatin-independent role of Polycomb-like 1 to stabilize p53 and promote cellular quiescence. Genes & development *29*, 2231-2243.
18. Buschmann, T., Fuchs, S. Y., Lee, C. G., Pan, Z. Q., and Ronai, Z. (2000). SUMO-1 modification of Mdm2 prevents its self-ubiquitination and increases Mdm2 ability to ubiquitinate p53. Cell *101*, 753-762.
19. Camacho, C. V., Mukherjee, B., McEllin, B., Ding, L. H., Hu, B., Habib, A. A., Xie, X. J., Nirodi, C. S., Saha, D., Story, M. D.*, et al.* (2010). Loss of p15/Ink4b accompanies tumorigenesis triggered by complex DNA double-strand breaks. Carcinogenesis *31*, 1889-1896.
20. Cappadocia, L., Pichler, A., and Lima, C. D. (2015). Structural basis for catalytic activation by the human ZNF451 SUMO E3 ligase. Nature structural & molecular biology *22*, 968-975.
21. Carr, H. S., Zuo, Y., Oh, W., and Frost, J. A. (2013). Regulation of focal adhesion kinase activation, breast cancer cell motility, and amoeboid invasion by the RhoA guanine nucleotide exchange factor Net1. Molecular and cellular biology *33*, 2773-2786.
22. Cerami, E., Gao, J., Dogrusoz, U., Gross, B. E., Sumer, S. O., Aksoy, B. A., Jacobsen, A., Byrne, C. J., Heuer, M. L., Larsson, E.*, et al.* (2012). The cBio cancer genomics portal: an open platform for exploring multidimensional cancer genomics data. Cancer discovery *2*, 401-404.

23. Chan, K. T., Bennin, D. A., and Huttenlocher, A. (2010). Regulation of adhesion dynamics by calpain-mediated proteolysis of focal adhesion kinase (FAK). The Journal of biological chemistry *285*, 11418-11426.
24. Chang, F., Lemmon, C. A., Park, D., and Romer, L. H. (2007). FAK potentiates Rac1 activation and localization to matrix adhesion sites: a role for betaPIX. Molecular biology of the cell *18*, 253-264.
25. Chen, H. C., Huang, H. Y., Chen, Y. L., Lee, K. D., Chu, Y. R., Lin, P. Y., Hsu, C. C., Chu, P. Y., Huang, T. H., Hsiao, S. H., and Leu, Y. W. (2015). Methylation of the Tumor Suppressor Genes HIC1 and RassF1A Clusters Independently From the Methylation of Polycomb Target Genes in Colon Cancer. Annals of surgical oncology.
26. Chen, L., Gibbons, D. L., Goswami, S., Cortez, M. A., Ahn, Y. H., Byers, L. A., Zhang, X., Yi, X., Dwyer, D., Lin, W.*, et al.* (2014a). Metastasis is regulated via microRNA-200/ZEB1 axis control of tumour cell PD-L1 expression and intratumoral immunosuppression. Nature communications *5*, 5241.
27. Chen, Q., Xu, R., Zeng, C., Lu, Q., Huang, D., Shi, C., Zhang, W., Deng, L., Yan, R., Rao, H.*, et al.* (2014b). Down-regulation of Gli transcription factor leads to the inhibition of migration and invasion of ovarian cancer cells via integrin beta4-mediated FAK signaling. PloS one *9*, e88386.
28. Cheong, M. S., Park, H. C., Hong, M. J., Lee, J., Choi, W., Jin, J. B., Bohnert, H. J., Lee, S. Y., Bressan, R. A., and Yun, D. J. (2009). Specific domain structures control abscisic acid-, salicylic acid-, and stress-mediated SIZ1 phenotypes. Plant physiology *151*, 1930-1942.
29. Chien, Y., Kim, S., Bumeister, R., Loo, Y. M., Kwon, S. W., Johnson, C. L., Balakireva, M. G., Romeo, Y., Kopelovich, L., Gale, M., Jr.*, et al.* (2006). RalB GTPase-mediated activation of the IkappaB family kinase TBK1 couples innate immune signaling to tumor cell survival. Cell *127*, 157-170.
30. Chipuk, J. E., Maurer, U., Green, D. R., and Schuler, M. (2003). Pharmacologic activation of p53 elicits Bax-dependent apoptosis in the absence of transcription. Cancer cell *4*, 371-381.
31. Cho, J. H., Robinson, J. P., Arave, R. A., Burnett, W. J., Kircher, D. A., Chen, G., Davies, M. A., Grossmann, A. H., VanBrocklin, M. W., McMahon, M., and Holmen, S. L. (2015). AKT1 Activation Promotes Development of Melanoma Metastases. Cell reports *13*, 898-905.
32. Choi, H. J., Park, J. H., Park, J. H., Lee, K. B., and Oh, S. M. (2015). Pc2-mediated SUMOylation of WWOX is essential for its suppression of DU145 prostate tumorigenesis. FEBS letters.
33. Chung, C. D., Liao, J., Liu, B., Rao, X., Jay, P., Berta, P., and Shuai, K. (1997). Specific inhibition of Stat3 signal transduction by PIAS3. Science (New York, NY) *278*, 1803-1805.

34. Coffin, J. D., Harrison, J., Schwartz, S., and Heimark, R. (1991). Angioblast differentiation and morphogenesis of the vascular endothelium in the mouse embryo. Developmental biology *148*, 51-62.
35. Coffin, J. D., and Poole, T. J. (1991). Endothelial cell origin and migration in embryonic heart and cranial blood vessel development. The Anatomical record *231*, 383-395.
36. Collavin, L., Gostissa, M., Avolio, F., Secco, P., Ronchi, A., Santoro, C., and Del Sal, G. (2004). Modification of the erythroid transcription factor GATA-1 by SUMO-1. Proceedings of the National Academy of Sciences of the United States of America *101*, 8870-8875.
37. Conway, S. J., Kruzynska-Frejtag, A., Kneer, P. L., Machnicki, M., and Koushik, S. V. (2003). What cardiovascular defect does my prenatal mouse mutant have, and why? Genesis *35*, 1-21.
38. Costa, M. W., Lee, S., Furtado, M. B., Xin, L., Sparrow, D. B., Martinez, C. G., Dunwoodie, S. L., Kurtenbach, E., Mohun, T., Rosenthal, N., and Harvey, R. P. (2011). Complex SUMO-1 regulation of cardiac transcription factor Nkx2-5. PloS one *6*, e24812.
39. Dadakhujaev, S., Salazar-Arcila, C., Netherton, S. J., Chandhoke, A. S., Singla, A. K., Jirik, F. R., and Bonni, S. (2014). A novel role for the SUMO E3 ligase PIAS1 in cancer metastasis. Oncoscience *1*, 229-240.
40. Das, A. K., Sato, M., Story, M. D., Peyton, M., Graves, R., Redpath, S., Girard, L., Gazdar, A. F., Shay, J. W., Minna, J. D., and Nirodi, C. S. (2006). Non-small-cell lung cancers with kinase domain mutations in the epidermal growth factor receptor are sensitive to ionizing radiation. Cancer research *66*, 9601-9608.
41. Davidovich, C., Wang, X., Cifuentes-Rojas, C., Goodrich, K. J., Gooding, A. R., Lee, J. T., and Cech, T. R. (2015). Toward a consensus on the binding specificity and promiscuity of PRC2 for RNA. Molecular cell *57*, 552-558.
42. Dawlaty, M. M., Malureanu, L., Jeganathan, K. B., Kao, E., Sustmann, C., Tahk, S., Shuai, K., Grosschedl, R., and van Deursen, J. M. (2008). Resolution of sister centromeres requires RanBP2-mediated SUMOylation of topoisomerase IIalpha. Cell *133*, 103-115.
43. Dbouk, H. A., Weil, L. M., Perera, G. K., Dellinger, M. T., Pearson, G., Brekken, R. A., and Cobb, M. H. (2014). Actions of the protein kinase WNK1 on endothelial cells are differentially mediated by its substrate kinases OSR1 and SPAK. Proceedings of the National Academy of Sciences of the United States of America *111*, 15999-16004.
44. Dellinger, M. T., Meadows, S. M., Wynne, K., Cleaver, O., and Brekken, R. A. (2013). Vascular endothelial growth factor receptor-2 promotes the development of the lymphatic vasculature. PloS one *8*, e74686.

45. Dieckhoff, P., Bolte, M., Sancak, Y., Braus, G. H., and Irniger, S. (2004). Smt3/SUMO and Ubc9 are required for efficient APC/C-mediated proteolysis in budding yeast. Molecular microbiology *51*, 1375-1387.
46. Dunworth, W. P., Cardona-Costa, J., Bozkulak, E. C., Kim, J. D., Meadows, S., Fischer, J. C., Wang, Y., Cleaver, O., Qyang, Y., Ober, E. A., and Jin, S. W. (2014). Bone morphogenetic protein 2 signaling negatively modulates lymphatic development in vertebrate embryos. Circulation research *114*, 56-66.
47. Eifler, K., and Vertegaal, A. C. (2015). SUMOylation-Mediated Regulation of Cell Cycle Progression and Cancer. Trends in biochemical sciences *40*, 779-793.
48. Eisenhardt, N., Chaugule, V. K., Koidl, S., Droescher, M., Dogan, E., Rettich, J., Sutinen, P., Imanishi, S. Y., Hofmann, K., Palvimo, J. J., and Pichler, A. (2015). A new vertebrate SUMO enzyme family reveals insights into SUMO-chain assembly. Nature structural & molecular biology *22*, 959-967.
49. Eke, I., Deuse, Y., Hehlgans, S., Gurtner, K., Krause, M., Baumann, M., Shevchenko, A., Sandfort, V., and Cordes, N. (2012). beta(1)Integrin/FAK/cortactin signaling is essential for human head and neck cancer resistance to radiotherapy. The Journal of clinical investigation *122*, 1529-1540.
50. Erster, S., Mihara, M., Kim, R. H., Petrenko, O., and Moll, U. M. (2004). In vivo mitochondrial p53 translocation triggers a rapid first wave of cell death in response to DNA damage that can precede p53 target gene activation. Molecular and cellular biology *24*, 6728-6741.
51. Ezratty, E. J., Partridge, M. A., and Gundersen, G. G. (2005). Microtubule-induced focal adhesion disassembly is mediated by dynamin and focal adhesion kinase. Nature cell biology *7*, 581-590.
52. Fairchild, A., Harris, K., Barnes, E., Wong, R., Lutz, S., Bezjak, A., Cheung, P., and Chow, E. (2008). Palliative thoracic radiotherapy for lung cancer: a systematic review. J Clin Oncol *26*, 4001-4011.
53. Feldser, D. M., Kostova, K. K., Winslow, M. M., Taylor, S. E., Cashman, C., Whittaker, C. A., Sanchez-Rivera, F. J., Resnick, R., Bronson, R., Hemann, M. T., and Jacks, T. (2010). Stage-specific sensitivity to p53 restoration during lung cancer progression. Nature *468*, 572-575.
54. Feng, N., Wang, Z., Zhang, Z., He, X., Wang, C., and Zhang, L. (2015). miR-487b promotes human umbilical vein endothelial cell proliferation, migration, invasion and tube formation through regulating THBS1. Neuroscience letters *591*, 1-7.
55. Feng, Y., Wu, H., Xu, Y., Zhang, Z., Liu, T., Lin, X., and Feng, X. H. (2014). Zinc finger protein 451 is a novel Smad corepressor in transforming growth factor-beta signaling. The Journal of biological chemistry *289*, 2072-2083.

56. Forler, D., Rabut, G., Ciccarelli, F. D., Herold, A., Kocher, T., Niggeweg, R., Bork, P., Ellenberg, J., and Izaurralde, E. (2004). RanBP2/Nup358 provides a major binding site for NXF1-p15 dimers at the nuclear pore complex and functions in nuclear mRNA export. Molecular and cellular biology *24*, 1155-1167.
57. Franken, N. A., Rodermond, H. M., Stap, J., Haveman, J., and van Bree, C. (2006). Clonogenic assay of cells in vitro. Nat Protoc *1*, 2315-2319.
58. Frisch, S. M., Schaller, M., and Cieply, B. (2013). Mechanisms that link the oncogenic epithelial-mesenchymal transition to suppression of anoikis. Journal of cell science *126*, 21-29.
59. Galanty, Y., Belotserkovskaya, R., Coates, J., Polo, S., Miller, K. M., and Jackson, S. P. (2009). Mammalian SUMO E3-ligases PIAS1 and PIAS4 promote responses to DNA double-strand breaks. Nature *462*, 935-939.
60. Garcia-Dominguez, M., and Reyes, J. C. (2009). SUMO association with repressor complexes, emerging routes for transcriptional control. Biochimica et biophysica acta *1789*, 451-459.
61. Gazdar, A. F., Girard, L., Lockwood, W. W., Lam, W. L., and Minna, J. D. (2010). Lung cancer cell lines as tools for biomedical discovery and research. Journal of the National Cancer Institute *102*, 1310-1321.
62. Geiss-Friedlander, R., and Melchior, F. (2007). Concepts in sumoylation: a decade on. Nature reviews Molecular cell biology *8*, 947-956.
63. Gibbons, D. L., Lin, W., Creighton, C. J., Zheng, S., Berel, D., Yang, Y., Raso, M. G., Liu, D. D., Wistuba, II, Lozano, G., and Kurie, J. M. (2009). Expression signatures of metastatic capacity in a genetic mouse model of lung adenocarcinoma. PloS one *4*, e5401.
64. Gil del Alcazar, C. R., Hardebeck, M. C., Mukherjee, B., Tomimatsu, N., Gao, X., Yan, J., Xie, X. J., Bachoo, R., Li, L., Habib, A. A., and Burma, S. (2014). Inhibition of DNA double-strand break repair by the dual PI3K/mTOR inhibitor NVP-BEZ235 as a strategy for radiosensitization of glioblastoma. Clinical cancer research : an official journal of the American Association for Cancer Research *20*, 1235-1248.
65. Gil, J., Bernard, D., and Peters, G. (2005). Role of polycomb group proteins in stem cell self-renewal and cancer. DNA and cell biology *24*, 117-125.
66. Giorgi, C., Ito, K., Lin, H. K., Santangelo, C., Wieckowski, M. R., Lebiedzinska, M., Bononi, A., Bonora, M., Duszynski, J., Bernardi, R.*, et al.* (2010). PML regulates apoptosis at endoplasmic reticulum by modulating calcium release. Science (New York, NY) *330*, 1247-1251.
67. Golubovskaya, V. M., Conway-Dorsey, K., Edmiston, S. N., Tse, C. K., Lark, A. A., Livasy, C. A., Moore, D., Millikan, R. C., and Cance, W. G. (2009). FAK overexpression and p53 mutations are highly correlated in human breast

cancer. International journal of cancer Journal international du cancer *125*, 1735-1738.
68. Gomez Perdiguero, E., Klapproth, K., Schulz, C., Busch, K., Azzoni, E., Crozet, L., Garner, H., Trouillet, C., de Bruijn, M. F., Geissmann, F., and Rodewald, H. R. (2015). Tissue-resident macrophages originate from yolk-sac-derived erythro-myeloid progenitors. Nature *518*, 547-551.
69. Gorlich, D., and Mattaj, I. W. (1996). Nucleocytoplasmic transport. Science (New York, NY) *271*, 1513-1518.
70. Guan, X. (2015). Cancer metastases: challenges and opportunities. Acta pharmaceutica Sinica B *5*, 402-418.
71. Guo, W., Wang, H., Zhao, W., Zhu, J., Ju, B., and Wang, X. (2001). Effect of all-trans retinoic acid and arsenic trioxide on tissue factor expression in acute promyelocytic leukemia cells. Chinese medical journal *114*, 30-34.
72. Gupta, M. K., Gulick, J., Liu, R., Wang, X., Molkentin, J. D., and Robbins, J. (2014). Sumo E2 enzyme UBC9 is required for efficient protein quality control in cardiomyocytes. Circulation research *115*, 721-729.
73. Gysin, S., Salt, M., Young, A., and McCormick, F. (2011). Therapeutic strategies for targeting ras proteins. Genes & cancer *2*, 359-372.
74. Hamada, M., Haeger, A., Jeganathan, K. B., van Ree, J. H., Malureanu, L., Walde, S., Joseph, J., Kehlenbach, R. H., and van Deursen, J. M. (2011). Ran-dependent docking of importin-beta to RanBP2/Nup358 filaments is essential for protein import and cell viability. The Journal of cell biology *194*, 597-612.
75. Hay, R. T. (2005). SUMO: a history of modification. Molecular cell *18*, 1-12.
76. Hehlgans, S., Eke, I., and Cordes, N. (2012). Targeting FAK radiosensitizes 3-dimensional grown human HNSCC cells through reduced Akt1 and MEK1/2 signaling. International journal of radiation oncology, biology, physics *83*, e669-676.
77. Heo, K. S., Chang, E., Takei, Y., Le, N. T., Woo, C. H., Sullivan, M. A., Morrell, C., Fujiwara, K., and Abe, J. (2013). Phosphorylation of protein inhibitor of activated STAT1 (PIAS1) by MAPK-activated protein kinase-2 inhibits endothelial inflammation via increasing both PIAS1 transrepression and SUMO E3 ligase activity. Arteriosclerosis, thrombosis, and vascular biology *33*, 321-329.
78. Hochstrasser, M. (2001). SP-RING for SUMO: new functions bloom for a ubiquitin-like protein. Cell *107*, 5-8.
79. Hoefer, J., Schafer, G., Klocker, H., Erb, H. H., Mills, I. G., Hengst, L., Puhr, M., and Culig, Z. (2012). PIAS1 is increased in human prostate cancer and enhances proliferation through inhibition of p21. The American journal of pathology *180*, 2097-2107.

80. Huang, X., and Darzynkiewicz, Z. (2006). Cytometric assessment of histone H2AX phosphorylation: a reporter of DNA damage. Methods in molecular biology *314*, 73-80.
81. Ip, H. S., Wilson, D. B., Heikinheimo, M., Tang, Z., Ting, C. N., Simon, M. C., Leiden, J. M., and Parmacek, M. S. (1994). The GATA-4 transcription factor transactivates the cardiac muscle-specific troponin C promoter-enhancer in nonmuscle cells. Molecular and cellular biology *14*, 7517-7526.
82. Ivanschitz, L., Takahashi, Y., Jollivet, F., Ayrault, O., Le Bras, M., and de The, H. (2015). PML IV/ARF interaction enhances p53 SUMO-1 conjugation, activation, and senescence. Proceedings of the National Academy of Sciences of the United States of America *112*, 14278-14283.
83. Iwasa, T., Okamoto, I., Suzuki, M., Nakahara, T., Yamanaka, K., Hatashita, E., Yamada, Y., Fukuoka, M., Ono, K., and Nakagawa, K. (2008). Radiosensitizing effect of YM155, a novel small-molecule survivin suppressant, in non-small cell lung cancer cell lines. Clin Cancer Res *14*, 6496-6504.
84. Jackson, S. P., and Durocher, D. (2013). Regulation of DNA damage responses by ubiquitin and SUMO. Molecular cell *49*, 795-807.
85. Jacobsen, R. N., Forristal, C. E., Raggatt, L. J., Nowlan, B., Barbier, V., Kaur, S., van Rooijen, N., Winkler, I. G., Pettit, A. R., and Levesque, J. P. (2014). Mobilization with granulocyte colony-stimulating factor blocks medullar erythropoiesis by depleting F4/80(+)VCAM1(+)CD169(+)ER-HR3(+)Ly6G(+) erythroid island macrophages in the mouse. Experimental hematology *42*, 547-561 e544.
86. Johnson, E. S., and Blobel, G. (1997). Ubc9p is the conjugating enzyme for the ubiquitin-like protein Smt3p. The Journal of biological chemistry *272*, 26799-26802.
87. Johnson, E. S., and Gupta, A. A. (2001). An E3-like factor that promotes SUMO conjugation to the yeast septins. Cell *106*, 735-744.
88. Kadare, G., Toutant, M., Formstecher, E., Corvol, J. C., Carnaud, M., Boutterin, M. C., and Girault, J. A. (2003). PIAS1-mediated sumoylation of focal adhesion kinase activates its autophosphorylation. The Journal of biological chemistry *278*, 47434-47440.
89. Kagey, M. H., Melhuish, T. A., and Wotton, D. (2003). The polycomb protein Pc2 is a SUMO E3. Cell *113*, 127-137.
90. Kalamarz, M. E., Paddibhatla, I., Nadar, C., and Govind, S. (2012). Sumoylation is tumor-suppressive and confers proliferative quiescence to hematopoietic progenitors in Drosophila melanogaster larvae. Biology open *1*, 161-172.
91. Kang, X., Qi, Y., Zuo, Y., Wang, Q., Zou, Y., Schwartz, R. J., Cheng, J., and Yeh, E. T. (2010). SUMO-specific protease 2 is essential for suppression of

polycomb group protein-mediated gene silencing during embryonic development. Molecular cell *38*, 191-201.
92. Karvonen, U., Jaaskelainen, T., Rytinki, M., Kaikkonen, S., and Palvimo, J. J. (2008). ZNF451 is a novel PML body- and SUMO-associated transcriptional coregulator. Journal of molecular biology *382*, 585-600.
93. Kelley, C., Blumberg, H., Zon, L. I., and Evans, T. (1993). GATA-4 is a novel transcription factor expressed in endocardium of the developing heart. Development (Cambridge, England) *118*, 817-827.
94. Khan, A. A., Lee, A. J., and Roh, T. Y. (2015). Polycomb group protein-mediated histone modifications during cell differentiation. Epigenomics *7*, 75-84.
95. Knight, R. A., Scarabelli, T. M., and Stephanou, A. (2012). STAT transcription in the ischemic heart. Jak-Stat *1*, 111-117.
96. Koni, P. A., Joshi, S. K., Temann, U. A., Olson, D., Burkly, L., and Flavell, R. A. (2001). Conditional vascular cell adhesion molecule 1 deletion in mice: impaired lymphocyte migration to bone marrow. The Journal of experimental medicine *193*, 741-754.
97. Konstantinidou, G., Bey, E. A., Rabellino, A., Schuster, K., Maira, M. S., Gazdar, A. F., Amici, A., Boothman, D. A., and Scaglioni, P. P. (2009). Dual phosphoinositide 3-kinase/mammalian target of rapamycin blockade is an effective radiosensitizing strategy for the treatment of non-small cell lung cancer harboring K-RAS mutations. Cancer research *69*, 7644-7652.
98. Konstantinidou, G., Ramadori, G., Torti, F., Kangasniemi, K., Ramirez, R. E., Cai, Y., Behrens, C., Dellinger, M. T., Brekken, R. A., Wistuba, II*, et al.* (2013). RHOA-FAK is a required signaling axis for the maintenance of KRAS-driven lung adenocarcinomas. Cancer discovery *3*, 444-457.
99. Konstantinov, I. E., Coles, J. G., Boscarino, C., Takahashi, M., Goncalves, J., Ritter, J., and Van Arsdell, G. S. (2004). Gene expression profiles in children undergoing cardiac surgery for right heart obstructive lesions. The Journal of thoracic and cardiovascular surgery *127*, 746-754.
100. Lacaud, G., Robertson, S., Palis, J., Kennedy, M., and Keller, G. (2001). Regulation of hemangioblast development. Annals of the New York Academy of Sciences *938*, 96-107; discussion 108.
101. Lao, M., Shi, M., Zou, Y., Huang, M., Ye, Y., Qiu, Q., Xiao, Y., Zeng, S., Liang, L., Yang, X., and Xu, H. (2015). Protein Inhibitor of Activated STAT3 Regulates Migration, Invasion, and Activation of Fibroblast-like Synoviocytes in Rheumatoid Arthritis. Journal of immunology (Baltimore, Md : 1950).
102. Lee, H. Y., Johnson, K. D., Fujiwara, T., Boyer, M. E., Kim, S. I., and Bresnick, E. H. (2009). Controlling hematopoiesis through sumoylation-dependent regulation of a GATA factor. Molecular cell *36*, 984-995.
103. Lewis, P. W., Muller, M. M., Koletsky, M. S., Cordero, F., Lin, S., Banaszynski, L. A., Garcia, B. A., Muir, T. W., Becher, O. J., and Allis, C. D.

(2013). Inhibition of PRC2 activity by a gain-of-function H3 mutation found in pediatric glioblastoma. Science (New York, NY) *340*, 857-861.
104. Li, C. W., Xia, W., Huo, L., Lim, S. O., Wu, Y., Hsu, J. L., Chao, C. H., Yamaguchi, H., Yang, N. K., Ding, Q.*, et al.* (2012). Epithelial-mesenchymal transition induced by TNF-alpha requires NF-kappaB-mediated transcriptional upregulation of Twist1. Cancer research *72*, 1290-1300.
105. Li, X. Y., Zhou, X., Rowe, R. G., Hu, Y., Schlaepfer, D. D., Ilic, D., Dressler, G., Park, A., Guan, J. L., and Weiss, S. J. (2011). Snail1 controls epithelial-mesenchymal lineage commitment in focal adhesion kinase-null embryonic cells. The Journal of cell biology *195*, 729-738.
106. Lim, S. T., Chen, X. L., Lim, Y., Hanson, D. A., Vo, T. T., Howerton, K., Larocque, N., Fisher, S. J., Schlaepfer, D. D., and Ilic, D. (2008). Nuclear FAK promotes cell proliferation and survival through FERM-enhanced p53 degradation. Molecular cell *29*, 9-22.
107. Lim, S. T., Miller, N. L., Chen, X. L., Tancioni, I., Walsh, C. T., Lawson, C., Uryu, S., Weis, S. M., Cheresh, D. A., and Schlaepfer, D. D. (2012). Nuclear-localized focal adhesion kinase regulates inflammatory VCAM-1 expression. The Journal of cell biology *197*, 907-919.
108. Liu, B., Liao, J., Rao, X., Kushner, S. A., Chung, C. D., Chang, D. D., and Shuai, K. (1998). Inhibition of Stat1-mediated gene activation by PIAS1. Proceedings of the National Academy of Sciences of the United States of America *95*, 10626-10631.
109. Liu, B., Mink, S., Wong, K. A., Stein, N., Getman, C., Dempsey, P. W., Wu, H., and Shuai, K. (2004). PIAS1 selectively inhibits interferon-inducible genes and is important in innate immunity. Nature immunology *5*, 891-898.
110. Liu, B., Tahk, S., Yee, K. M., Fan, G., and Shuai, K. (2010). The ligase PIAS1 restricts natural regulatory T cell differentiation by epigenetic repression. Science (New York, NY) *330*, 521-525.
111. Liu, B., Tahk, S., Yee, K. M., Yang, R., Yang, Y., Mackie, R., Hsu, C., Chernishof, V., O'Brien, N., Jin, Y.*, et al.* (2014a). PIAS1 regulates breast tumorigenesis through selective epigenetic gene silencing. PloS one *9*, e89464.
112. Liu, B., Yang, Y., Chernishof, V., Loo, R. R., Jang, H., Tahk, S., Yang, R., Mink, S., Shultz, D., Bellone, C. J.*, et al.* (2007). Proinflammatory stimuli induce IKKalpha-mediated phosphorylation of PIAS1 to restrict inflammation and immunity. Cell *129*, 903-914.
113. Liu, B., Yee, K. M., Tahk, S., Mackie, R., Hsu, C., and Shuai, K. (2014b). PIAS1 SUMO ligase regulates the self-renewal and differentiation of hematopoietic stem cells. The EMBO journal *33*, 101-113.
114. Lopez-Laso, E., Mateos-Gonzalez, M. E., Perez-Navero, J. L., Camino-Leon, R., Briones, P., and Neilson, D. E. (2009). [Infection-triggered familial or

recurrent acute necrotizing encephalopathy]. Anales de pediatria (Barcelona, Spain : 2003) *71*, 235-239.
115. Luo, S. W., Zhang, C., Zhang, B., Kim, C. H., Qiu, Y. Z., Du, Q. S., Mei, L., and Xiong, W. C. (2009). Regulation of heterochromatin remodelling and myogenin expression during muscle differentiation by FAK interaction with MBD2. The EMBO journal *28*, 2568-2582.
116. Maeda, T., Ito, K., Merghoub, T., Poliseno, L., Hobbs, R. M., Wang, G., Dong, L., Maeda, M., Dore, L. C., Zelent, A.*, et al.* (2009). LRF is an essential downstream target of GATA1 in erythroid development and regulates BIM-dependent apoptosis. Developmental cell *17*, 527-540.
117. Mahajan, R., Delphin, C., Guan, T., Gerace, L., and Melchior, F. (1997). A small ubiquitin-related polypeptide involved in targeting RanGAP1 to nuclear pore complex protein RanBP2. Cell *88*, 97-107.
118. Marchenko, N. D., Zaika, A., and Moll, U. M. (2000). Death signal-induced localization of p53 protein to mitochondria. A potential role in apoptotic signaling. The Journal of biological chemistry *275*, 16202-16212.
119. McKean, D. M., Sisbarro, L., Ilic, D., Kaplan-Alburquerque, N., Nemenoff, R., Weiser-Evans, M., Kern, M. J., and Jones, P. L. (2003). FAK induces expression of Prx1 to promote tenascin-C-dependent fibroblast migration. The Journal of cell biology *161*, 393-402.
120. McKenna, C. C., Ojeda, A. F., Spurlin, J., 3rd, Kwiatkowski, S., and Lwigale, P. Y. (2014). Sema3A maintains corneal avascularity during development by inhibiting Vegf induced angioblast migration. Developmental biology *391*, 241-250.
121. Meadows, S. M., Ratliff, L. A., Singh, M. K., Epstein, J. A., and Cleaver, O. (2013). Resolution of defective dorsal aortae patterning in Sema3E-deficient mice occurs via angiogenic remodeling. Developmental dynamics : an official publication of the American Association of Anatomists *242*, 580-590.
122. Melchior, F., Schergaut, M., and Pichler, A. (2003). SUMO: ligases, isopeptidases and nuclear pores. Trends in biochemical sciences *28*, 612-618.
123. Mierke, C. T. (2013). The role of focal adhesion kinase in the regulation of cellular mechanical properties. Physical biology *10*, 065005.
124. Millay, D. P., O'Rourke, J. R., Sutherland, L. B., Bezprozvannaya, S., Shelton, J. M., Bassel-Duby, R., and Olson, E. N. (2013). Myomaker is a membrane activator of myoblast fusion and muscle formation. Nature *499*, 301-305.
125. Minty, A., Dumont, X., Kaghad, M., and Caput, D. (2000). Covalent modification of p73alpha by SUMO-1. Two-hybrid screening with p73 identifies novel SUMO-1-interacting proteins and a SUMO-1 interaction motif. The Journal of biological chemistry *275*, 36316-36323.

126. Moilanen, A. M., Karvonen, U., Poukka, H., Yan, W., Toppari, J., Janne, O. A., and Palvimo, J. J. (1999). A testis-specific androgen receptor coregulator that belongs to a novel family of nuclear proteins. The Journal of biological chemistry *274*, 3700-3704.
127. Muller, S., Matunis, M. J., and Dejean, A. (1998a). Conjugation with the ubiquitin-related modifier SUMO-1 regulates the partitioning of PML within the nucleus. The EMBO journal *17*, 61-70.
128. Muller, S., Miller, W. H., Jr., and Dejean, A. (1998b). Trivalent antimonials induce degradation of the PML-RAR oncoprotein and reorganization of the promyelocytic leukemia nuclear bodies in acute promyelocytic leukemia NB4 cells. Blood *92*, 4308-4316.
129. Myers, C. T., and Krieg, P. A. (2013). BMP-mediated specification of the erythroid lineage suppresses endothelial development in blood island precursors. Blood *122*, 3929-3939.
130. Nacerddine, K., Lehembre, F., Bhaumik, M., Artus, J., Cohen-Tannoudji, M., Babinet, C., Pandolfi, P. P., and Dejean, A. (2005). The SUMO pathway is essential for nuclear integrity and chromosome segregation in mice. Developmental cell *9*, 769-779.
131. Nagai, M., Moriyama, T., Mehmood, R., Tokuhiro, K., Ikawa, M., Okabe, M., Tanaka, H., and Yoneda, Y. (2011). Mice lacking Ran binding protein 1 are viable and show male infertility. FEBS letters *585*, 791-796.
132. Neilson, D. E. (2010). The interplay of infection and genetics in acute necrotizing encephalopathy. Current opinion in pediatrics *22*, 751-757.
133. Neilson, D. E., Adams, M. D., Orr, C. M., Schelling, D. K., Eiben, R. M., Kerr, D. S., Anderson, J., Bassuk, A. G., Bye, A. M., Childs, A. M.*, et al.* (2009). Infection-triggered familial or recurrent cases of acute necrotizing encephalopathy caused by mutations in a component of the nuclear pore, RANBP2. American journal of human genetics *84*, 44-51.
134. Netherton, S. J., and Bonni, S. (2010). Suppression of TGFbeta-induced epithelial-mesenchymal transition like phenotype by a PIAS1 regulated sumoylation pathway in NMuMG epithelial cells. PloS one *5*, e13971.
135. Nicoletti, I., Migliorati, G., Pagliacci, M. C., Grignani, F., and Riccardi, C. (1991). A rapid and simple method for measuring thymocyte apoptosis by propidium iodide staining and flow cytometry. J Immunol Methods *139*, 271-279.
136. Niskanen, E. A., Malinen, M., Sutinen, P., Toropainen, S., Paakinaho, V., Vihervaara, A., Joutsen, J., Kaikkonen, M. U., Sistonen, L., and Palvimo, J. J. (2015). Global SUMOylation on active chromatin is an acute heat stress response restricting transcription. Genome biology *16*, 153.
137. Nowak, M., and Hammerschmidt, M. (2006). Ubc9 regulates mitosis and cell survival during zebrafish development. Molecular biology of the cell *17*, 5324-5336.

138. Okubo, S., Hara, F., Tsuchida, Y., Shimotakahara, S., Suzuki, S., Hatanaka, H., Yokoyama, S., Tanaka, H., Yasuda, H., and Shindo, H. (2004). NMR structure of the N-terminal domain of SUMO ligase PIAS1 and its interaction with tumor suppressor p53 and A/T-rich DNA oligomers. The Journal of biological chemistry *279*, 31455-31461.
139. Olson, E. N., Brennan, T. J., Chakraborty, T., Cheng, T. C., Cserjesi, P., Edmondson, D., James, G., and Li, L. (1991). Molecular control of myogenesis: antagonism between growth and differentiation. Molecular and cellular biochemistry *104*, 7-13.
140. Palvimo, J. J. (2007). PIAS proteins as regulators of small ubiquitin-related modifier (SUMO) modifications and transcription. Biochemical Society transactions *35*, 1405-1408.
141. Pang, C. J., Lemsaddek, W., Alhashem, Y. N., Bondzi, C., Redmond, L. C., Ah-Son, N., Dumur, C. I., Archer, K. J., Haar, J. L., Lloyd, J. A., and Trudel, M. (2012). Kruppel-like factor 1 (KLF1), KLF2, and Myc control a regulatory network essential for embryonic erythropoiesis. Molecular and cellular biology *32*, 2628-2644.
142. Park, J. H., Lee, B. L., Yoon, J., Kim, J., Kim, M. A., Yang, H. K., and Kim, W. H. (2010). Focal adhesion kinase (FAK) gene amplification and its clinical implications in gastric cancer. Human pathology *41*, 1664-1673.
143. Paro, R., and Hogness, D. S. (1991). The Polycomb protein shares a homologous domain with a heterochromatin-associated protein of Drosophila. Proceedings of the National Academy of Sciences of the United States of America *88*, 263-267.
144. Patil, H., Saha, A., Senda, E., Cho, K. I., Haque, M., Yu, M., Qiu, S., Yoon, D., Hao, Y., Peachey, N. S., and Ferreira, P. A. (2014). Selective impairment of a subset of Ran-GTP-binding domains of ran-binding protein 2 (Ranbp2) suffices to recapitulate the degeneration of the retinal pigment epithelium (RPE) triggered by Ranbp2 ablation. The Journal of biological chemistry *289*, 29767-29789.
145. Phelps, R. M., Johnson, B. E., Ihde, D. C., Gazdar, A. F., Carbone, D. P., McClintock, P. R., Linnoila, R. I., Matthews, M. J., Bunn, P. A., Jr., Carney, D.*, et al.* (1996). NCI-Navy Medical Oncology Branch cell line data base. Journal of cellular biochemistry Supplement *24*, 32-91.
146. Pichler, A., Gast, A., Seeler, J. S., Dejean, A., and Melchior, F. (2002). The nucleoporin RanBP2 has SUMO1 E3 ligase activity. Cell *108*, 109-120.
147. Poux, S., McCabe, D., and Pirrotta, V. (2001). Recruitment of components of Polycomb Group chromatin complexes in Drosophila. Development (Cambridge, England) *128*, 75-85.
148. Prieto-Granada, C. N., Wiesner, T., Messina, J. L., Jungbluth, A. A., Chi, P., and Antonescu, C. R. (2015). Loss of H3K27me3 Expression Is a Highly

Sensitive Marker for Sporadic and Radiation-induced MPNST. The American journal of surgical pathology.
149. Pylayeva-Gupta, Y., Grabocka, E., and Bar-Sagi, D. (2011). RAS oncogenes: weaving a tumorigenic web. Nature reviews Cancer *11*, 761-774.
150. Pylayeva, Y., Gillen, K. M., Gerald, W., Beggs, H. E., Reichardt, L. F., and Giancotti, F. G. (2009). Ras- and PI3K-dependent breast tumorigenesis in mice and humans requires focal adhesion kinase signaling. The Journal of clinical investigation *119*, 252-266.
151. Qin, Y., Xu, J., Aysola, K., Begum, N., Reddy, V., Chai, Y., Grizzle, W. E., Partridge, E. E., Reddy, E. S., and Rao, V. N. (2011). Ubc9 mediates nuclear localization and growth suppression of BRCA1 and BRCA1a proteins. Journal of cellular physiology *226*, 3355-3367.
152. Rabellino, A., Carter, B., Konstantinidou, G., Wu, S. Y., Rimessi, A., Byers, L. A., Heymach, J. V., Girard, L., Chiang, C. M., Teruya-Feldstein, J., and Scaglioni, P. P. (2012). The SUMO E3-ligase PIAS1 regulates the tumor suppressor PML and its oncogenic counterpart PML-RARA. Cancer research *72*, 2275-2284.
153. Ramirez, R. D., Sheridan, S., Girard, L., Sato, M., Kim, Y., Pollack, J., Peyton, M., Zou, Y., Kurie, J. M., Dimaio, J. M.*, et al.* (2004). Immortalization of human bronchial epithelial cells in the absence of viral oncoproteins. Cancer research *64*, 9027-9034.
154. Roberts, W. G., Ung, E., Whalen, P., Cooper, B., Hulford, C., Autry, C., Richter, D., Emerson, E., Lin, J., Kath, J.*, et al.* (2008). Antitumor activity and pharmacology of a selective focal adhesion kinase inhibitor, PF-562,271. Cancer research *68*, 1935-1944.
155. Rodenhuis, S., Slebos, R. J., Boot, A. J., Evers, S. G., Mooi, W. J., Wagenaar, S. S., van Bodegom, P. C., and Bos, J. L. (1988). Incidence and possible clinical significance of K-ras oncogene activation in adenocarcinoma of the human lung. Cancer research *48*, 5738-5741.
156. Rogers, R. S., Horvath, C. M., and Matunis, M. J. (2003). SUMO modification of STAT1 and its role in PIAS-mediated inhibition of gene activation. The Journal of biological chemistry *278*, 30091-30097.
157. Rytinki, M. M., Kaikkonen, S., Pehkonen, P., Jaaskelainen, T., and Palvimo, J. J. (2009). PIAS proteins: pleiotropic interactors associated with SUMO. Cellular and molecular life sciences : CMLS *66*, 3029-3041.
158. Sachdev, S., Bruhn, L., Sieber, H., Pichler, A., Melchior, F., and Grosschedl, R. (2001). PIASy, a nuclear matrix-associated SUMO E3 ligase, represses LEF1 activity by sequestration into nuclear bodies. Genes & development *15*, 3088-3103.

159. Sakin, V., Richter, S. M., Hsiao, H. H., Urlaub, H., and Melchior, F. (2015). Sumoylation of the GTPase Ran by the RanBP2 SUMO E3 Ligase Complex. The Journal of biological chemistry *290*, 23589-23602.
160. Santti, H., Mikkonen, L., Anand, A., Hirvonen-Santti, S., Toppari, J., Panhuysen, M., Vauti, F., Perera, M., Corte, G., Wurst, W.*, et al.* (2005). Disruption of the murine PIASx gene results in reduced testis weight. Journal of molecular endocrinology *34*, 645-654.
161. Serrels, A., Lund, T., Serrels, B., Byron, A., McPherson, R. C., von Kriegsheim, A., Gomez-Cuadrado, L., Canel, M., Muir, M., Ring, J. E.*, et al.* (2015). Nuclear FAK Controls Chemokine Transcription, Tregs, and Evasion of Anti-tumor Immunity. Cell *163*, 160-173.
162. Seufert, W., Futcher, B., and Jentsch, S. (1995). Role of a ubiquitin-conjugating enzyme in degradation of S- and M-phase cyclins. Nature *373*, 78-81.
163. Shalaby, F., Rossant, J., Yamaguchi, T. P., Gertsenstein, M., Wu, X. F., Breitman, M. L., and Schuh, A. C. (1995). Failure of blood-island formation and vasculogenesis in Flk-1-deficient mice. Nature *376*, 62-66.
164. Sieg, D. J., Hauck, C. R., and Schlaepfer, D. D. (1999). Required role of focal adhesion kinase (FAK) for integrin-stimulated cell migration. Journal of cell science *112 (Pt 16)*, 2677-2691.
165. Singh, R. R., Sedani, S., Lim, M., Wassmer, E., and Absoud, M. (2015). RANBP2 mutation and acute necrotizing encephalopathy: 2 cases and a literature review of the expanding clinico-radiological phenotype. European journal of paediatric neurology : EJPN : official journal of the European Paediatric Neurology Society *19*, 106-113.
166. Son, K., Smith, T. C., and Luna, E. J. (2015). Supervillin binds the Rac/Rho-GEF Trio and increases Trio-mediated Rac1 activation. Cytoskeleton (Hoboken, NJ) *72*, 47-64.
167. Spektor, T. M., Congdon, L. M., Veerappan, C. S., and Rice, J. C. (2011). The UBC9 E2 SUMO conjugating enzyme binds the PR-Set7 histone methyltransferase to facilitate target gene repression. PloS one *6*, e22785.
168. Stade, K., Vogel, F., Schwienhorst, I., Meusser, B., Volkwein, C., Nentwig, B., Dohmen, R. J., and Sommer, T. (2002). A lack of SUMO conjugation affects cNLS-dependent nuclear protein import in yeast. The Journal of biological chemistry *277*, 49554-49561.
169. Stefater, J. A., 3rd, Lewkowich, I., Rao, S., Mariggi, G., Carpenter, A. C., Burr, A. R., Fan, J., Ajima, R., Molkentin, J. D., Williams, B. O.*, et al.* (2011). Regulation of angiogenesis by a non-canonical Wnt-Flt1 pathway in myeloid cells. Nature *474*, 511-515.
170. Stehmeier, P., and Muller, S. (2009). Phospho-regulated SUMO interaction modules connect the SUMO system to CK2 signaling. Molecular cell *33*, 400-409.

171. Sturgeon, C. M., Chicha, L., Ditadi, A., Zhou, Q., McGrath, K. E., Palis, J., Hammond, S. M., Wang, S., Olson, E. N., and Keller, G. (2012). Primitive erythropoiesis is regulated by miR-126 via nonhematopoietic Vcam-1+ cells. Developmental cell *23*, 45-57.
172. Sturgeon, C. M., Ditadi, A., Awong, G., Kennedy, M., and Keller, G. (2014). Wnt signaling controls the specification of definitive and primitive hematopoiesis from human pluripotent stem cells. Nature biotechnology *32*, 554-561.
173. Tahk, S., Liu, B., Chernishof, V., Wong, K. A., Wu, H., and Shuai, K. (2007). Control of specificity and magnitude of NF-kappa B and STAT1-mediated gene activation through PIASy and PIAS1 cooperation. Proceedings of the National Academy of Sciences of the United States of America *104*, 11643-11648.
174. Takahashi, Y., Toh-e, A., and Kikuchi, Y. (2001). A novel factor required for the SUMO1/Smt3 conjugation of yeast septins. Gene *275*, 223-231.
175. Tamplin, O. J., Durand, E. M., Carr, L. A., Childs, S. J., Hagedorn, E. J., Li, P., Yzaguirre, A. D., Speck, N. A., and Zon, L. I. (2015). Hematopoietic stem cell arrival triggers dynamic remodeling of the perivascular niche. Cell *160*, 241-252.
176. Tsai, C. T., Ikematsu, K., Sakai, S., Matsuo, A., and Nakasono, I. (2011). Expression of Bcl2l1, Clcf1, IL-28ra and Pias1 in the mouse heart after single and repeated administration of chlorpromazine. Legal medicine *13*, 221-225.
177. Ueno, H., and Weissman, I. L. (2006). Clonal analysis of mouse development reveals a polyclonal origin for yolk sac blood islands. Developmental cell *11*, 519-533.
178. Vertegaal, A. C. (2007). Small ubiquitin-related modifiers in chains. Biochemical Society transactions *35*, 1422-1423.
179. Wang, G., Li, W., Cui, J., Gao, S., Yao, C., Jiang, Z., Song, Y., Yuan, C. J., Yang, Y., Liu, Z., and Cai, L. (2004a). An efficient therapeutic approach to patients with acute promyelocytic leukemia using a combination of arsenic trioxide with low-dose all-trans retinoic acid. Hematological oncology *22*, 63-71.
180. Wang, H. B., Dembo, M., Hanks, S. K., and Wang, Y. (2001). Focal adhesion kinase is involved in mechanosensing during fibroblast migration. Proceedings of the National Academy of Sciences of the United States of America *98*, 11295-11300.
181. Wang, J., Feng, X. H., and Schwartz, R. J. (2004b). SUMO-1 modification activated GATA4-dependent cardiogenic gene activity. The Journal of biological chemistry *279*, 49091-49098.
182. Wang, J., Li, A., Wang, Z., Feng, X., Olson, E. N., and Schwartz, R. J. (2007). Myocardin sumoylation transactivates cardiogenic genes in pluripotent 10T1/2 fibroblasts. Molecular and cellular biology *27*, 622-632.

183. Wang, J., Zhang, H., Iyer, D., Feng, X. H., and Schwartz, R. J. (2008). Regulation of cardiac specific nkx2.5 gene activity by small ubiquitin-like modifier. The Journal of biological chemistry *283*, 23235-23243.
184. Wang, L., Wansleeben, C., Zhao, S., Miao, P., Paschen, W., and Yang, W. (2014). SUMO2 is essential while SUMO3 is dispensable for mouse embryonic development. EMBO reports *15*, 878-885.
185. Ward, K. K., Tancioni, I., Lawson, C., Miller, N. L., Jean, C., Chen, X. L., Uryu, S., Kim, J., Tarin, D., Stupack, D. G*., et al.* (2013). Inhibition of focal adhesion kinase (FAK) activity prevents anchorage-independent ovarian carcinoma cell growth and tumor progression. Clinical & experimental metastasis *30*, 579-594.
186. Wassef, M., Rodilla, V., Teissandier, A., Zeitouni, B., Gruel, N., Sadacca, B., Irondelle, M., Charruel, M., Ducos, B., Michaud, A*., et al.* (2015). Impaired PRC2 activity promotes transcriptional instability and favors breast tumorigenesis. Genes & development *29*, 2547-2562.
187. Weinberg, F., Hamanaka, R., Wheaton, W. W., Weinberg, S., Joseph, J., Lopez, M., Kalyanaraman, B., Mutlu, G. M., Budinger, G. R., and Chandel, N. S. (2010). Mitochondrial metabolism and ROS generation are essential for Kras-mediated tumorigenicity. Proceedings of the National Academy of Sciences of the United States of America *107*, 8788-8793.
188. Weissman, A. M. (2001). Themes and variations on ubiquitylation. Nature reviews Molecular cell biology *2*, 169-178.
189. Wilson, C., Nicholes, K., Bustos, D., Lin, E., Song, Q., Stephan, J. P., Kirkpatrick, D. S., and Settleman, J. (2014). Overcoming EMT-associated resistance to anti-cancer drugs via Src/FAK pathway inhibition. Oncotarget *5*, 7328-7341.
190. Yang, L., Lin, C., Liu, W., Zhang, J., Ohgi, K. A., Grinstein, J. D., Dorrestein, P. C., and Rosenfeld, M. G. (2011a). ncRNA- and Pc2 methylation-dependent gene relocation between nuclear structures mediates gene activation programs. Cell *147*, 773-788.
191. Yang, Y., Ahn, Y. H., Chen, Y., Tan, X., Guo, L., Gibbons, D. L., Ungewiss, C., Peng, D. H., Liu, X., Lin, S. H*., et al.* (2014). ZEB1 sensitizes lung adenocarcinoma to metastasis suppression by PI3K antagonism. The Journal of clinical investigation *124*, 2696-2708.
192. Yang, Y., Ahn, Y. H., Gibbons, D. L., Zang, Y., Lin, W., Thilaganathan, N., Alvarez, C. A., Moreira, D. C., Creighton, C. J., Gregory, P. A*., et al.* (2011b). The Notch ligand Jagged2 promotes lung adenocarcinoma metastasis through a miR-200-dependent pathway in mice. The Journal of clinical investigation *121*, 1373-1385.
193. Yu, L., Ji, W., Zhang, H., Renda, M. J., He, Y., Lin, S., Cheng, E. C., Chen, H., Krause, D. S., and Min, W. (2010). SENP1-mediated GATA1

deSUMOylation is critical for definitive erythropoiesis. The Journal of experimental medicine *207*, 1183-1195.

194. Yun, J., Mullarky, E., Lu, C., Bosch, K. N., Kavalier, A., Rivera, K., Roper, J., Chio, II, Giannopoulou, E. G., Rago, C.*, et al.* (2015). Vitamin C selectively kills KRAS and BRAF mutant colorectal cancer cells by targeting GAPDH. Science (New York, NY) *350*, 1391-1396.

195. Zhang, F. P., Mikkonen, L., Toppari, J., Palvimo, J. J., Thesleff, I., and Janne, O. A. (2008). Sumo-1 function is dispensable in normal mouse development. Molecular and cellular biology *28*, 5381-5390.

196. Zhang, Y., Gong, Y., Hu, D., Zhu, P., Wang, N., Zhang, Q., Wang, M., Aldeewan, A., Xia, H., Qu, X.*, et al.* (2015). Nuclear SIPA1 activates integrin beta1 promoter and promotes invasion of breast cancer cells. Oncogene *34*, 1451-1462.

197. Zheng, S., El-Naggar, A. K., Kim, E. S., Kurie, J. M., and Lozano, G. (2007). A genetic mouse model for metastatic lung cancer with gender differences in survival. Oncogene *26*, 6896-6904.

VITAE

Jerfiz D. Constanzo was born in La Romana, Dominican Republic, on February 8th, 1988. Jerfiz Graduated From Colegio Santa Rosa de Lima in May 2006. He moved to Puerto Rico and enrolled at Universidad Metropolitana (UMET), San Juan, Puerto Rico, where he obtained his bachelor degree in Biology. During his time at UMET he was awarded the national science foundation (NSF) scholarship for high academic achievement among other meritorious awards. In August 2010, he enrolled in the Graduate School of Biomedical Sciences at the University of Texas Southwestern Medical Center. He joined the Cancer Biology program and conducted his dissertation research under the guidance of Dr. Pier Paolo Scaglioni M.D. He successfully defended his thesis on January 2015 and was awarded the degree Doctor of Philosophy. Jerfiz lives in Dallas with Wife Mariya and daughter Eliana Marie.

Current Address:

5720 Forest Park Road

Apt. #3109

Dallas, TX 75235